Synthesis and characterization of magnetic gold nanomaterials and their application in the reduction of methylene blue

Emmanuel Jabulani Lukhele

199130779

Thesis submitted in fulfilment of the requirements for the degree

Master of Applied Sciences: Chemistry

in the Faculty of Applied Sciences at the

Cape Peninsula University of Technology

Supervisor: Professor Nikoletta B. Báthori (CPUT)

Co-supervisor: Dr Rehana Malgas-Enus (SU)

Bellville Campus

March 2022

CPUT Copyright information

The thesis may not be published either in part (in scholarly, scientific or technical journals), or as a whole (as a monograph), unless permission has been obtained from the University.

Declaration

I, Emmanuel Jabulani Lukhele, declare that the content of this thesis/dissertation my own unaided work, and that the thesis has not previously been submitted for academic examination towards any qualification. Furthermore, it represents my own opinions and not necessarily those of Cape Peninsula University of Technology.

Signed  Date 07 February 2022

Abstract

This thesis reports the synthesis and full characterization of phosphine-stabilized gold nanomagnetic materials. These nanomagnetic materials were modified on the surface for the treatment of wastewater from the textile industry. It was subsequently used as catalysts for the reduction, removal and recyclability studies of methylene blue dyes in an aqueous solution. It is commonly known that dyes from the textile industry are toxic to the environment through the wastewater stream and the reduction and/or removal of these dyes are a crucial study needed to keep our water safe and clean for human usage.

The synthesis of these nanomagnetic materials involved the making of naked superparamagnetic iron oxide nanoparticles (SPIONs) and this nanoparticle (**EJL1**) was prepared using the commonly used co-precipitation method. The metal precursor used for these naked SPIONs involved the mixing of two iron precursors ($FeCl_2.4H_2O$ and $FeCl_3.6H_2O$) in aqueous solution, with an addition of ammonium hydroxide (NH_4OH) solution to form a dark black precipitate, which indicates the formation of magnetite (Fe_3O_4), referred to as naked SPIONs in this thesis, due to its superparamagnetic properties. This was fully characterized using ultraviolet-visible spectroscopy (UV-Vis), Fourier-transform infrared spectroscopy (FT-IR), powder X-Ray diffraction (PXRD) and high-resolution transmission electron microscopy (HRTEM) techniques. From the FTIR. it could be confirmed that the Fe_3O_4 was obtained. The purity of the naked SPIONs was confirmed by using PXRD, as their diffraction pattern matched those of standard magnetite samples. The FT-IR spectrum showed the absorbance peaks that are characteristic of magnetite. The HRTEM confirmed an average particle size of 18.7 ± 5.6 nm.

The SPIONs was then modified by using chloroauric acid ($HAuCl_4.3H_2O$), which was reduced onto the SPIONs surface using two different reducing agents, namely sodium borohydride ($NaBH_4$) and sodium citrate ($Na_3C_6H_5O_7$). There were six catalysts successfully synthesized (**EJL2-EJL7**) using the direct gold-coating method. These were fully characterized using powder X-Ray diffraction (PXRD), ultraviolet visible spectroscopy (UV-Vis), Fourier-transform infrared spectroscopy (FT-IR), and high-resolution transmission electron microscopy (HRTEM), techniques. The ultraviolet visible spectroscopy clearly showed the difference in SPR peaks between the naked SPIONs and AuNPs. This proves that the reduction of these catalysts was successfully employed. The PXRD

concluded that the gold-coated nanoparticles were seen to have gold diffraction peaks which was confirmed by PXRD.

A well-known problem facing gold-coated nanoparticles (AuNPs) is their tendency to agglomerate, hence using a stabilizer on the AuNP surface to prevent agglomeration was important. Two phosphine ligands, 1,3,5-triaza-7-phosphaadamantane and triphenylphosphine, were used as stabilizer to produce phosphine-stabilized gold-coated SPIONs. Twelve phosphine-stabilized gold-coated SPIONs were successfully synthesized (**EJL8 to EJL19**). These were characterized using inductively coupled plasma spectroscopy (ICP), Fourier-transform infrared spectroscopy (FT-IR), high-resolution transmission electron microscopy (HRTEM) and ultraviolet visible spectroscopy (UV-Vis), techniques. From the FT-IR spectra it can be concluded that these ligands were successfully attached to the surface of the gold coated SPIONs as there was presence of -CH, C=C and C-N stretching frequencies which were not present on the naked SPIONs. From HRTEM, the TEM micrographs obtained showed that the gold coated SPIONs was not agglomerated, therefore the phosphine ligands stabilizer resolved this issue.

All the nanomagnetic materials used in this research had three different magnetite (Fe_3O_4) to gold (Au) metal ratios, namely 1:10, 1:50 and 1:100 respectively.

These catalysts were used for methylene blue (MB) dye reduction and removal from aqueous solution. The kinetics of this reaction using our range of nanomaterials are discussed and helped us found that the adsorbents not only reduce the MB, but also remove it completely from the aqueous solution when extracting the nanomaterial by applying an external magnetic field. The MB was desorbed from the nanoparticle surface by acetonitrile, after which the adsorbent could easily be recycled up to 5 times. Furthermore, since these catalysts have magnetic properties, they can be removed by applying an external magnetic field, making catalyst recovery and recyclability much easier.

Acknowledgement

I would first like to give praise and honour to God Almighty who provided me with strength to be able to do this research. There is a gospel song that comes has kept me going especially when the times got tough. It goes “Through it all, I have learned to trust in Jesus, I have learned to trust in God”. This indeed has been my anchor.

Secondly, I would like to thank Dr Rehana Malgas-Enus, this can truly be said, without you I would have not been able to have achieved the work I did for this research. Your endless support, your vast knowledge that you have shared with me, your guidance and push to be able to achieve this has made this journey worth it. You are more than a co-supervisor and supervisor to all the students in your research group, as your willingness to go above and beyond for the RME research group, may God truly bless you.

Thirdly, to Prof N. Bathori, you have been a complete blessing to this research and my accomplishment will not be a success have you not shown the willingness and the guidance you gave me through this research period. I look forward to working more with you soon once again.

Furthermore, I would like to acknowledge Mr WH Le Roux, the last two weeks of getting this thesis done with your willingness and positive attitude and encouragement you have given me. This would not be at all a success story without me stating my gratitude towards your very helpful spirit. The RME research group at large, I am proud to be associated with some amazing researchers and to all thanks for all the contributions made during this research journey.

Lastly, I wasn’t to acknowledge two more people in my personal life without them I would not have been able to do this. One being my mother has carried me in prayers to be able to achieve this thesis. Without your encouragement and prayers this would have not been possible. To Mr Sam Bobo, you have given me so much support and encouragement throughout this process. May God bless you as you also grow in your career.

Table of Contents

Abbreviations and Acronyms

^{13}C NMR- carbon nuclear magnetic resonance

^{1}H NMR- proton nuclear magnetic resonance

ATR- attenuated total reflectance

Au@MNPs- gold coated magnetic nanoparticles

FTIR- Fourier Transform Infra-Red spectroscopy

HRTEM- high resolution transmission electron microscopy

ICP-OES - inductively couple plasma optical emission spectroscopy

SPIONs- superparamagnetic iron oxide nanoparticles

MIONs- magnetic iron oxide nanoparticles

Mm- molar mass

MNPs- magnetic nanoparticles

nm- nanometer

PPh_3- triphenylphosphine

PTA- 1,3,5-triaza-7-phosphaadamandane

PXRD- powder X-ray diffraction

TEM- transmission electron microscopy

UV-Vis- ultraviolet-visible light spectroscopy

Chapter 1: Literature review

1.1 Introduction

Gold nanoparticles are particularly promising materials for use as catalysts due to their simple reductive preparation, reliable chemical stability and versatility in surface modification.[1] One way of rendering recyclable nanoparticle catalysts, is by surface functionalization of superparamagnetic nanoparticles. For superparamagnetic nanoparticles, their surface functionalization is a major breakthrough in research as it can bridge the gap between heterogeneous and homogeneous catalysis. Therefore, the introduction of nanomagnetic nanoparticles in a range of solid matrices allows for some already well-established procedures that have been tested for catalyst heterogenization that involves different techniques. For this project the interest is in magnetic separation. Magnetite is the most commonly used magnetic material due to its ability to support important homogeneous catalytically active metals.[2] In addition, there are several reports on the synthesis of magnetic core/shell nanoparticles which has a magnetite (Fe_3O_4) core and a metal or metal oxide shell.[3]

In the textile industry, synthetic dyes have been used to impart colour to fabrics; however, these dyes pose a serious threat to the environment due to their toxicity. The complex structure of dyes makes them difficult to degrade. Therefore, a perpetual method is needed to eradicate the dyes. Conventional methods have been reported,[4] some of which include coagulation-flocculation, sedimentation, membrane technologies (reverse osmosis, nanofiltration and dialysis), cloud point extraction, microbiological decomposition, aerobic and anaerobic degradation, chemical oxidation technologies (Fenton's reagent with hydrogen peroxide, photo-catalysis with UV radiation and ozonation), electrochemical treatment and adsorbents utilization (activated carbon, inorganic adsorbents such as silica or clays, synthetic ion-exchange resins and chitin-based adsorbents), but they are not efficient as the derivatives of the complex dyes remain in the water even after the treatment. The removal of these chemicals are expensive and complicated. Dyes cause many problems in the industry.[5] There are few factors that makes them problematic such as the dye concentration and duration of exposure to the environment. The azo dyes can have some sort of chronic side-effects when exposed to organisms. The presence of small quantities of dyes in water to an extent of less than 1 ppm, can be highly visibly seen due to their vibrant colours. The greatest environmental concern with dyes is their absorption and reflection of sunlight entering the water. Dyes can remain in the environment for an extended

period of time, because of their high thermal and photostability. For instance, the half-life of hydrolyzed Reactive Blue 19 is about 46 years at pH 7 and 25 °C. Many dyes and their breakdown products are carcinogenic, mutagenic and/or toxic to life.[6] Dyes are mostly introduced into the environment through industrial effluents. In recent times, nanoparticles have been found to be an effective approach to water purification.[7]

Therefore, we propose the use of modified gold-coated magnetic nanoparticles stabilized with phosphine ligands, as catalysts in the reduction of methylene blue dye in textile industry wastewater. These catalysts can also be recyclable due to their magnetic abilities.

1.2 Literature review

1.2.1 Nanoparticle materials

The nanomagnetic particle catalysis and surface functionalization has become a major component of chemistry. One of the major challenges facing chemists is the catalytic design and synthesis of environmentally benign catalysts.[8] The sustainability of the nanomagnetic catalysts must have specific features such as higher surface activity, lower preparation cost, great selectivity, great removal capabilities, good stability, ease of extraction and recyclability. The conventional catalysts can be homogeneous or heterogenous. The catalytic optimisation mechanistic studies based on advantages such as selectivity, surface modification, and activity is crucial. The challenges of separating homogeneous catalysts from reaction media can have a major restriction to their application in industry. Heterogenization of active catalysts with a solid support resulting in an active heterogeneous catalytic system, is an efficient strategy in order to achieve the isolation and separation of catalysts. The is just one disadvantage with the heterogeneous catalysts activities is that they are lower than those of their homogeneous counterparts. This is mostly because of their lower dimensionality that would enable the interaction between the components and the catalyst surface. Nanocatalysts, also referred to in this regard as semi-heterogeneous catalysts that has a large surface-to-volume ratios, have become more appealing as an alternative to conventional catalysts. This is due to their ability to be enhanced in its catalytic activity by stabilization while selectivity can be realized by tailoring

their particle shape, particle size, electronic structure and nanoparticle composition.[9] Nanotechnology is an emerging area, and several technological advancements have been possible in the fields of medicine, catalysis and environmental restoration. Nanoparticles possess remarkable catalytic, optical, magnetic, electronic, and thermal properties due to their specific properties like size, shape, and distribution as compared to their bulk analogues.[10]

Nano-catalysts can be recovered and isolated by different methods such as centrifugations as well as filtrations. The disadvantage of these methods is that they can hamper the sustainability and affordability of the nano-catalytic strategy. There are several ways that this can be overcome. Making use of magnetic nanoparticles (MNPs) has emerged as the most common practical and logical solution. This is due to the dynamic and efficient ways in which they can be removed from reaction mixtures using an external applied magnetic field. Therefore, the MNPs have emerged to be ideal catalysts or supports for nano-catalysts systems going forward. This field has produced a great amount of excellent and successful reviews.[11]

The MNPs can have a particle size range from nanometer to micrometer, which are desirable sizes to work with. They have also become attractive materials in more fields of applications, such as the medical- and biological industries.[12] The most promising particles are the iron oxide nanoparticles of various kinds, including their derivatives. These include magnetite (Fe_3O_4), maghemite (γ-Fe_2O_3) and hematite (α-Fe_2O_3), which are the most popular iron oxide nanoparticles. These nanoparticles of iron oxide are used widely as materials for different applications such as drug carriers,[13] drug release,[14] cancer therapy,[15] hyperthermia, magnetic separation, magnetic resonance imaging (MRI),[16] proton exchange membrane[17] and as sensors.[18] Of these oxide nanoparticles, the Fe_3O_4 nanoparticles are the most studied materials. This is because of their ability to respond to a magnetic field through their superparamagnetic behaviour at room temperature, using high saturation magnetization. Furthermore, their non-toxicity is a great advantage while their high biocompatibility is extremely suitable for biomedical applications.[19] The uniformity in particle size, shape and being well dispersed in solvents are a major requirement for most of these applications. One of the major factors within these applications is the particle size that affects the particle's properties. The size and shape of magnetite particles are generally controlled by the synthesis method. A variety of methods have been reported in the literature on the synthesis of magnetite nanoparticles, such as the chemical co-precipitation,[20] hydrolysis,[21] thermal decomposition[22] and sol-gel techniques.[23]

1.2.2 Gold-coated nanoparticles

There are some challenges that occur regarding magnetic nanoparticles (MNPs), which can be addressed by coating the MNPs with a gold layer to form gold-coated nanoparticles. These MNPs are not ideal with regards to being very active species especially in sensing applications. The challenge facing the use of MNPs in sensing is a result of MNPs having a large surface area to volume ratio and low surface charge at neutral pH; dispersions of these particles typically have a low stability with the MNPs tending to aggregate when dispersed in solvents.[24] The aggregation can be reduced with appropriate surface chemistry, which is also vital for sensing applications.[25] However, the surfaces of most magnetic materials are not highly compatible with well-defined surface chemistry as the alkanethiol system. The process of having gold-coated MNPs addresses all challenges mentioned above. They are not limited to but can include several others such as conductivity,[26] optical properties (localized surface plasmon resonance and surface enhanced Raman scattering),[27] biocompatibility,[28] bio-affinity through functionalization of amine/thiol terminal groups[29] and chemical stability by protecting the magnetic core from aggregation, oxidation and corrosion,[30] see **Figure 1.1**.

The gold (Au) within the nanoparticle sphere as a coating agent has become an area of intense research focus due to its fascinating chemical and electronic properties. It has been seen in a wide range of applications such as lubricant manufacture, pharmacology (drug delivery), cosmetology, and its particularly interesting use in catalysis.[31] These properties can vary with the morphology and particle size of the gold nanoparticles. Li *et al*.[32] demonstrated the synthesis of magnetic nanoparticles coated with AuNPs, where the magnetic nanoparticle acted as both reductant and template, and the particle size of the AuNPs catalysts can be varied with an increase in reaction time.[32] There are also several reports which describe the synthesis of various nanostructure morphologies such as spherical, hexagonal, rod like, cubic and planar nanoparticles. These various particle shapes can be achieved by modifying different experimental parameters. These parameters include the nanoparticle precursors, time, temperature, pH and reactant concentrations.[33] Pentagonal- and hexagonal gold-coated nanoparticles are considered to be more catalytically active when compared to other particle shapes because they possess more reactive surfaces.[34]

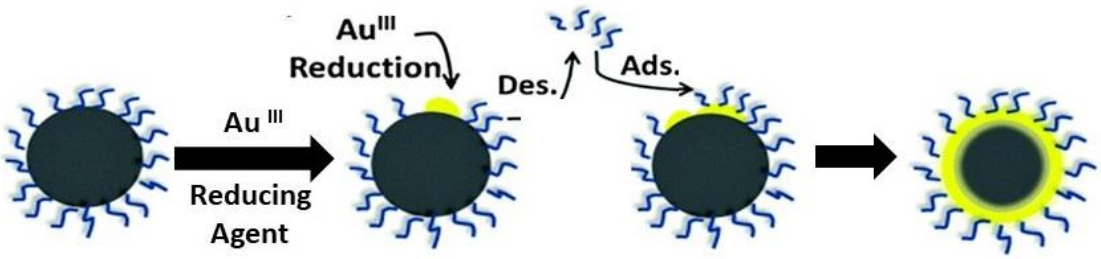

Figure 1.1: Gold coating of Fe_3O_4 nanoparticles process.

1.2.2.1 Direct gold coating

The direct gold coating method involves using the magnetic particles that are in aqueous or organic media. The most commonly employed procedure is the reduction of Au^{3+} onto the MNPs using reducing agents such as sodium citrate ($Na_3C_6H_5O_7$) or sodium borohydride ($NaBH_4$) in aqueous solution. This method of attachment of gold atoms to make a shell on the MNPs using the sodium citrate/borohydride reduction of gold chloride, is one of the simplest and robust methods used.[35] See **Figure 1.2**.

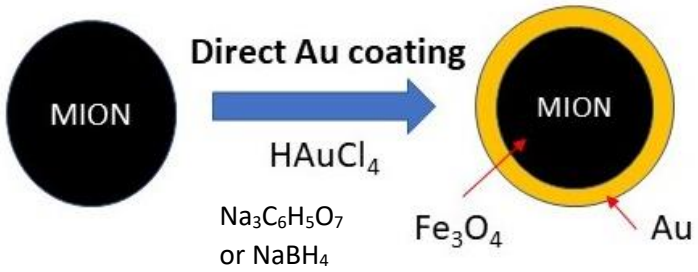

Figure 1.2: Direct Au-Coating method.

1.2.2.2 Indirect gold coating

The indirect gold coated nanoparticles are characterized by having a 'glue layer' between the magnetic core and the outer gold shell. The key for this method is with the glue-layer which requires a careful choice and preparation of the 'glue layer' to be able to achieve the gold coated MNPs that will have multifunctional properties. This glue-layer must be able to fully coat the MNPs surface to guarantee good chemical- and physical-stability. They should also have many

binding groups with the ability to chelate metal ions to promote gold shell growth, see **Figure 1.3**. There are few known materials that can be used as a glue-layer. The two most commonly used being poly-L-histidine, or polymer polyethylene-imine.[37]

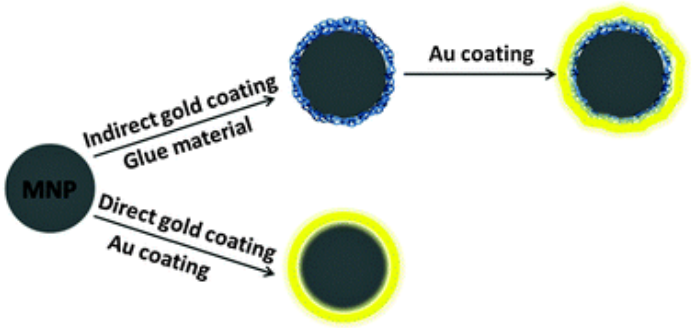

Figure 1.3: Gold coated magnetic nanoparticles (Au@MNPs).[36]

1.2.3 Stabilization of nanoparticles

Nanoparticle materials have a propensity to self-assemble or agglomerate into larger structures.[37] This has become a major issue which can be resolved by making use of stabilizers. There are many stabilizers such as polymers, heteroatom-containing ligands, dendrimers and long carbon chain ligands have been used successfully to prevent agglomeration or the propensity to self-assemble. The simplest and hence the most commonly used method to produce metal nanoparticles, is considered to be colloidal synthesis method.[38] This colloidal synthesis method typically involves the dissolution of an appropriate metal precursor simultaneously with a surfactant. The metal precursor is then reduced by an appropriate reducing agent ($Na_3C_6H_5O_7$ or $NaBH_4$) to generate the desired nanoparticles. This method also has its disadvantages as nanoparticles with wide size distributions are often obtained. This has prompted further research that is intended to optimize the surface modification, in order to narrow these particle size distributions.[39] There has been one area of research that has been successful in producing highly monodispersed nanoparticles, by making use of dendrimers as a template for the synthesis of the nanoparticles which has an ability to act as a cluster stabilizer. In this research, two phosphine ligands (PTA and PPh_3) will be used to stabilize the gold-coated

nanoparticles to prevent them from agglomeration, and also to tailor the solubility of the nanomaterials, as shown in **Figure 1.4**.

Figure 1.4: AuNPs stabilized using phosphine ligands.

1.2.4 Application of NPs in wastewater treatment

As discussed previously, the textile industry uses organic azo dyes which leads to environmental pollution and contamination that is highly toxic to both flora and fauna. These industrial wastewater effluents can contaminate the underground water, which will in turn contain toxic organic dyes which have serious effects on the aquatic ecosystem. These toxic azo dyes can be removed from contaminated wastewater using various methods. There has been a need for greener and simpler methods, since these current methods mostly make use of organic solvents which are high energy consuming processes. Therefore, the research has shifted to focus on the use of nanoparticles for this purpose. Most researchers are now developing different types of simpler and greener nano-systems for removal of toxic dyes within the wastewater treatment industry. These azo dyes' effluent discharges into the environment are currently a major concern due to both their high visibility, undesirability, and obstinacy. The investigation with serious efforts of researchers to be able to produce a safer and cleaner environment, is of great need as previously emphasized.[40] Methylene blue dye is our focus area of study for this research application. Methylene blue (MB) is a thiazine cationic dye is predominately used in industry for dyeing cottons, colouring paper, wools, and temporary hair colorants. The increase in the use of MB dye has a major impact on the health hazards as it is known to cause eye burns, which can

result in blindness in humans.[41] The removal of azo dyes in wastewater treatment using nanoparticles is fast becoming the preferred technique for wastewater treatment. This removal technique has advantages such as high efficiency, being good adsorbates and ease of upscaling. The adsorption technique has received tremendous attention due to its cost efficiency, easy access with high performance, and of most importance is its reusability. For the last few decades, researchers have shown a substantial interest in the use of activated carbon as the most useful technique for the removal of dye from organic and aqueous solutions. This application is limited due to the availability of activated carbon, as the raw materials related to activated carbon synthesis are expensive. Since the successful removal efficiency of dyes depends on the physicochemical characteristics of an absorbent, nanoparticles have received a great deal of attention due to their high surface-to volume ratio, highly ordered structure and their decreased particle size, within the environmental field.[42] Previous research work on magnetic separation as a reliable fast and convenient methods has been performed. These were done by using different iron oxides loaded on the activated carbon such as Fe_2O_3,[43] Au-Fe_3O_4,[44] and Fe_3O_4.[45]

From the literature, it has been shown that gold nanoparticles are very efficient catalysts, especially for the reduction of 4-nitrophenol. Likewise, AuNPs have been used to catalyze reductive dye degradation for a few azo dyes. As previously mentioned, agglomeration is a huge challenge in nanoparticle synthesis since highly reactive small gold nanoparticles usually tend to agglomerate. Therefore, they also require stabilizers to ensure that agglomeration is limited and/or prevented. Both support materials and stabilizing ligands can be modified successfully to prevent agglomeration for various applications.[46] Hence, researchers have focused on developing more effective methods for the treatment of wastewater.[47]

1.2.5 Effect of particle shape morphology

The particle shape morphology effect will be discussed as the surface functionalization of magnetic iron oxide nanoparticles below:

1.2.5.1 Surface functionalization of magnetic iron oxide nanoparticles (MIONs)

One of the inevitable problems associated with MIONs in the nano size range, is that they are highly unstable over long periods of time. This happens in two ways: (1) From the loss of dispersibility, where small nanoparticles tend to aggregate to form large particles therefore reducing the surface energy; (2) from the loss of magnetism, where naked MIONs are easily oxidized in air due to their increased ability to react with oxygen in the atmosphere. This is especially noted for magnetite and γ-maghemite nanoparticles. Therefore, the successful stabilisation of the naked MIONs is vital. In the biomedical applications, it is necessary to obtain water dispersible nanoparticles, because most biological media are neutral aqueous solutions. Four types of MIONS-based materials, have been synthetically attempted, including the core-shell structure, matrix dispersed structure, Janus-type heterostructures and shell-core-shell structure (Figure 1.5).[90]

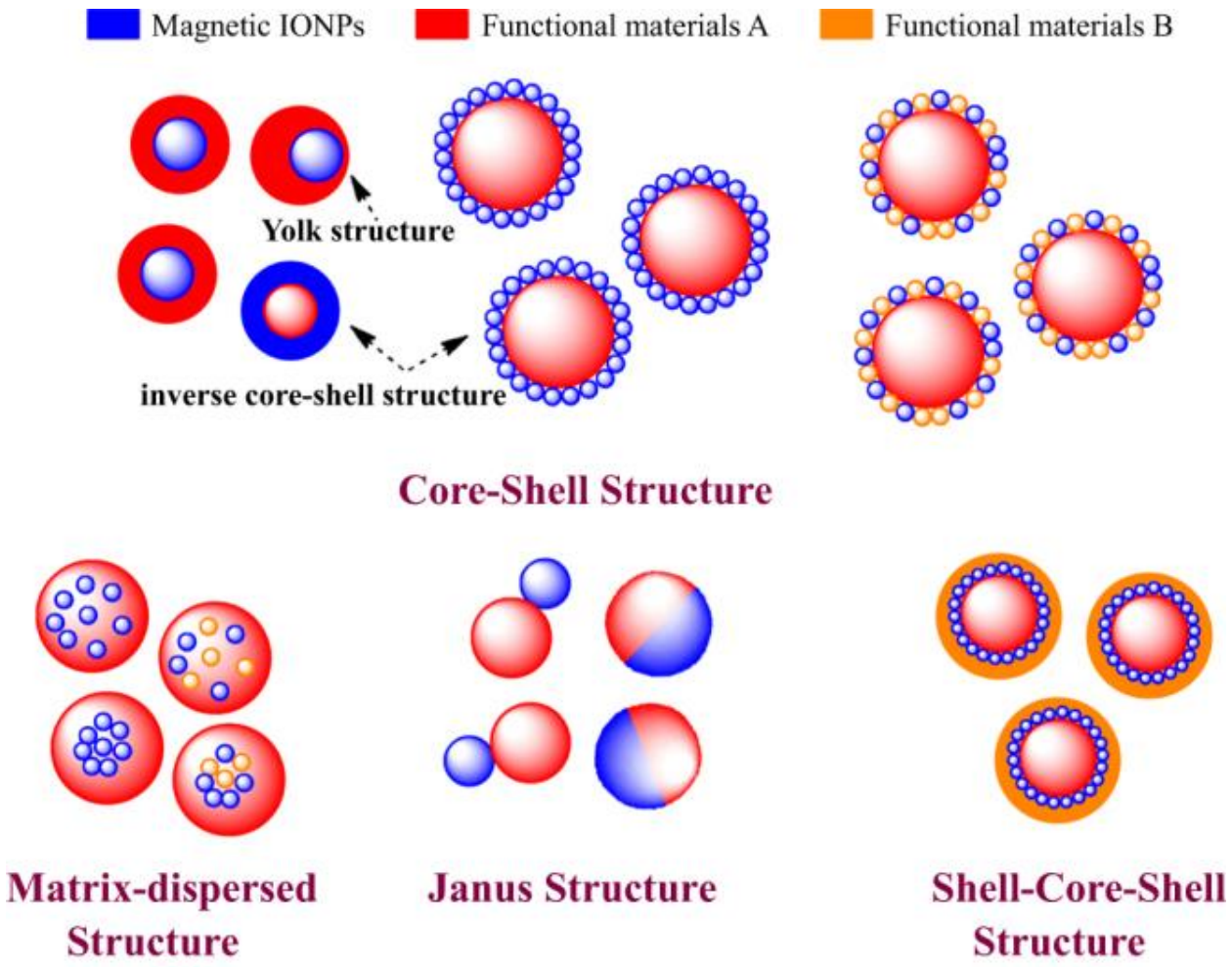

Figure 1.5: Structures of typical morphologies of nanomagnetic composite nanomaterials.[48]

The blue spheres represent MIONs while the other colours represent the non-magnetic entities and matrix materials. The non-magnetic entity can supply the composite material with more functionalities and properties and thus provides a multifunctional hybrid system.

1.2.5.1.1 Core-shell structure

The definition of the 'core-shell' structure is that iron oxide coats the surface of the core material. In the inverse core-shell structure, the MIONs will be coated on the surface of non-magnetic functional materials. Furthermore, the MIONs has the ability to combine one or more functional materials, and further coat with another functional material on a functionalized surface.[47]

1.2.5.1.2 Matrix-dispersed structure

For the matrix-dispersed structure, the MIONs are dispersed in a matrix to prevent the superparamagnetic nanoparticles from aggregating into large ferromagnetic species. Therefore, matrix-dispersed nanoparticles can be created in a variety of different states. Like being "dispersed in a continuous amorphous matrix, grafted on larger, mesoscale particles, or well defined, three-dimensional superstructures of nanoparticles".[47]

1.2.5.1.3 Janus structure

In the Janus structure, there is one side which is MIONs, and another side is then functional. This is usually more for the anisotropic nanomaterials. Surface chemical compositions of Janus structures are interesting for applications, even if one is not concerned with self-assembly.[47]

1.2.5.1.4 Shell-core-shell structure

The shell-core-shell structure of MIONs is where the MIONs are located between the two functional materials. Most applications require MIONs to be embedded in the non-magnetic

layers. This is to avoid aggregation and sedimentation of MIONs as well as to endow them with particular surface properties for specific applications. [47]

1.2.5.1.5 Aggregation and concentration

The aggregation states of nanoparticles are vital. These states of nanoparticles are dependent on several factors such as surface charge, composition, size, etc. An interesting trend has been observed; i.e., as the concentration of nanoparticles increases, the toxicity decreases.[49]

1.2.5.1.6 Surface coating and surface roughness

The surface properties of particles have a significant role for nanoparticles, as discussed previously. They play an important role in determining the outcome of their collaboration with the cells and other biological entities. Surface coating can affect several properties on nanoparticles but mostly the cytotoxic properties of nanoparticles by changing their physicochemical properties. These physicochemical properties are: (1) magnetic, (2) electric, (3) optical properties and (4) chemical reactivity. These properties can also alter the pharmacokinetics, distribution, accumulation, and toxicity of nanoparticles.[93]

1.3 Kinetics

Kinetics is an important method employed to understand better catalytic systems and their mechanisms for nanoparticles in their various applications. They provide mathematically conclusions pertaining to the different parameters to be proven for a particular application. There are different kinetics methods that have been studied for methylene blue dye degradation, like the photodegradation of MB using titanium dioxide powder by using elementary reactions.[50] For methylene blue, the kinetic studies are dependent on the use of bulk materials as the reduction of MB is a kinetically slow process. In the case of bulk catalysts, the molecules of MB cannot be adsorbed on the bulk material rapidly but can be made more facile by using the

appropriate nano-catalytic assemblies. “Therefore, in nano-catalytic material, the surface-to-volume ratio of the available absorption sites increases abundantly. Moreover, the accessibility of the MB molecules to these sites also exponentially increases with the decrease in the size of the catalyst. Thus, the nanomaterial considerably reduces the kinetic barrier during the reduction of MB”.[51]

For the purpose of this research thesis, the kinetic methods employed pertaining to the nanomagnetic studies preparation and for the methylene blue dye reduction in aqueous solution. This will be discussed in detail in chapter 3. To emphasize the importance of kinetics as mentioned above mentioned within the methylene blue reduction or removal processes.

1.4 Dye wastewater treatment

As previously mentioned, organic azo dyes have been found in many wastewater streams from the textile industry, and these toxic dyes have substantially been affecting human health and having a major impact on the environment[52], as shown in **Figure 1.5**. There are many health hazards that these toxic organic dyes can cause, such as skin irritation, blood disorder, liver, and kidney damage not excluding the poisoning of the central nervous system both in humans and animals due to their carcinogenicity and toxicity abilities.[53] The dye polluted wastewater is known to heavily interfere with ecosystems, due to blocking the sunlight inflowing into the water and hindering the photosynthetic processes.[54] The degradation, reduction and removal of these toxic compounds into non-toxic products is required before they are discharge into the water stream. The first synthetic dye, Mauve or Aniline-Purple, was discovered in 1856. Ever since, dyes have become an indispensable part of the textile and many other industries.[55] The list of the azo dyes used in the textile industries are many but to mention a few, Methyl violet, Brilliant Green, Bromophenol Blue, Ethyl Violet, Victoria Blue, Methyl Green, Pararosaniline, Cresol Red, and Basic Fuchsin.[56] There has been difficulties in removing these dyes as they are generally resistant to aerobic treatment process applied to municipal sewage water treatment sites, which are not well maintained resulting in these dyes getting into other water systems. This resistance to degradation, reduction, and removal, along with the high pollutant nature, these dyes pose a significant problem. It has become more than just important to have these dyes removed from the wastewater streams and crucial to hamper their toxicity. Most traditional methods have

failed to decolorize these organic dyes. The most suitable method is the adsorption of such organic dyes at low-cost and having resourceful solid supports and has been deliberated to be the simplest, most effective, and economical method. The current disadvantages of the used systems are that they require a larger amount of toxic chemicals and are not cost-effective.

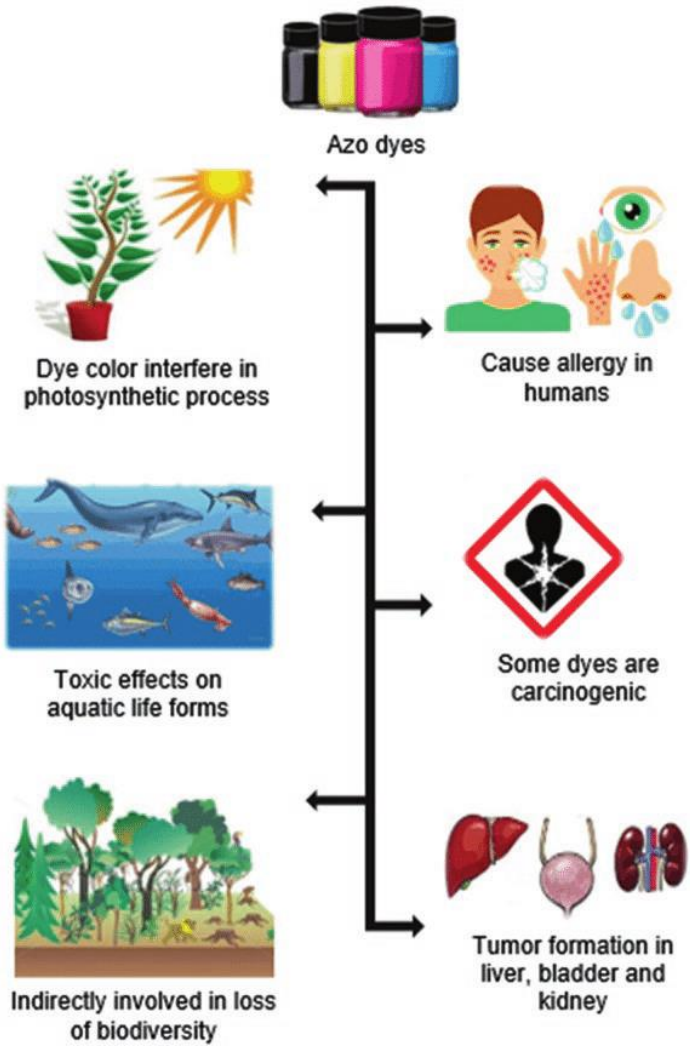

Figure 1.6: The effects of Azo dyes in wastewater.[57]

1.4.1 Nanoparticles as a solution for wastewater treatment

The reductive degradation method of coloured dyes in the wastewater streams with the presence of metal nanoparticles as treatment such as Au, Ag, Ni, Si and Fe, as catalyst is highly efficient, rapid, simple, and economic.[58] Since there is a need for greener systems this approach

has been found to be much greener compared to other approaches. This is because it does not only reduce the chromophore groups but has the capabilities to break the large organic pollutant molecules into small molecules,[59] which can then be biodegradable. The reductive degradation process is a much faster process when compared to the widely used photocatalytic oxidative degradation. Furthermore, photocatalytic processes require irradiation, and it is well known that this process requires and consume very high amounts of energy. The reduction of dyes using sodium borohydride ($NaBH_4$) occurs by electron transfer. These electron transfers are from the BH_4^- (ions) to the dye molecule. There is a large redox potential difference between the electron donor (BH^-_4 ion) and acceptor (dyes) species, which makes the electron transfer process difficult and less environmentally friendly.[60] This reductive degradation by $NaBH_4$ on the dyes is thermodynamically favourable, but it is kinetically difficult. Metal nanoparticles act as catalyst for reduction; as silver, gold, or platinum acts as an electron relay system because their redox potential falls in between the donor (BH^-_4) and the acceptor (dye molecule). The process is well known, as the metal nanoparticles assists the electron transfer from donor to acceptor, as already stipulated, thereby making the degradation process more favourable thermodynamically and kinetically.[61] This implies that the catalytic efficiency of metal nanoparticles will be increasing as their surface to volume ratio increases, and are directly proportional.[62] The Fermi potential, surface plasmon resonance and catalytic efficiency of gold nanoparticles make them potential candidates for the use as a catalyst for electron-transfer reactions. The high Fermi potential of gold nanoparticles reduces the potential difference between BH^-_4 and the dye molecule. The synthesis of gold nanoparticles with proper redox potential is significant and challenging too. The functionalization of these nanoparticles enhances the stability of the AuNPs by using a reliable stabilizer to prevent the nanoparticles from agglomerating.

Though Fe_3O_4 has been exploited for degradation of anilines, phenols, nitrophenol and dye pollutants, and its magnetic separability contributes to its widespread applications, the magnetism promotes the coagulation of magnetite nanoparticles resulting in suppressed adsorption performance. Thus, researchers are working on the immobilization of magnetite on a solid support like bentonite, biochar and organic polymeric materials which can minimize the coagulation of magnetic nanoparticles.[63] In this project we look at the synthesis, mechanistic design and evaluation of gold-coated phosphine-stabilized magnetic nanoparticles as nano-catalysts for the use in reductive discoloration, degradation, and removal of methylene blue. For

this application, the immobilization of monometallic gold nanoparticles (AuNPs) on supports such as magnetite is used as catalysts in heterogeneous catalytic processes. These catalysts will be successfully modified with 1,3,5-triaza-7-phosphaadamantane (PTA) on the surface of the gold-coated magnetite. The nano-sized magnetic iron oxide nanoparticles (MION's) will be synthesized using the co-precipitation method.[64] The characterization of these catalysts will be performed using Fourier Transform Infrared spectroscopy (FTIR), transmission electron microscopy (TEM), ultraviolet-visible spectroscopy (UV-Vis) and powder X-ray diffraction (PXRD). Powder XRD could confirm the formation of nanocrystal inverse spinal phase magnetite. These magnetic nano-catalysts will be used as catalysts in the reduction of azo dyes. The catalysts should provide ease of recovery and recyclability.

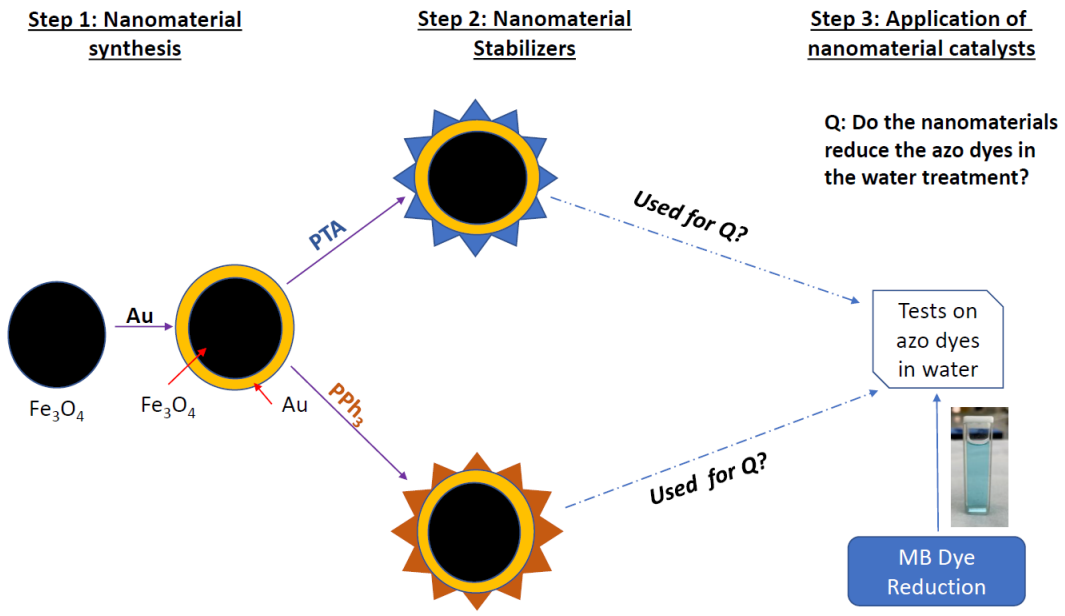

Figure 1.7: Experimental design of the proposed research project.

1.5 Hypotheses or research questions

1.5.1 Hypotheses

The hypotheses regarding this research project is and follows:

- Gold modified magnetic nanoparticles can reduce azo dyes from textile industry wastewater.

1.5.2 Research questions

The research questions regarding this project are as follows:

- Can the synthesis of the modified magnetic nanoparticle be obtained?
- Could gold-modified magnetic nanoparticles reduce azo dyes used in the textile industry?
- Are these magnetic nanoparticles recyclable, and do they maintain their activity after multiple cycles?

1.6 Aims and objectives

Gold coated magnetic nanoparticles will be synthesized and stabilized with two ligands, 1,3,5-triaza-7-phosphaadamantane and triphenylphosphine. The stabilized gold nanomaterials will then be used as catalysts in the dye degradation of methylene blue. General analytical methods (UV-VIS, FTIR, ICP), electron microscopy (SEM, TEM), thermo-analytical methods (DSC, TGA) and X-ray methods (PXRD) will be used to characterize the nanomaterials. In alignment with the research questions, the following objectives will be adhered to, regarding the synthesis method process of magnetic gold-coated nanoparticles and their applications in dye reduction and degradation.

Synthesis of naked magnetite nanoparticles and their characterization.

- Synthesis of gold (Au) nanoparticles with different gold: magnetite loading ratio and their characterization.
- Synthesis of modified gold nanoparticles with different phosphine stabilized nanoparticles and their characterization.
- All the above-mentioned nanoparticles applications will be used in dye degradation for the textile industry.

This thesis has been divided into four chapters, where **Chapter 1** will cover the literature background on the methods for the catalysts for wastewater treatment. The focus of this chapter will be more on the use of superparamagnetic iron oxide nanoparticles (SPIONs): their design

synthesis methods, reduction using gold and their modification with phosphine ligands, and their use in the reduction/removal of methylene blue dye in wastewater.

Chapter 2 will cover the synthesis methods and characterization of naked SPIONs by a co-precipitation method. Magnetite nanoparticles produced by chemical co-precipitation are normally not pure and usually have in their presence other traces of iron oxide species. In order to produce pure magnetite (Fe_3O_4) nanoparticles, the optimisation of this method was carried out by varying the total iron (Fe) concentration and temperature. The synthesis and characterization of gold-coated (AuNPs) nanoparticles that were stabilized with phosphine ligands will also be covered. The characterization of the nanoparticles was carried out by using infrared spectroscopy (IR), powder X-ray diffraction (PXRD), Ultraviolet-Visible (UV-Vis) Spectroscopy, Inductively Coupled Plasma (ICP) and high-resolution transmission electron microscopy (HRTEM).

In **Chapter 3**, naked SPIONs and AuNPs synthesized by optimized reaction conditions were used in the reduction and removal of methylene blue dye. These studies were done mainly by monitoring the disappearance of the methylene blue band via Ultraviolet-Visible (UV-Vis) Spectroscopy. A possible mechanism that will explain the interaction between methylene blue, $NaBH_4$ and the surface of AuNPs catalysts has been proposed. The interaction kinetics and thermodynamics studies were also investigated.

Chapter 4 gives the summary and conclusion of the research findings, as well as suggestions for future work.

1.7 Delimitation of the research

- No scale-up formulation will be attempted.
- Biological testing of formed materials will not be conducted

1.8 References

[1] H. Maleki, A. Simchi, M. Imani, and B.F.O Coats, Size-controlled synthesis of superparamagnetic iron oxide nanoparticles and their surface coating by gold for biomedical applications, Journal of magnetism and magnetic materials, (2012) 324, 3997-4005.

[2] M. B. Gawade, P. S. Branco and R. S. Varma, Nano-magnetite (Fe_2O_3) as a support for recyclable catalysts in the development of sustainable methodologies, Chemical Society Reviews, (2013) 42, 3371-3393.

[3] Z. Xu, Y. Hou and S. Sun, Magnetic Core/Shell Fe_3O_4/Au/Ag Nanoparticles with tunable plasmonic properties, Journal of the American Chemical Society Communications, (2007) 129 (28), 8698-8699.

[4] P. Saikia, A. T. Miah and P. P. Das, Highly efficient catalytic reductive degradation of various organic dyes by Au/CeO2-TiO2 nano-hybrid, Journal of Chemical Sciences (2017) 129, 81-93.

[5] N. T. Nandhini, S. Rajeshkumar, and S. Mythili, The possible mechanism of eco-friendly synthesized nanoparticles on hazardous dyes degradation, Biocatalysis and Agricultural Biotechnology, (2019) 19, 101138, 1-10.

[6] M. I. Kiron, Problems caused by textile dyes in the environment, Textile learner (one stop solution for textiles), (2011) 04, 4786-4787.

[7] N. T. Nandhini, S. Rajeshkumar, and S. Mythili, The possible mechanism of eco-friendly synthesized nanoparticles on hazardous dyes degradation, Biocatalysis and Agricultural Biotechnology, (2019) 19, 101138, 1-10.

[8] R. B. Nasir Baig, R. S. Varma, Magnetically retrievable catalysts for organic synthesis, Chemical Communications, (2013) 49, 752-770.

[9] D. Astruc, Wiley-VCH Verlag GmbH & Co. KGaA: Weinheim, In transition-metal Nanoparticles in Catalysis, (2008).

[10] S. Raina, A. Roy, and N. Bharadvaja, Degradation of dyes using biologically synthesized silver and copper nanoparticles, Environmental Nanotechnology, Monitoring & Management, (2020) 13,100278, 1-5.

[11] Y. Zhu, L. P. Stubbs, F. Ho, R. Liu, C. P. Ship, J. A. Maguire, and N. S. Hosmane, Magnetic Nanocomposites: A new perspective in catalysis, ChemCatChem, (2010) 2, 365-374.

[12] H. Iida, K. Takayanagi, T. Nakanishi, T. Osaka, Synthesis of Fe_3O_4 nanoparticles with various sizes and magnetic properties by controlled hydrolysis, Journal of Colloid and Interface Science, (2007) 314, 274-280.

[13] J. Yang, S. B. Park, H. G. Yoon, Y. M. Huh, and S. Haan, Preparation of poly ε-caprolactone nanoparticles containing magnetite for magnetic drug carrier, International Journal of Pharmaceutics, (2006) 324, 185-190.

[14] L. Zhou, J. Yuan, W. Yuan, X. Sui, S. Wu, Z. Li, and D. Shen, Synthesis, characterization, and controllable drug release of pH-sensitive hybrid magnetic nanoparticles, Journal of Magnetism and Magnetic Materials, (2009) 321, 2799-2804.

[15] B. X. Hu, K. G. Neoh, and E. T Kang, Cellular response to magnetic nanoparticles "PEGylated" via surface-initiated atom transfer radical polymerization, Biomacromolecules, (2006) 27, 5725-5733.

[16] Z. Ma, and H. Liu, Synthesis and surface modification of magnetic particles for application in biotechnology and biomedicine, China Particuology, (2007) 5, 1-10.

[17] S. B. Brijmohan, and M. T. Shaw, Magnetic ion-exchange nanoparticles and their application in proton exchange membranes, Journal of Membrane Science, (2007) 303, 64-710.

[18] Y. L. Luo, L. H. Fan, F. Xu, Y. S. Chen, Zhang, and Q. N. Wei, Synthesis and characterization of Fe_3O_4/PPy/P(MAA-co-AAm) trilayered composite microspheres with electric, magnetic and pH response characteristics, Material Chemistry and Physics, (2010) 120, 590-597.

[19] R. Kumar, B. S. Inbaraj, and B. H. Chen, Surface modification of superparamagnetic iron nanoparticles with calcium salt of poly(γ-glutamic acid) as coating material, Materials Research Bulletin, (2010) 45. 1603-1607.

[20] X. Liu, M. D. Kaminski, Y. Guan, H. Chen, and A. J. Roisengart, Preparation and characterization of hydrophobic superparamagnetic magnetite gel, Journal of Magnetism and Magnetic Materials, (2006) 306, 248-253.

[21] I. J. Bruce, J. Taylor, M. Todd, M. J. Davies, E. Borioni, C. Sangregorio, and T. Sen, Synthesis, characterization and application of silica-magnetite nanocomposites, Journal of Magnetism and Magnetic Materials, (2004) 284, 145-160.

[22] S. Asuha, B. Suyala, X. Siqintana, and S. Zhao, Direct synthesis of Fe_3O_4 nanopowder by thermal decomposition of Fe-urea complex and its properties, Journal of Alloys Compounds, (2011) 509, 2870-2873.

[23] B. Unal, Z. Durmus, H. Kavas, A. Baykal, and M. S. Toprak, Synthesis, conductivity and dielectric characterization of salicylic acid- Fe_3O_4 nanocomposite, Materials Chemistry and Physics, (2010) 123, 184-190.

[24] K. G. de Souza, G. F. Andrade, I. Vasconcelos, I. M. D. Viana, C. Fernandes and E. M. B. de Sousa, Magnetic solid-phase extraction based on mesoporous silica-coated magnetic nanoparticles for analysis of oral antidiabetic drugs in human plasma, Materials Science and Engineering C, (2014) 40, 275-280.

[25] J. J. Gooding and S. Ciampi, The molecular level modification of surfaces: from self-assembled monolayers to complex molecular assemblies, Chemical Society Reviews, (2011) 40, 2704-2718.

[26] S. H. Koening and K. E. Kellar, Theory of $1/T_1$ and $1/T_2$ NMRD profiles of solutions of magnetic nanoparticles, Magnetic Resonance in Medicine, (1995) 34, 227-233.

[27] D. Yang, X. C. Pang, Y. J. He, Y. Q. Wang, G. X. Chen, W. Z. Wang and Z. Q. Lin, Precisely Size-Tunable Magnetic/Plasmonic Core/Shell Nanoparticles with Controlled Optical Properties, Angewandte Chemie International Edition, (2015) 54, 12091-12096.

[28] H. Y. Park, M. J. Schadt, L. Wang, I. I. Slim, P. N. Njoki, S. H. Kim, M. Y. Jang, J. Luo and C. J. Zhong, Fabrication of magnetic core@shell Fe oxide@Au nanoparticles for interfacial bioactivity and bio-separation, Langmuir, (2007) 23, 9050-9056.

[29] J. L. Lyon, D. A. Fleming, M. B. Stone, P. Schiffer and M. E. Williams, Synthesis of Fe Oxide Core/Au Shell nanoparticles by iterative hydroxylamine seeding, Nano Letters, (2004) 4, 719-723.

[30] I. Y. Goon, L. M. H. Lai, M. Lim. P. Munroe, J. J. Gooding and R. Amal. Fabrication and dispersion of gold-shell-protected magnetite nanoparticles: systematic control using polyethyleneimine, Chemical Materials, (2009) 21, 673-723.

[31] D. T. Thompson, Using gold nanoparticles for catalysis, Nano Today, (2007) 2, 40-43.

[32] K. Li, T. Jiao, R. Xing, G. Zou, J. Zhou, I. Zhang, and Q. Peng, Fabrication of tunable hierarchical magnetic coated gold nanoparticles nanocomposites constructed by self-reduction reactions with enhanced catalytic performances, Science China Materials, (2018) 61, 728-736.

[33] Y. Ofir, B. Samantha, and V. M. Rotello, Polymer and biopolymer mediated self-assembly of gold nanoparticles, Chemical Society Reviews, (2018) 37, 1814-1825.

[34] M. Kumari, A. Mishra, S. Pandey, S. P. Singh, V. Chaudhry, M. K. R. Mudiam, S. Shukla, P. Kakkar, and C. S. Nautiyal, Physico-chemical condition optimisation during biosynthesis lead to development of improved and catalytically efficient gold nanoparticles, Scientific Reports, (2016) 6, 27575-27583.

[35] W. H. De Jong, W. I. Hagens, O. Krystek, M. C. Burger, A. J. A. M. Sips and R. E. Geertsma, Particle size-dependent organ distribution of gold nanoparticles after intravenous administration, Biomaterials, vol 29, no 12, 2008:1912-1919

[36] S. M. Silva, R. Tavallaie, L. Sandiford, R. D. Tilley and J. Gooding, Gold coated magnetic nanoparticles: from preparation to surface modification for analytical and biomedical applications, Chemical Communications, (2016) 52, 7528-7540.

[37] K. T. Wu, Y. D. Yao, C. R. C. Wang, P. F. Chen, and E. T. Yeh, Magnetic field induced optical transmission study in an iron nanoparticle ferrofluid, Journal of Applied Physics, (1999) 85, 5959-5961.

[38] Y. Xia, T. D. Nguyen, M. Yang, B. Lee, A. Santos, P. Podsiadlo, Z. Tang, S. C. Glotzer, and N. A. Kotov, Self-assembly of self-limiting monodisperse supraparticles from polydisperse nanoparticles, Nature Nanotechnology, (2011) 6, 580-587.

[39] R. K. DeLong, C. M. Reynolds, Y. Malcolm, A. Schaeffer, T. Severs, and A. J. Wanekaya, Functionalized gold nanoparticles for the binding, stabilization, and delivery of therapeutic DNA, RNA, and other biological macromolecules, Nanotechnology Science and Applications, (2010) 3, 53-63.

[40] G. Mezohegyi, F. P. van der Zee, J. Font, A. Fortuny and A. Fabregat, Towards advanced aqueous dye removal processes: A short review on the versatile role of activated carbon, Journal of Environmental Management, (2012) 102, 148-164.

[41] M. Ghaedi, M. Roosta, A. M. Ghaedi, A. Ostovan, I. Tyagi, S. Argarwal and V. K. Gupta, Removal of methylene blue by silver nanoparticles loaded on activated carbon by an ultrasound-assisted device: optimisation by experimental design methodology, Res. Che. Intermed, Springer, (2015) 12, 110-152.

[42] D. Nayeri, and S. A. Mousavi, Dye removal from water and wastewater by nanosized metal oxides-modified activated carbon: a review in recent research, Journal of Environmental health science and engineering, (2020) 18, 1671-1689.

[43] Q. Chen, Z. Tang, H. Li, M. Wu, Q. Zhao, and B. Pan. An electron-scale comparative study on the adsorption of six divalent heavy metal cations on MnFe2O4@ CAC hybrid: experimental and DFT investigations. Chemical Engineering Journal. 2020;381:122656

[44] M. Singh, H. S. Dosanjh, and H. Singh. Surface modified spinel cobalt ferrite nanoparticles for cationic dye removal: kinetics and thermodynamics studies. Journal of Water Process Eng. 2016;11:152–161.

[45] P. Saini, R. Sharma, R. P. Pant, and R. K. Kotnala. Ultrafast adsorption of organic dyes by activated-carbon@ Fe_3O_4 nanoscale composites: An effective solution for water purification. Indian Journal for Pure Applied Physics. (2018) 56, 187–195.

[46] Y. C. Chang, and D. H. Chen, Catalytic reduction of 4-nitrophenol by magnetically recoverable Au nanocatalyst, Journal of Hazardous Materials, (2009) 165, 664-669.

[47] T. Robinson, G. McMullan, R. Marchant, and P. Nigam, Remediation of dyes in textile effluent: a critical review on current treatment technologies with a proposal alternative, Journal of Bioresource Technology, (2001) 77, 247-225.

[48] W. Wu, Z. Wu, T. Yu, C. Jiang and W. Kim, Recent progress on magnetic iron oxide nanoparticles: synthesis, surface functional strategies and biomedical applications. National Institute for Materials Science, Science and Technology of Advanced Materials, (2015) 16, 023501-023544.

[49] M. A Gatoo, S. Naseem, M. Y. Arfat, A. Mohmood Dar, K. Qasim and A. Zubair, Physicochemical properties of nanomaterials: Implication in associated toxic manifestations. BioMed Research International, (2014), 1-8.

[50] Y. Ono, T. Rachi, T. Okuda, M. Yokouchi, Y. Kamimoto, A. Nakajima, and K. Okada. Kinetics study for photodegradation of methylene blue by titanium dioxide powder prepared by selective leaching method, Journal of Physics and Chemistry of Solids, (2012) 73, 343-349.

[51] R. begum, J. Najeeb, A. Sattar, K. Naseem, A. Irfan. A. G. Al-Sehemi and Z. H. Farooqi, chemical reduction of methylene blue in the presence of nanocatalysts: a critical review, Reviews in Chemical Engineering., (2019) 36, 6.

[52] X. Chen, Z. Zheng, X. Ke, E. Jaatinen, T. Xie, D. Wang, C. Guo, J. Zhao and H. Zhu, Supported silver nanoparticles as photocatalysts under ultraviolet and visible light irradiation, Green Chemistry, (2010) 12 (3), 414-419.

[53] M. Shamsipur, and H. R. Rajabi, O. Khani, Pure and Fe^{3+} -doped ZnS quantum dots as novel and sufficient nanophotocatalyst: synthesis, characterization and use for decolorization of Victoria blue R, Material Science in Semiconductor Processing, (2013) 16, 1154-1161.

[54] N. K. R. Bogireddy, H. A. K. Kumar, and B. K. Mandal, Biofabricated silver nanoparticles as green catalyst in the degradation of different textile dyes, Journal of Environmental Chemical Engineering, (2016) 4, 56-64.

[55] W. H. Perkin, On Mauve or Aniline-Purple, Proceedings of the Royal Society of London, Life, Earth and Health Sciences, (1963) 12, 713-715.

[56] S. Singh, V. C. Srivastava, and I. D. Mall, Mechanism of dye degradation during electrochemical treatment, Journal of Physical Chemistry, (2013) C117 (29), 15229-15240.

[57] G. Singh, S. K. Dwivedi, J. Mishra, Role of Fungal Enzymes in the removal of Azo Dyes, Microbial Enzymes: Roles and Application in Industries (2020) 11, 231-257

[58] Y. M. Ju, S. G. Yang, Y. C. Ding, C. Sun, A. Q. Zhang, and L. H. Wang, Microwave-assisted rapid photocatalytic degradation of malachite green in TiO_2 suspensions: mechanism and pathways, Journal of Physical Chemistry, (2008) A 112, 11172-11177.

[59] A. R. Khaskheli, S. Naz, R. A. Soomro, S. Ozel, A. Aljabour, N. H. Kalwar, A. W. Mahesar, I. H. Patir, and M. Ersoz, L-lysine derived nickel nanoparticles for reductive degradation of organic dyes, Advanced Materials Letters, (2016) 7 (8), 616-621.

[60] G. Wilkinson, R. D. Gillard, and J. A. McCleverty, Comprehensive Co-ordination Chemistry. The Synthesis, Reactions, Properties and Applications of Coordination Compounds. V.3. Main Group and Early Transition Elements, Pergamon Press, Oxford, UK, (1987) 19 (1).

[61] R. A. Soomro, A. Nafady, A. T. H. Sirajajuddin, N. H. Sherazi, M. R Kalwar, and K. R. Hallam, Catalytic reductive degradation of methyl orange using air resilient copper nanostructures, Journal of Nanomater, (2015), 136164, 1-11.

[62] F. Wang, M. Shao, L. Cheng, D. Chen, Y. Fu, and D. D. D. Ma, Si/Pd nanostructure with high catalytic activity in degradation of eosin Y. Materials Research Bulletin, (2009) 44, 126-129.

[63] D. Wan, W. Li, G. Wang, K. Chen, L. Lu, and Q. Hu, Adsorption and heterogeneous degradation of rhodamine B on the surface of magnetic bentonite material. Application of Surface Science (2015) 349, 988-996.

[64] A. Sabarudin, R. Wahid, F. C. Nalle, R. A. Shobirin, and D. J. D. H. Santjojo, Designed structure and magnetic characteristic studies of magnetic iron oxide (Fe_3O_4) nanoparticles coated by polyvinyl alcohol and polyvinyl alcohol-linked with glutaraldehyde, Rasayan Journal of Chemistry, (2017) 10 (4), 1261-1270.

Chapter 2: Synthesis and characterisation of SPIONs and magnetic Au phosphine nanoparticles

2.1 Introduction

In this chapter, the synthesis and characterization of the naked superparamagnetic iron oxide nanoparticles (SPIONs), as well as magnetic gold nanoparticles (AuNPs) stabilized with phosphine ligands as catalysts. The synthesis of naked SPIONs were carried out by using the most commonly used co-precipitation method.[1] The co-precipitation method is considered to be the best method for the synthesis of naked magnetite (Fe_3O_4) nanoparticles used for adsorption of metal ions from solutions. Total iron concentration used were for Fe^{2+} was at 0.0275M and Fe^{3+} was at 0.0127M. The colloidal synthesis method is considered to be the most versatile and simplistic manner to produce nanoparticles.[2] This synthesis method normally involves the suspension of a suitable metal precursor together with a surfactant. The metal precursor is then reduced using the appropriate reducing agent to make the desired nanoparticles. However, using this process leads to nanoparticles that have a wide particle size distribution. This has therefore incited more research into the optimisation of the surface surfactant in order to obtain narrow particle size distributions.[3] Therefore, the magnetic AuNPs stabilized catalysts were synthesized by a direct method,[4] and two phosphine chain ligands were used to stabilize the gold-coated nanoparticles to prevent them from agglomeration, and also to tailor the solubility of the nanomaterials. The SPIONs, as well as the stabilized AuNPs, were characterized using Fourier-transform infrared spectroscopy (FT-IR), the powder X-Ray diffraction (PXRD), ultraviolet-visible (UV-Vis) spectroscopy and high-resolution transmission electron microscopy (HRTEM).

As mentioned in chapter 1, catalysis is a very important key component of chemistry. The challenges facing many chemists nowadays is the design and making use of greener and environmentally benign catalysts.[5] Iron oxides exist in many forms in nature. Magnetite (Fe_3O_4), maghemite (γ-Fe_2O_3), and hematite (α-Fe_2O_3) are the most common. In recent years, the synthesis and utilization of iron oxide nanomaterials (NMs) with novel properties and functions have been widely studied, due to their size in nano-range, high surface area to volume ratios and superparamagnetism. There are many scientific disciplines that have a wide interest in magnetite (Fe_3O_4) due to its ability to have superparamagnetic properties.[6] Fe_3O_4 is a black ferromagnetic mineral that consists of an inverse spinel crystal structure. This spinel crystal structure contains 32 O^{2-} anions, 16 Fe^{3+} and 8 Fe^{2+} cations, respectively. Fe_3O_4 differs from most other iron oxides, like maghemite and hematite, in that it contains both di-valent and tri-valent iron ions. There has

been a various studies developed for magnetite nanoparticles that are continuing all the time. These continuous studies are done for the optimisation processes methods to obtain the preferred properties for their application.[7] The modification of magnetite nanoparticles is mostly achieved by controlling their particle size, crystallite size, and shape, is one of the main objectives within the chemistry fields to explore their full potential in different applications.[8] The SPIONs will be reported as **EJL1** which will subsequently be modified to form gold-coated magnetic nanoparticles and stabilized with phosphine ligands, as catalysts to be used in the reduction and removal of methylene blue. These gold-coated magnetic nanoparticles, which are stabilized with phosphine ligands, will be reported as **EJL2** to **EJL19**. These catalysts will also contain different metal loadings and the effect therefore will be investigated. Subsequently the effect of the reducing agents and the different phosphine ligands used will be investigated.

2.2 Results and discussion

2.2.1 Synthesis of uncapped superparamagnetic iron oxide nanoparticles (SPIONs)

The metal precursor of $FeCl_2.4H_2O$ (Fe^{2+}) and $FeCl_3.6H_2O$ (Fe^{3+}) were dissolved to form a bright yellow solution. On addition of NH_4OH solution, the colour of the solution changed steadily from the initial bright yellow to brown, then dark brown, and ultimately turned to a very black colour, refer to **Figure 2.1a&b**. The latter colour was an indication of the formation of magnetite (Fe_3O_4). The precipitation of the metal precursor Fe^{3+} and Fe^{2+} usually occurs at a pH range of 3-9 to form Fe(III) and Fe(II) hydroxides, respectively. Moreover, the iron (III) hydroxide was decayed into another compound of FeOOH. The then formed FeOOH reacted with the $Fe(OH)_2$ to produce the Fe_3O_4. The use of the low ratios of Fe^{2+}: Fe^{3+} at 1:2 was aimed to be able to achieve a high yield of magnetite and to restrain the oxidation from Fe^{2+} to Fe^{3+}.[9]

(a)

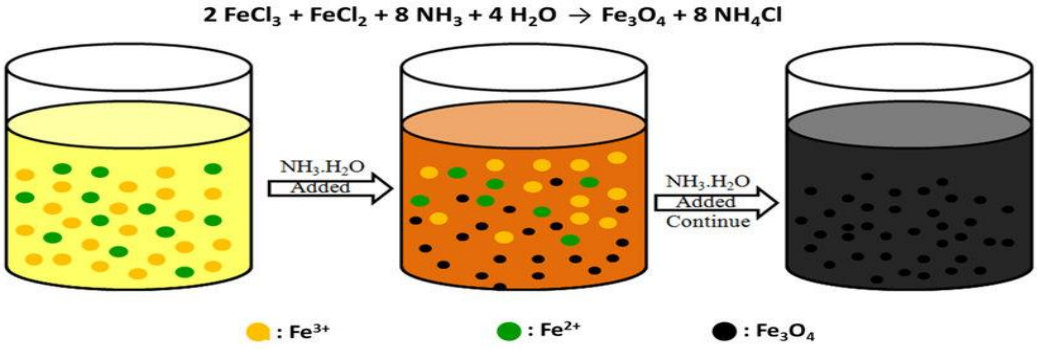

(b)

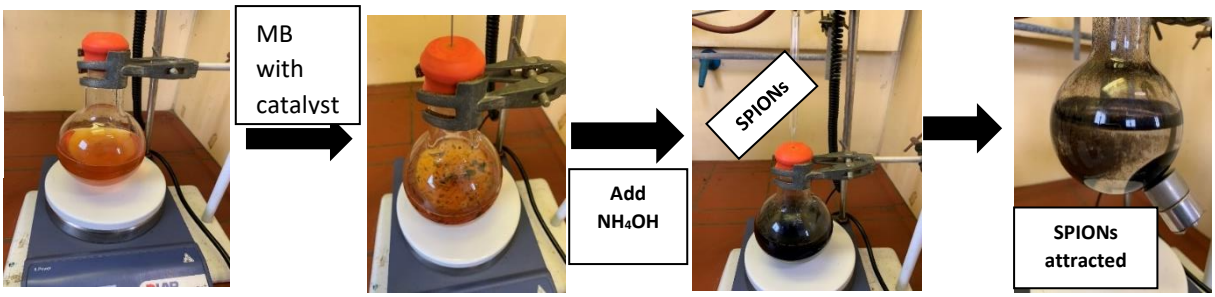

Figure 2.1b: The synthesis of the naked SPIONs by co-precipitation performed in the lab.

The co-precipitation stoichiometric reaction (**equation 1**) for the synthesis of magnetite nanoparticles is as indicated:[11]

$$Fe^{2+}{}_{(aq)} + 2\,Fe^{3+}{}_{(aq)} + 8\,OH^{-}{}_{(aq)} \rightarrow Fe_3O_{4(s)} + 4\,H_2O_{(l)} \qquad (1)$$

The complete precipitation occurs at pH levels between 9 to 14. These should be monitored before the magnetite is stored. This pH should be brought to pH of 7 by washing the magnetite with excess deionized water. Also, the reaction should be performed under non-oxidising environment to avoid oxidation of the magnetite nanoparticles. Kim Ahn and co-workers, expanded on the mechanistic formation pathway of Fe_3O_4 nanoparticles by the co-precipitation method. What they determined as seen from the **equations 2-5**, was that the formation of magnetite nanoparticles is a development resulting from phase transformations best described using the equations:[12]

$$Fe^{3+} + 3\,OH^{-} \rightarrow Fe(OH)_3 \qquad (2)$$

$$Fe(OH)_3 \rightarrow FeOOH + H_2O \qquad (3)$$

$$Fe^{2+} + 2\,OH^{-} \rightarrow Fe(OH)_2 \qquad (4)$$

$$FeOOH + Fe(OH)_2 \rightarrow Fe_3O_4 \downarrow + 2\,H_2 \qquad (5)$$

2.2.2 Characterization of uncapped superparamagnetic iron oxide nanoparticles (SPIONs)

The SPIONs were examined for their structural, morphological and magnetic characteristics by making use of Fourier-transform infrared spectroscopy (FT-IR), ultraviolet-visible (UV-Vis) spectroscopy, powder X-Ray diffraction (PXRD), and high-resolution transmission electron microscopy (HRTEM).

2.2.2.1 Infrared spectroscopy (SPIONs)

The SPIONs as prepared was characterized using IR spectroscopy, as shown in **Figure 2.2**. The SPIONs was diluted with KBr, grounded using a mortar and pestle, into fine powder which was pressed into a KBr-pellet. Magnetite (SPIONs-**EJL1**) is a blended cubic oxide that contains $^{2}/_{3}$ Fe^{3+} and $^{1}/_{3}$ Fe^{2+} cations, respectively we expect these peaks for each kind of site. Therefore, the absorption intensity at λ = 583 cm^{-1}, can be assigned to Fe-O stretching vibration modes of the tetrahedral and octahedral sites. Moreover, the bands intensity at λ = 2360 cm^{-1} can be assigned to the stretching vibration of CO_2 in the atmosphere during analysis. The spectra also display additional intensity bands at round λ = 1403 cm^{-1} and 1134 cm^{-1}, and these bands can be attributed to the unreacted FeOOH or $Fe(OH)_2$ species, which from the equations mentioned above is seen as the intermediates in the synthesis process of the formation of magnetite nanoparticles. The absorption peak at 3447 cm^{-1} is observed and can be originated by the hydroxyl functionality (OH) present in water.

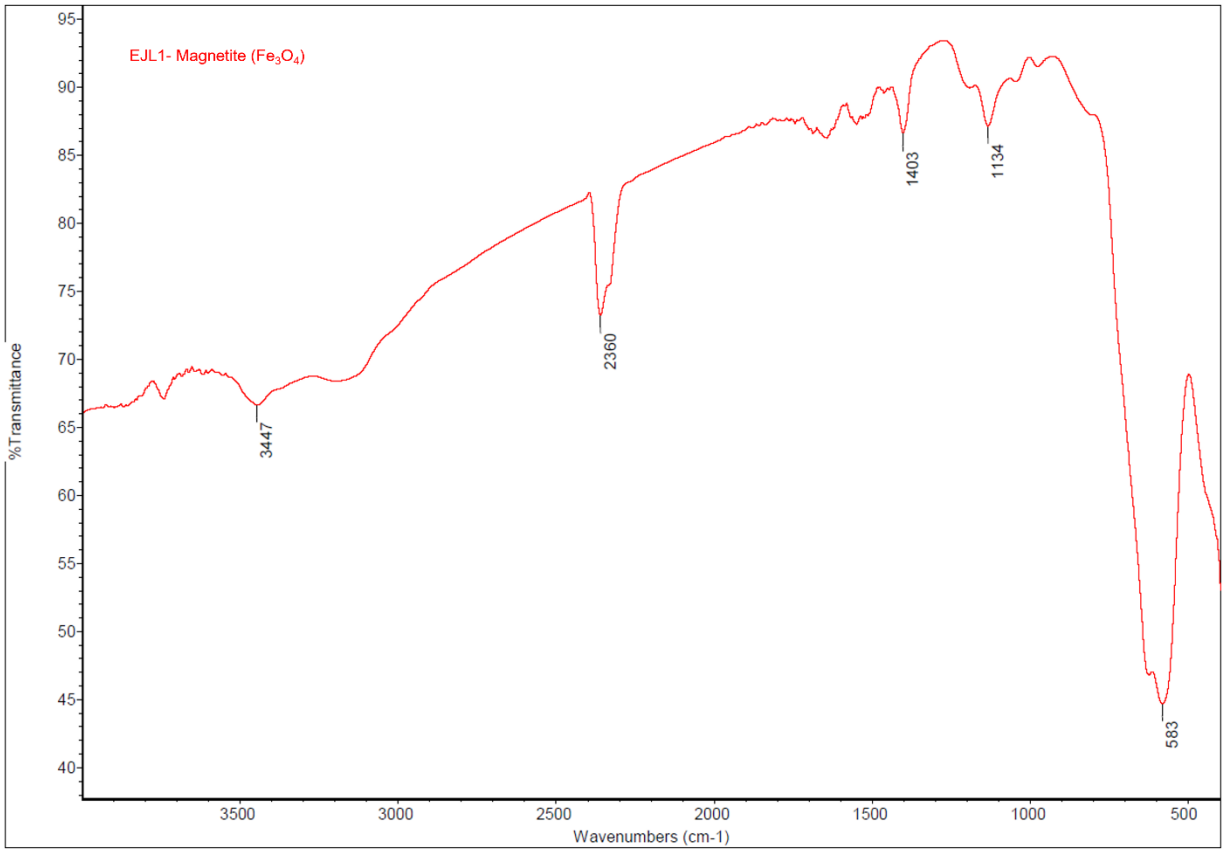

Figure 2.2: The FT-IR spectra of the naked magnetic iron oxide nanoparticles.

2.2.2.2 Ultraviolet visible spectroscopy (SPIONs)

This technique was used to confirm nanoparticle formation by detection of the surface plasma resonance (SPR) band. The SPIONs as prepared was characterized using UV-Vis spectroscopy, as shown in **Figure 2.3**. The absorbance of the SPIONs showed a very visible SPR peak, λ = 390 nm. This is a characteristic of magnetite nanoparticles.[13] No other peaks were observed in the spectrum, indicating the high purity of the synthesized magnetite by co-precipitation method.

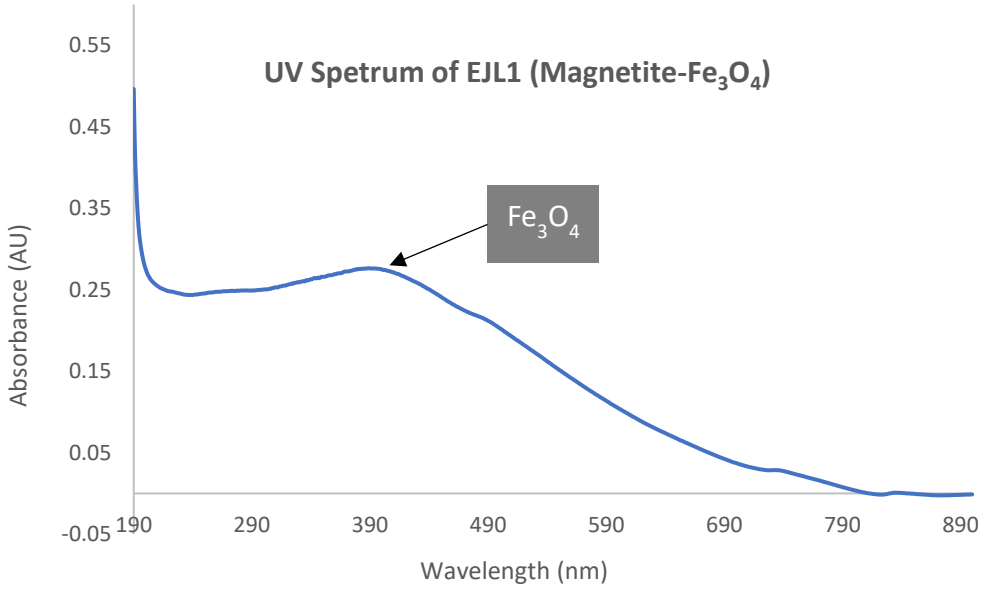

Figure 2.3: UV-Vis absorption spectra of Fe_3O_4 nanoparticles.

2.2.2.3 High resolution transmission electron microscopy (SPIONs)

This technique was performed to determine the morphology (shape), the average particle size, and particle size distribution of the unmodified SPIONs (**EJL1**). The three TEM images taken at 50 nm, 20 nm and 10 nm shows a spherical morphology agglomerated and polydisperse nanoparticles. The size distribution of the particles on average was found to be 18.7 ± 5.6 nm. Refer to **Figure 2.4.**

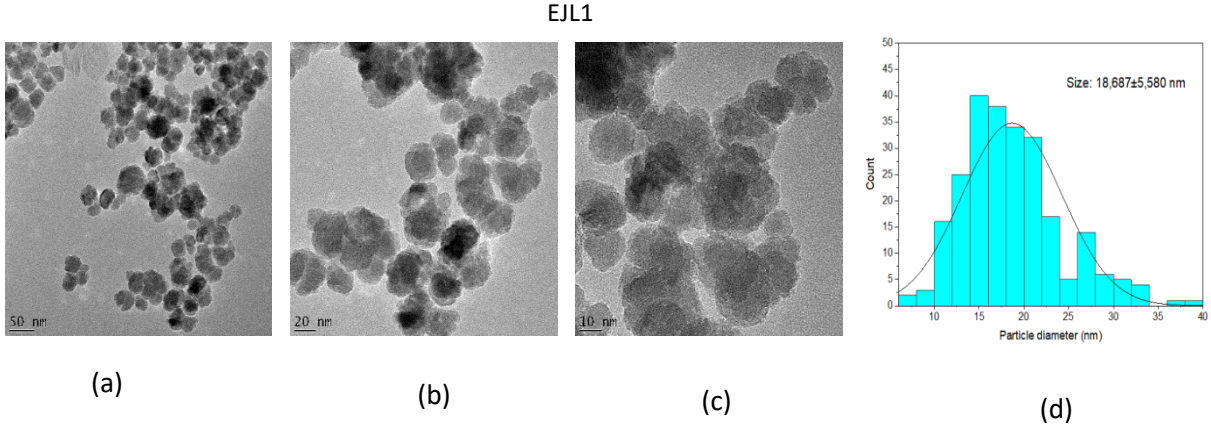

Figure 2.4: HRTEM images of EJL1 with the particle size histograms of the unmodified SPIONs.

2.2.2.4 Powder X-ray diffraction (SPIONs)

This technique was used to determine the solid phases present on the magnetite. This also examined the crystallinity and phase purity. **Figure 2.5** shows diffractograms of naked SPIONs. These reactions were carried out at 25 °C. The diffractogram of magnetite shows the corresponding diffraction peaks that have miller indices (*hkl*) values at 220, 311, 400, 422, 333, 440 and 622. This diffraction pattern does match well with those specifically of standard magnetite samples. This is as per JCPDS cards No. 00-011-0614 with a cubic spine structure.

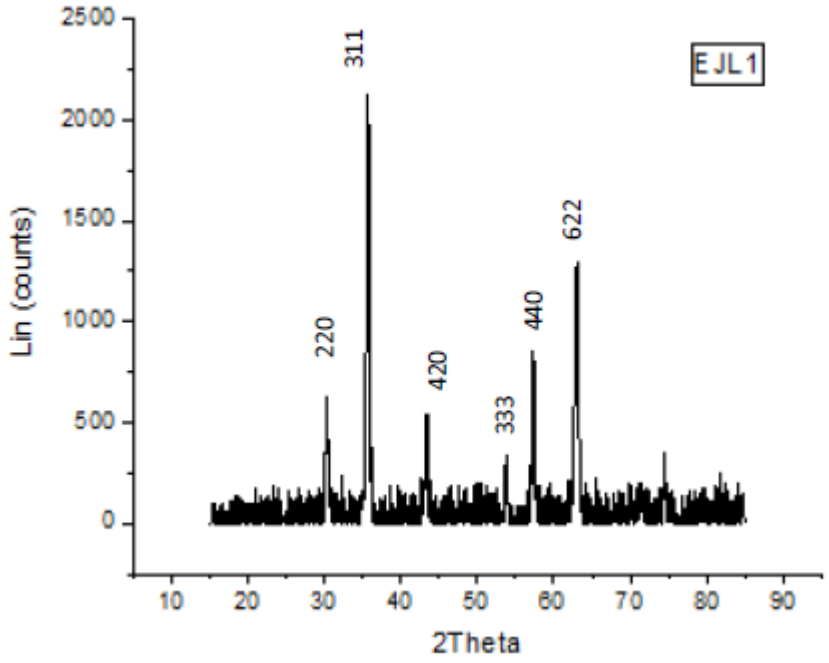

Figure 2.5: Powder X-Ray Diffraction (PXRD) analysis of the unmodified SPIONs.

2.2.3 Synthesis of gold coated SPIONs

SPIONs show a hydrophilic character because of the presence of hydroxyl groups on their surface. This creates hydrophilic interaction between the particles triggering their agglomeration. Once the magnetite had been prepared, the next step was the coat the SPIONs using gold (III) chloride trihydrate ($HAuCl_4.3H_2O$). The gold was reduced onto the magnetite surface using two different reducing agents, either sodium borohydride ($NaBH_4$) or sodium citrate ($Na_3C_6H_5O_7$). There were 6 catalysts synthesized (**EJL2-EJL7**), refer to **Table 2.1**, that were coated with gold on SPIONs.

These catalysts were varied in their metal loadings with different ratios of Fe_3O_4:Au in a 1:10, 1:50 and 1:100 fashion or respectively 1:0.1, 1:0.05 and 1:0.01. These metal loadings were achieved by keeping the magnetite (Fe_3O_4) metal concentration constant whilst varying the gold metal concentration to make up the metal loading ratios.

Table 2.1: List of gold coated AuNPs with their metal loadings

SAMPLE CODE	RATIO OF Fe_3O_4: Au	REDUCING AGENT
EJL1	Magnetite (SPION)	
EJL2	10:1	$NaBH_4$
EJL3	50:1	$NaBH_4$
EJL4	100:1	$NaBH_4$
EJL5	10:1	$Na_3C_6H_5O_7$
EJL6	50:1	$Na_3C_6H_5O_7$
EJL7	100:1	$Na_3C_6H_5O_7$

As mentioned in chapter 1, the synthesis of magnetic nanoparticles coated with AuNPs, where the magnetic nanoparticle acted as both template and reductant ($NaBH_4$ or $Na_3C_6H_5O_7$). The particle size of the AuNPs varied with increase in reaction time.[14] There have been several reports which have describe the synthesis of the various nanostructures such as spherical, hexagonal, rod like, cubic, planar, oval like and branched nanoparticles, to mention but a few, refer to **Figure 2.6**.[15] The various structural shapes are attained by regulating the different experimental parameters such as the temperature, pH, concentration, nanoparticle precursor and time, as already known.[16] Hexagonal- and pentagonal gold coated nanoparticles are considered to be more catalytically active compared to other shapes because of the presence of more reactive qualities, like surface and sites.[17]

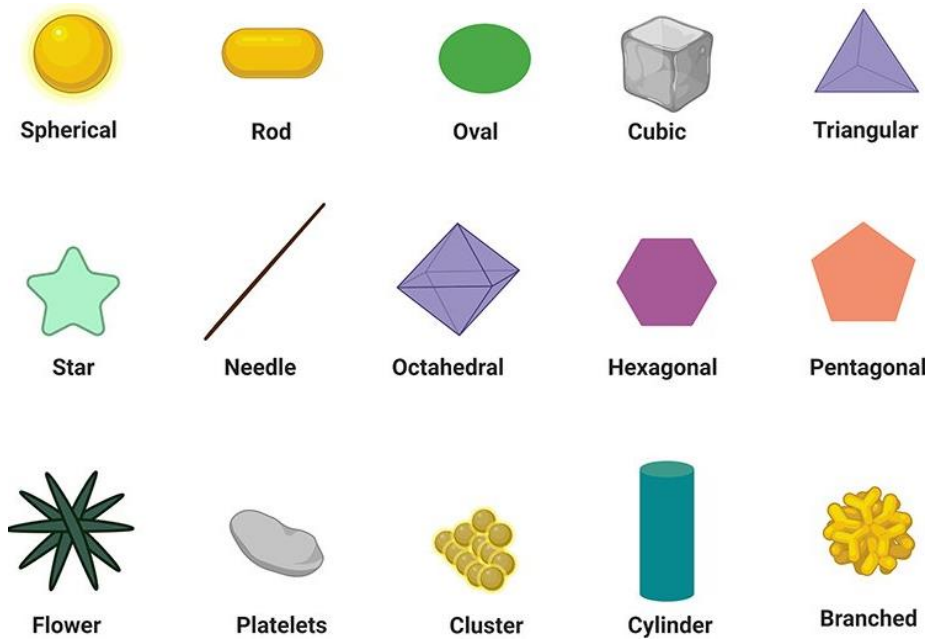

Figure 2.6: Various shapes of nanoparticles.[14]

There are two predominant ways for coating gold onto the nanoparticle, being direct and indirect gold coated. For this study the direct gold coating method was conducted.

2.2.4 Characterization of gold coated SPIONs

The gold coated SPIONs, also referred to as gold-coated nanoparticles (AuNPs) were considered for their structural, morphological as well as their magnetic characteristics using the following analytical techniques, the ultraviolet-visible (UV-Vis) spectroscopy, Fourier-transform infrared spectroscopy (FT-IR), powder X-Ray diffraction (PXRD), and high-resolution transmission electron microscopy (HRTEM).

2.2.4.1 Infrared spectroscopy (AuNPs)

The Fourier-transform infrared (FT-IR) spectra of unmodified as well as modified SPIONs were taken from the range 400 – 4000 cm^{-1} has been shown in **Figure 2.7**, in which the values of importance bands intensities were displayed. The unmodified naked SPIONs (**EJL1**) showed a broad band around 3445 cm^{-1}, indicative of the presence of -OH functionalities on the nanoparticles surface, while a strong frequency around 584 cm^{-1} represents a characteristic

frequency of Fe-O related to the magnetite. The vibrational frequency at 1627 cm^{-1} observed in the FT-IR spectra of sodium citrate treated magnetite nanoparticles (**EJL6**), which are characteristic of the carboxylate functional group, whilst the medium intensity frequency at 1402 cm^{-1} represents the -CH vibration. These results confirmed the attachment of sodium citrate on the magnetite nanoparticle surface. The spectrum of the sodium borohydride (**EJL3**) has a frequency at 834 cm^{-1}, indicative of the wagging frequency of BH_4. Whilst the medium intensity frequency at 1418 cm^{-1} represents the -CH vibration. These results confirmed the attachment of sodium borohydride on the magnetite nanoparticle surface. The metal ratio of the 1:50 samples were used for the FT-IR representative spectra.

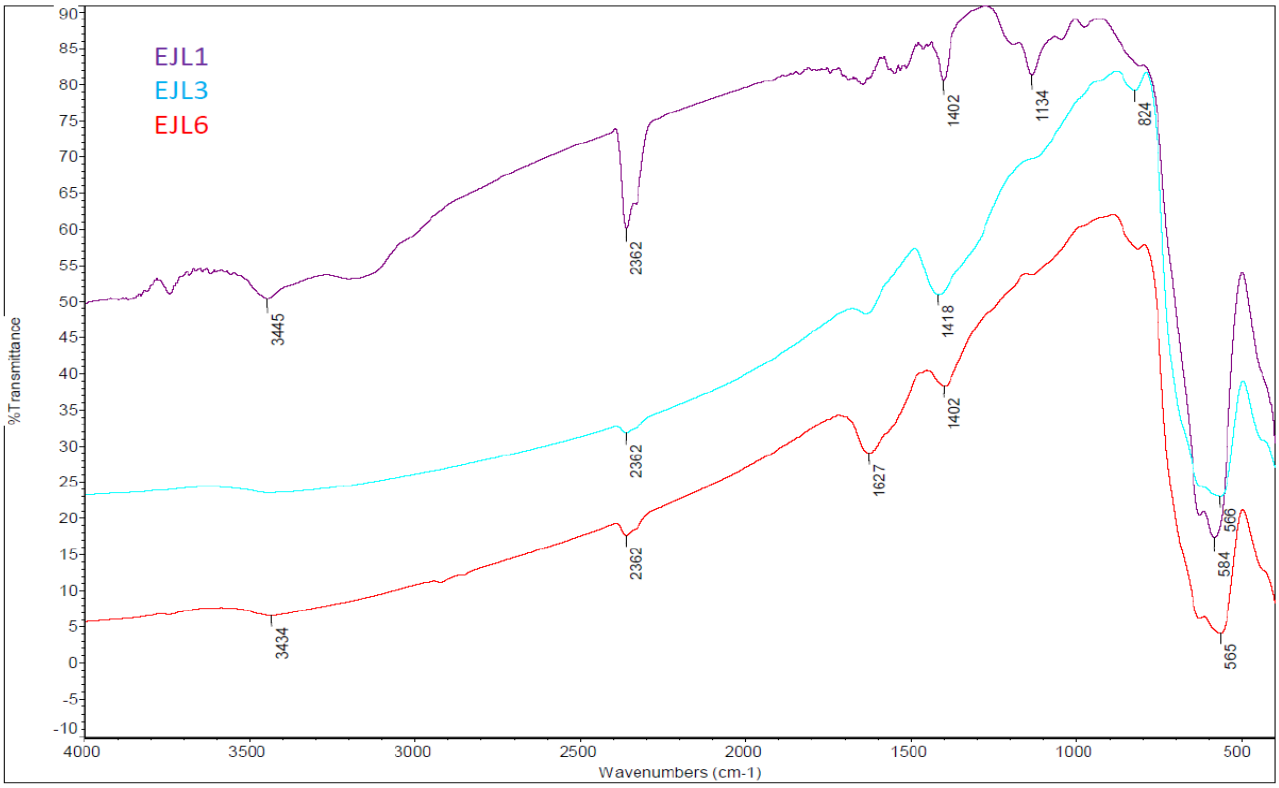

Figure 2.7: Infra-red spectra of gold coated nanoparticles (AuNPs).

2.2.4.2 Ultraviolet-visible spectroscopy (AuNPs)

Figure 2.8 represents UV-vis absorption spectra of the SPIONs with the AuNPs catalysts. This AuNPs were modified by using the reducing agents on the SPIONs to get the direct coating of the gold on the surface. There are increased absorbance maxima corresponding to the SPR bands in the gold coated SPIONs, compared to the naked SPIONs that only showed a singular visible SPR

peak, λ = 390 nm. The SPR peak for the AuNPs that was reduced using $NaBH_4$ showed absorbance peaks at λ = 260 nm and 380 nm, respectively. Also, there are two SPR peaks observed for the AuNPs that were reduced using $Na_3C_6H_5O_7$, with absorbance peaks at λ = 290 and 350 nm. These confirm that there was a successful reduction of the gold onto the SPIONs surface. Resulting in gold-coated SPIONs.

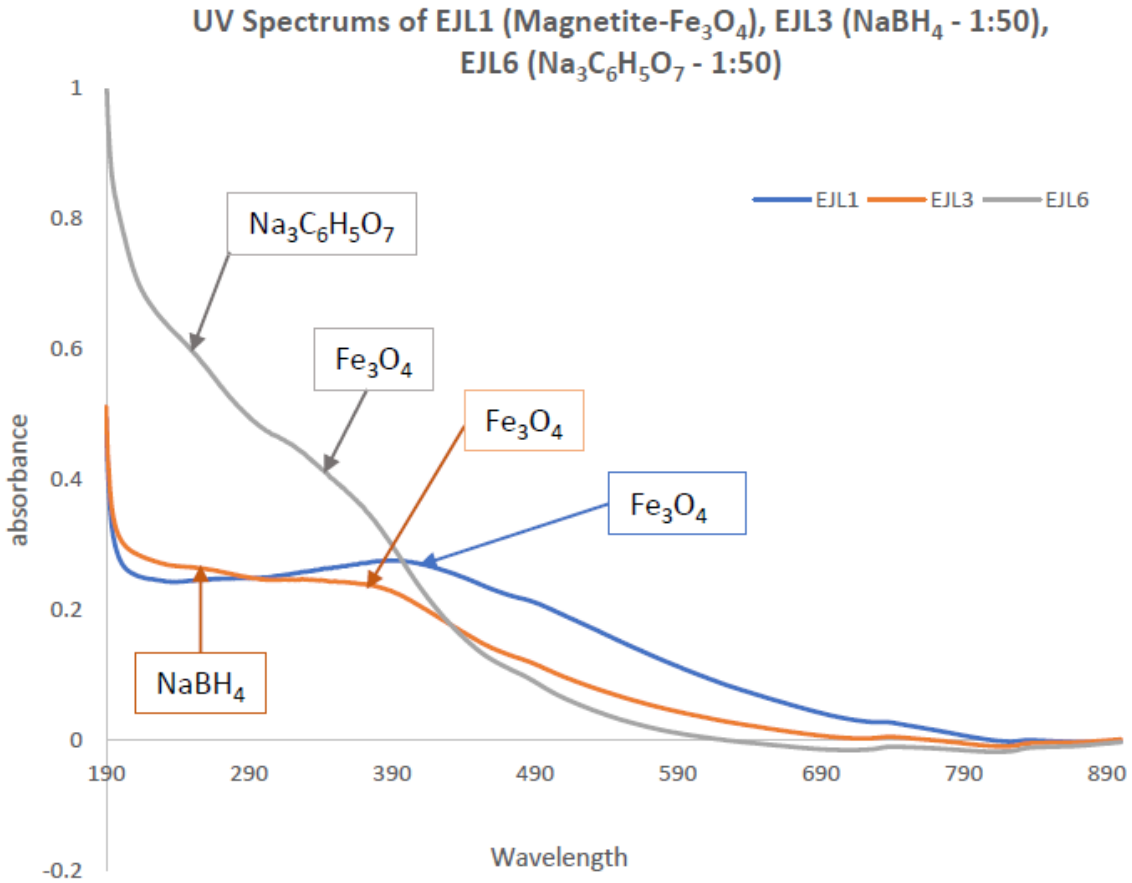

Figure 2.8. UV-vis spectra of the SPIONs and AuNPs.

2.2.4.3 High-resolution transmission electron microscopy (AuNPs)

The particle average size and size distributions of the AuNPs were investigated by means of HRTEM, see **Figure 2.9**. These particles are normally spherical, agglomerated and polydisperse. Their particle average sizes of **EJL2**, **EJL3** and **EJL4** are 22.53 ± 6.0 nm, 18.73 ± 6.0 nm and 27.30 ± 10.8 nm, respectively. These were the AuNPs that were reduced using the $NaBH_4$ reducing agent. The average particle sizes of **EJL5**, **EJL6** and **EJL7** are 16.87 ± 4.2 nm, 19.48 ± 5.7 nm, 17.12 ± 4.7 nm. These were the AuNPs that were reduced using the $Na_3C_6H_5O_7$ reducing agent. Particle

sizes are summarised in **Table 2.2**. It can be seen that the particle size dimensions for the AuNPs catalysts reduced by $Na_3C_6H_5O_7$ reducing agent are much smaller than those reduced with $NaBH_4$ reducing agent. This is due to the fact that $Na_3C_6H_5O_7$ is known as to have both properties of being a reducing agent as well as a stabilizer. Thus, dual property that $Na_3C_6H_5O_7$ resulted in size control of the nanoparticles.

The most commonly used method for the synthesis of gold nanoparticles involves the reduction of tetrachloroauric acid ($HAuCl_4$) by small amounts of citric acid. This method was introduced by Turkevich *et al.* in 1951 and further refined by Frens in 1973.[18] In this method, hot tetrachloroauric acid reacts with a small amount of sodium citrate solution. The citrate ions act as both a reducing agent, and a capping agent. Reduction occurs according to the equations (6) and (7):

$$Na_3C_6H_5O_7 + 3\,H^+ \rightarrow C_6H_8O_7 + 3\,Na^+ \quad (6)$$

$$2\,HAuCl_4 + 3\,C_6H_8O_7 \rightarrow 2\,Au + 3\,C_5H_6O_5 + 8\,HCl + 3\,CO_2 \quad (7)$$

In the traditional Frens' method, small amount of sodium citrate to tetrachloroauric ($HAuCl_4$) acid is used without particular attention to pH. The typical conclusion observed is as follows, the particle size decreases as the ratio of citrate to tetrachloroauric acid increases. This is consistent with the mechanism where part of the sodium citrate is used to reduce Au^{3+} to Au^0. Making the remaining sodium citrate ions, i.e., a capping agent, to be available for stabilising the nanoparticles. The nanoparticles keep on aggregating until the total surface area of all particles becomes small enough to be covered by the existing citrate ions. Hence, higher concentrations of sodium citrate will result in less particle aggregation. Then the final size of the particles decreases.[19]

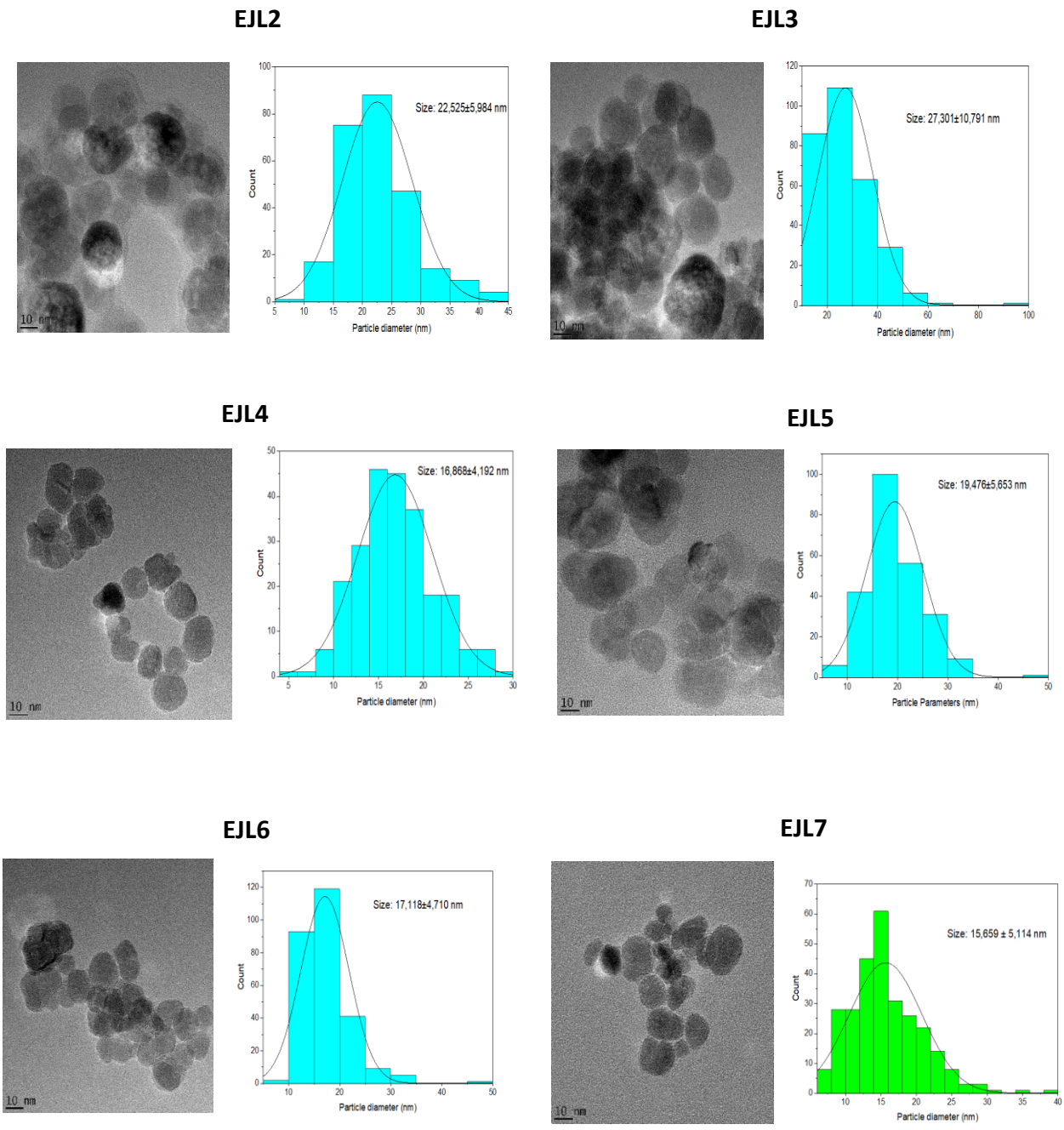

Figure 2.9: HRTEM images, particle size histograms of the gold coated SPIONs. EJL7, green colour has no significant at all.

Table 2.2: Summary list of gold coated AuNPs particle size distribution.

SAMPLE CODE	RATIO OF Fe_3O_4: Au	REDUCING AGENT	PARTICLE SIZE (NM)
EJL2	10:1	$NaBH_4$	22.53 ± 6.0
EJL3	50:1	$NaBH_4$	18.73 ± 6.0
EJL4	100:1	$NaBH_4$	27.30 ± 10.8
EJL5	10:1	$Na_3C_6H_5O_7$	16.87 ± 4.2
EJL6	50:1	$Na_3C_6H_5O_7$	19.48 ± 5.7
EJL7	100:1	$Na_3C_6H_5O_7$	17.12 ± 4.7

2.2.4.4 Powder X-Ray diffraction (SPIONs)

Figure 2.10 shows the PRXD patterns for the gold coated nanoparticles modified iron oxide by (a) sodium citrate and (b) sodium borohydride. Six characteristics diffraction peaks for Fe_3O_4 with the miller indices (*hkl*) values: (220), (311), (400), (422), (333), (440) and (622), as previously seen on the naked SPIONs PXRD shown in **Figure 2.5** are also visible on these PXRD patterns. Additional peaks associated with gold/syn are highlighted with a gold-stars on PXRD pattern, (**Figure 2.10)**. These show that the resultant nanoparticles were with a spinal structure. The result also revealed that the coating process did not result in the phase change of Fe_3O_4. The strong and sharp peaks proved that the samples were well crystallized.[20]

(a)

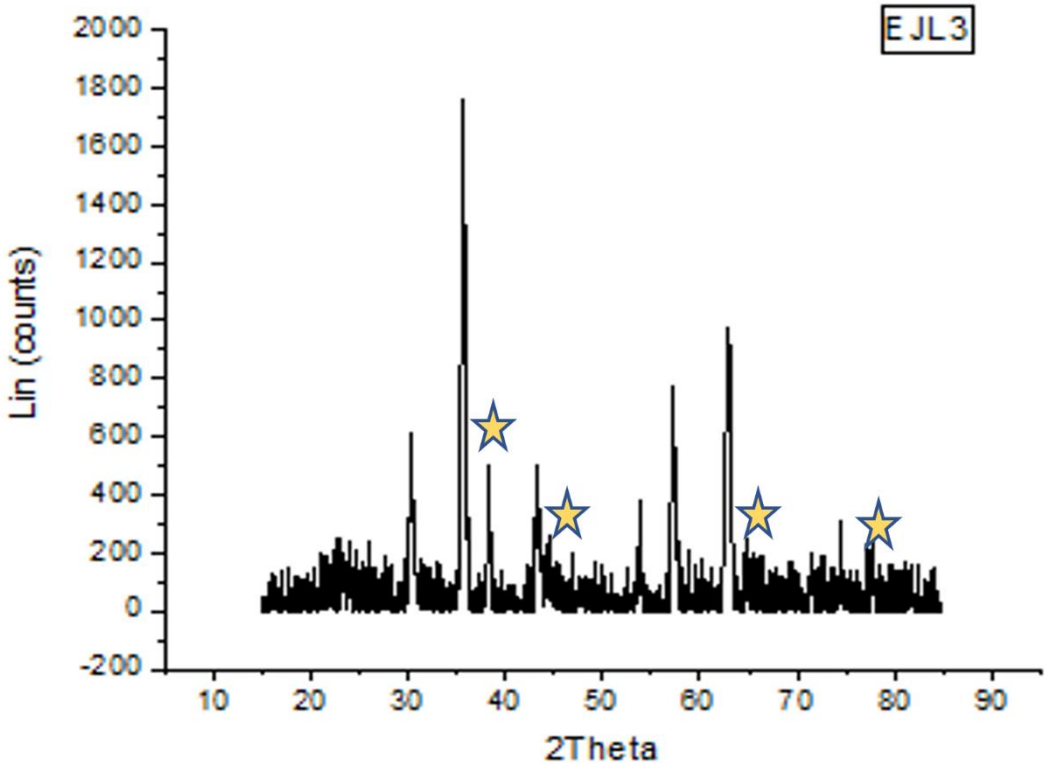

(b)

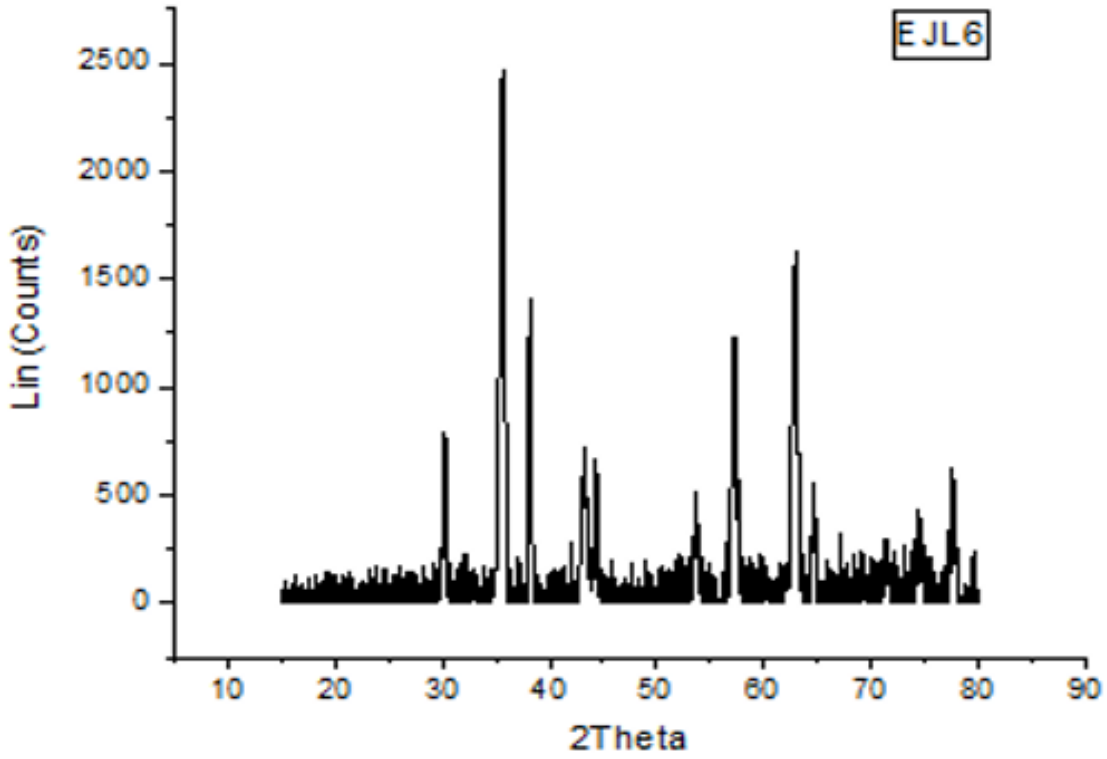

Figure 2.10: PXRD patterns of the AuNPs modified with (a) $NaBH_4$ and (b) $Na_3C_6H_5O_7$ iron oxide nanoparticles

2.2.5 Stabilization of gold coated SPIONs

It is known that the SPIONs do aggregate and agglomerate very easily. This is due to the short-range van der Waals forces between the adjacent particles. This leads to limiting their application with their very problematic hydrophilic character that causes agglomeration. When particles are dissolved in liquid media, they collide with one another. The stability of suspension depends on the interactions between two particles. The attractive forces between particles result in their aggregation and the suspension is not stable. To overcome these attractive interactions and improve stability, equally short-range repulsive forces are required.[21] For this purpose, magnetic nanoparticles have been coated with several materials, including chitosan, starch, poly(ethylene glycol) and poly(vinyl alcohol).[22] Therefore, modifying iron oxide nanoparticles have attracted attention because of the ease of preparation resulting in well-dispersed biocompatible nanoparticles.[23] Stabilization of these gold-coated nanoparticles with two different phosphine ligands (PTA and PPh_3), was done to avoid agglomeration and possibly improve their activity. A set of 12 (**EJL8 to EJL19**) stabilized AuNPs were performed as in (see **Table 2.3).** They consisted

of a set of three different metal loadings, two different reducing agents being used ($NaBH_4$ and $Na_3C_6H_5O_7$) as well as two different phosphine ligand stabilizers.

Table 2.3: List of stabilized gold coated SPIONs with their metal loadings

SAMPLE CODE	RATIO OF Fe_3O_4: Au	REDUCING AGENT	STABILIZER LIGANDS
EJL8	10:1	$NaBH_4$	PTA
EJL9	50:1	$NaBH_4$	PTA
EJL10	100:1	$NaBH_4$	PTA
EJL11	10:1	$Na_3C_6H_5O_7$	PTA
EJL12	50:1	$Na_3C_6H_5O_7$	PTA
EJL13	100:1	$Na_3C_6H_5O_7$	PTA
EJL14	10:1	$Na_3C_6H_5O_7$	PPh_3
EJL15	50:1	$Na_3C_6H_5O_7$	PPh_3
EJL16	100:1	$Na_3C_6H_5O_7$	PPh_3
EJL17	10:1	$NaBH_4$	PPh_3
EJL18	50:1	$NaBH_4$	PPh_3
EJL19	100:1	$NaBH_4$	PPh_3

2.2.6 Characterization of stabilized gold coated SPIONs

The stabilized gold coated SPIONs, were studied for their structural, morphological, and magnetic characteristics using the following analytical techniques, the Fourier-transform infrared spectroscopy (FT-IR), inductively coupled plasma spectroscopy (ICP), high resolution transmission electron microscopy (HRTEM) and ultraviolet-visible (UV-Vis) spectroscopy.

2.2.6.1 Infrared spectroscopy

The FT-IR spectra of unmodified as well as modified stabilized gold coated SPIONs were taken from the range 400 – 4000 cm^{-1} have been represented in **Figure 2.11**, in which the values of important frequencies were highlighted. The unmodified naked SPIONs (**EJL1**), as well as the stabilized gold coated magnetite, showed a broad band around 3440 - 3447 cm^{-1}, indicative of the presence of -OH functionalities on the nanoparticles surface, while a strong frequency around 583 - 630 cm^{-1} representative of the Fe-O vibration related to the magnetite present in all the catalysts. There are also the CO_2 vibrational frequencies around 2360 cm^{-1}, corresponding to the atmosphere during analysis. In the IR spectra of stabilized gold coated, **EJL9-EJL19**, characteristic

C=C vibrational stretches at around 1628 - 1643 cm^{-1} was observed. Whilst the medium intensity frequency at around 1404 - 1411 cm^{-1} represents the -CH vibration. These results confirmed the coordination of sodium citrate on the magnetite nanoparticles surface. The IR spectrum of **EJL12** has a frequency at 913 cm^{-1} indicative of the aromatic -CH out-of-plane bending vibrations. There were also bending frequencies at around 1029 – 1226 cm^{-1}, which can be assigned to the C-N amine functionality in **EJL9, EJL15** and **EJL18**. These results confirmed the coordination of the two different phosphine ligands to the gold coated magnetite nanoparticles. The metal ratio of the 1:50 samples were used for the FT-IR representative spectra. See also **Table 2.4** for the monitored vibrational frequencies of interest in this study.

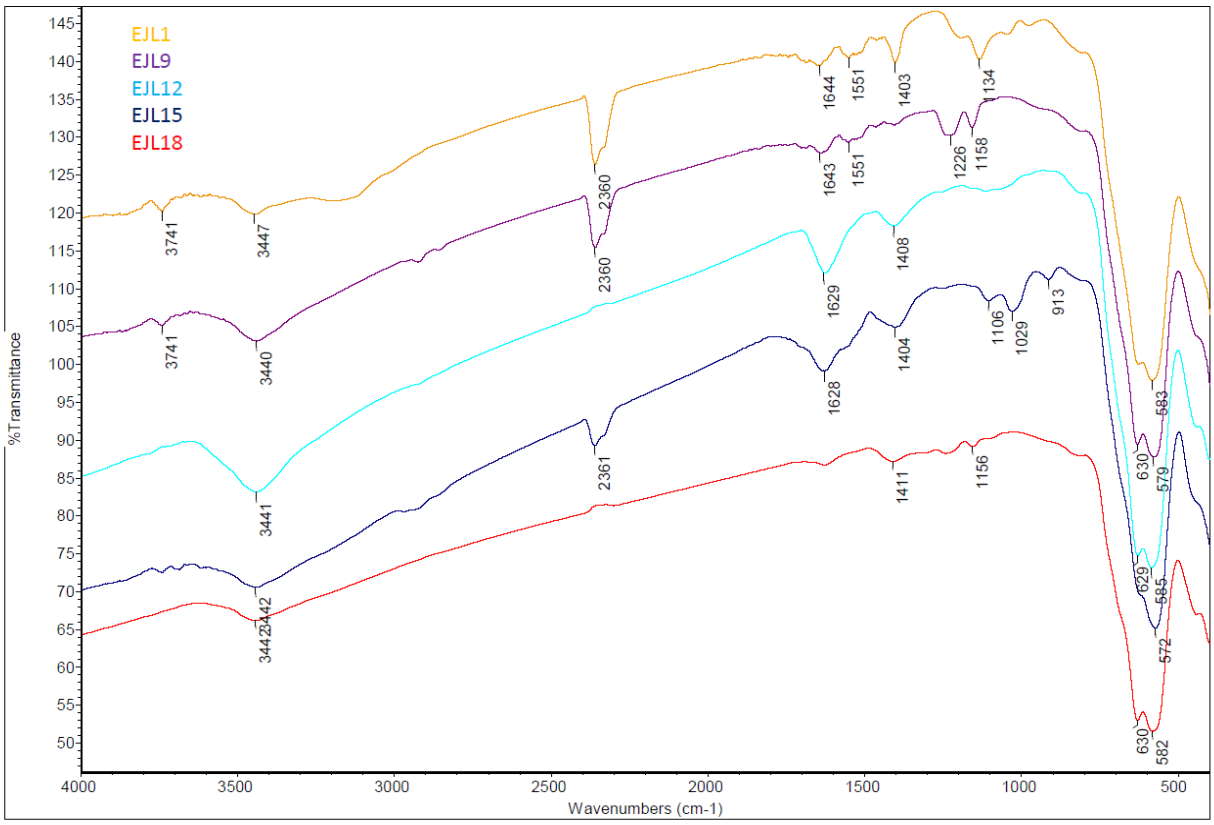

Figure 2.11: Infra-red spectra of gold coated nanoparticles (AuNPs).

Table 2.4. List of IR absorption bends peaks of interest

SAMPLE CODE	O-H (cm^{-1})	FE-O (cm^{-1})	C-N (cm^{-1})	-CH (cm^{-1})	ARYL C=C (cm^{-1})	ARYL -CH OP* (cm^{-1})
EJL1	3447	583				
EJL9	3440	579/630	1226/1158		1643	
EJL12	3441	585/629		1408	1629	
EJL15	3442	572	1106/1029	1404	1628	913
EJL18	3442	582/630	1156	1411	1628	

2.2.6.2 Ultraviolet visible spectroscopy

UV-Vis absorption spectra of the stabilized gold coated SPIONs are shown in **Figure 2.12**. These stabilized catalysts were modified by using the reducing agents on the SPIONs and stabilized by capping with phosphine ligands. It can be seen that the stabilized gold coated ligands where the same reducing agent was used form a similar spectrum, where the absorbance visible SPR peak for these that was reduced using $NaBH_4$ whether stabilized by PTA or PPh_3 showed absorbance peaks at λ = 260 nm and 380 nm peaks and the ones reduced using $Na_3C_6H_5O_7$ whether stabilized by PTA or PPh_3 showed absorbance peaks at λ = 290 and 350 nm. The naked SPIONs only showed a very visible SPR peak, λ at about 390 nm. These do confirm that there was a reduction done by the reducing agent to coat the gold on the surface of the SPIONs as well as this modification was well stabilized by the phosphine ligands.

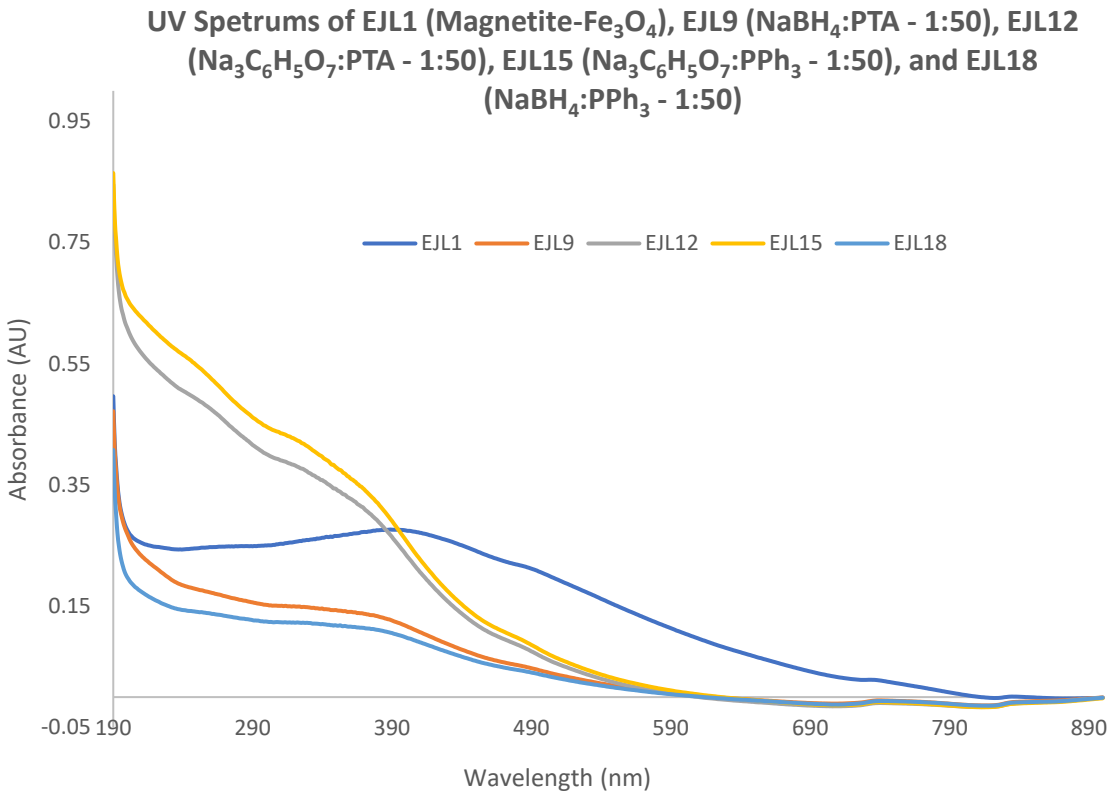

Figure 2.12. UV-vis spectra of the SPIONs and stabilized gold coated SPIONs.

2.2.6.3 High resolution transmission electron microscopy

The average size and size distributions of the stabilized gold coated SPIONs were investigated by means of HRTEM, shown in **Figure 2.13**. These particles are generally spherical, non-agglomerated and polydisperse. The average particle sizes of **EJL8**, **EJL9** and **EJL10** are 17.48 ± 5.3 nm, 18.42 ± 6.9 nm and 18.19 ± 6.3 nm, respectively. These were the catalysts that were reduced using the $NaBH_4$ reducing agent and stabilized with PTA. The average particle sizes of **EJL11**, **EJL12** and **EJL13** are 21.21 ± 6.5 nm, 16.75 ± 5.4 nm, 17.99 ± 5.4 nm. These were the catalysts that were reduced using the $Na_3C_6H_5O_7$ reducing agent and stabilized with PTA. The average particle sizes of **EJL14**, **EJL15** and **EJL16** are 18.66 ± 5.1 nm, 20.40 ± 6.2 nm and 19.50 ± 5.5 nm. These were the catalysts that were reduced using the $NaBH_4$ reducing agent and stabilized with PPh_3. The average particle sizes of **EJL17**, **EJL18** and **EJL19** are 17.38 ± 6.0 nm, 17.42 ± 4.7 nm, 17.92 ± 5.2 nm. These were the catalysts that were reduced using the $Na_3C_6H_5O_7$ reducing agent and stabilized with PPh_3. These set of catalysts as listed have different metal loadings and the

summary of the particle size is shown on **Table 2.5**. From the TEM images it can be seen that these catalysts are not agglomerated and on some it shows how the stabilizer has encapsulated the gold coated nanoparticle.

EJL8

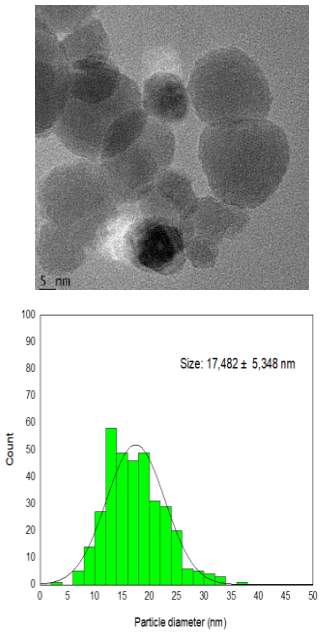

EJL9

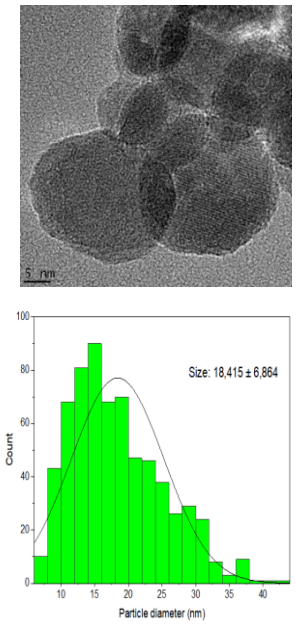

EJL10

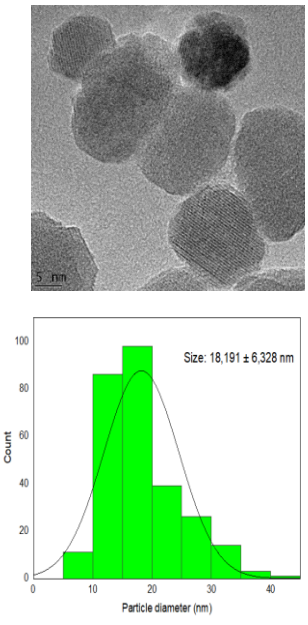

EJL11

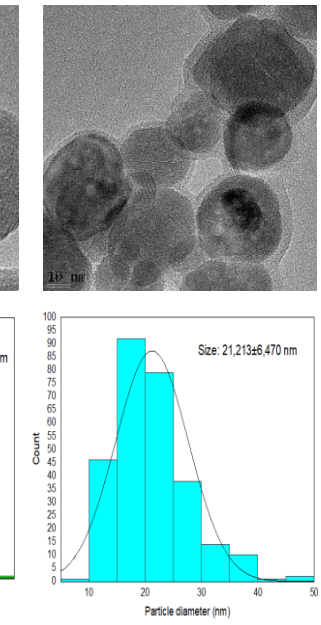

EJL16

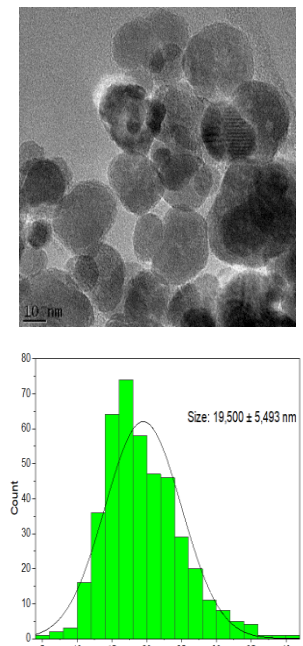

EJL17

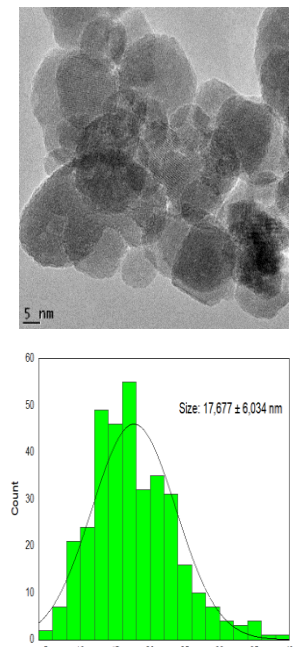

EJL18

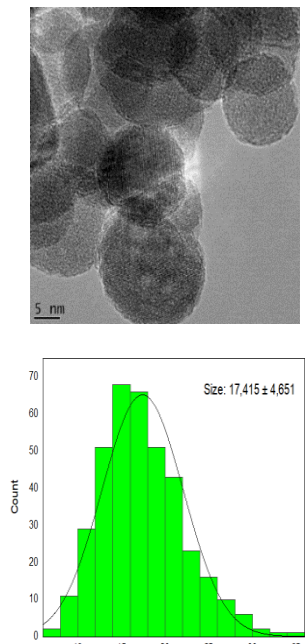

EJL19

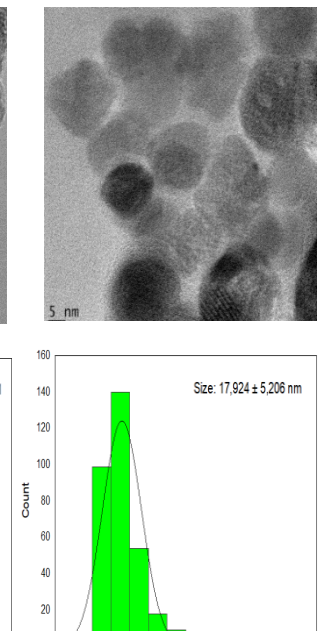

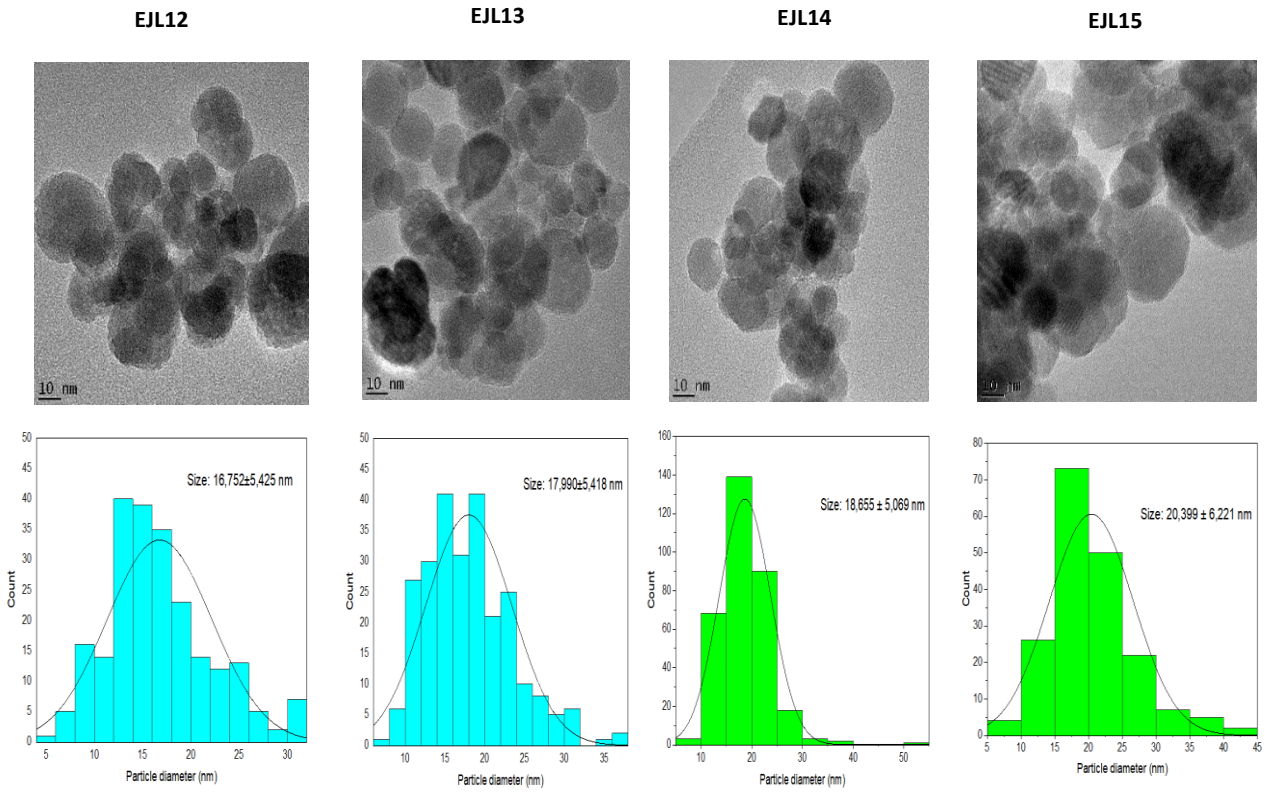

Figure 2.13: HRTEM images, particle size histograms of the stabilized gold coated SPIONs.

Table 2.5: Summary list of stabilized gold coated SPIONs particle size distribution.

SAMPLE CODE	RATIO OF FE_3O_4: AU	REDUCING AGENT	STABILIZER LIGAND	PARTICLE SIZE (NM)
EJL8	10:1	$NaBH_4$	PTA	17.48 ± 5.3
EJL9	50:1	$NaBH_4$	PTA	18.42 ± 6.9
EJL10	100:1	$NaBH_4$	PTA	18.19 ± 6.3
EJL11	10:1	$Na_3C_6H_5O_7$	PTA	21.21 ± 6.5
ELJ12	50:1	$Na_3C_6H_5O_7$	PTA	16.75 ± 5.4
EJL13	100:1	$Na_3C_6H_5O_7$	PTA	17.99 ± 5.4
EJL14	10:1	$Na_3C_6H_5O_7$	PPh_3	18.66 ± 5.1
EJL15	50:1	$Na_3C_6H_5O_7$	PPh_3	20.40 ± 6.2
EJL16	100:1	$Na_3C_6H_5O_7$	PPh_3	19.50 ± 5.5
EJL17	10:1	$NaBH_4$	PPh_3	17.38 ± 6.0
EJL18	50:1	$NaBH_4$	PPh_3	17.42 ± 4.7
EJL19	100:1	$NaBH_4$	PPh_3	17.92 ± 5.2

2.2.6.4 Inductive coupled plasma spectroscopy

ICP was used to determine the gold concentration and loading on the magnetite surface. The Ametek, Spectro Arcos, ICP-OES spectrometer was used. The concentration of metal ions in the supernatant solutions was determined by Inductively Coupled Plasma Optical Emission Spectroscopy (ICP-OES) with a Liberty Series II spectrometer (Varian, Australia). The calibration standards were matrix complemented to acid concentrations of the samples.

The ICP results presented in a histogram, **Figure 2.14**, showed that when comparing the metal loadings of the ratios for catalysts set group [**EJL8** (1:10), **EJL9** (1:50) and **EJL10** (1:100)], the Au content decreases from the highest Au content 1:10 (1:0.1) ratio, to 1:50 (1:0.05) ratio, with the least 1:100 (1:0.01) ratio, this is the trend that proves the Au metal loading was performed successfully and was coated directly to the SPIONs. This also confirms that the sample preparation method used for this stabilized gold coated SPIONs as the highest Au content was in 1:10 ratio, followed by 1:50 and 1:100 having the least Au content used. This observation is clear trend for all the 4 sets as seen in the histogram.

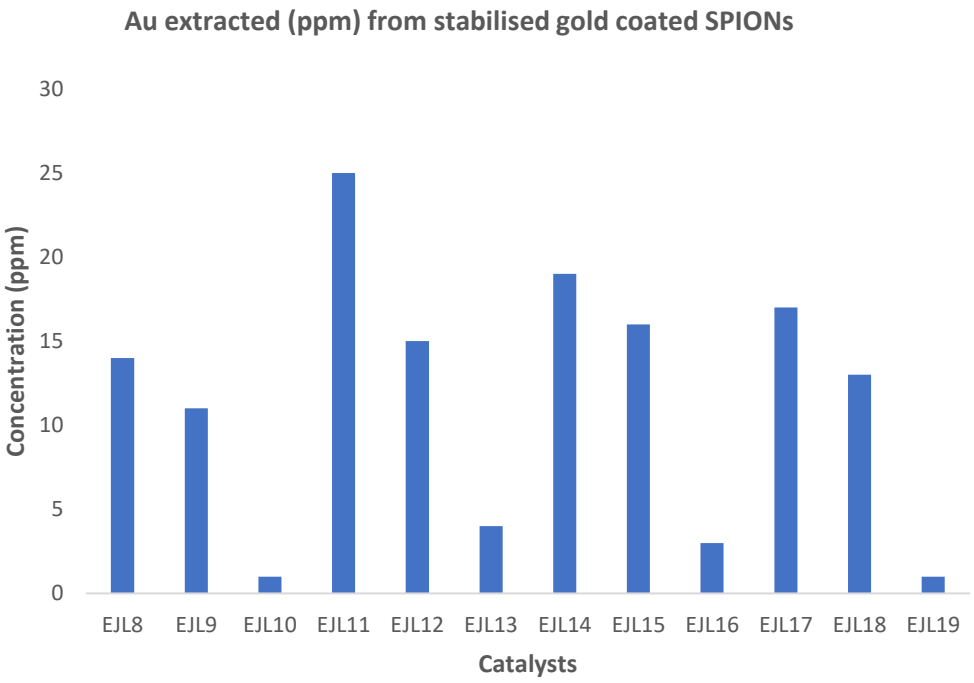

Figure 2.14: Histogram ICP results for Au extractions on AuNPs.

2.3 Conclusion

The superparamagnetic iron oxide nanoparticles (SPIONs) were synthesized successfully using the co-precipitation method using the Fe^{2+} and Fe^{3+} precursors with the molar ratio of 2:1. The Infrared spectroscopy confirmed that the magnetite was obtained as the IR spectrum showed the absorbance peaks that adhere to the characteristic of magnetite. The purity of the SPIONs was confirmed by using the powder X-ray diffraction pattern matched well with those of standard magnetite samples. The HRTEM confirmed the average particle size, and these sizes were in a good nanometres scale, as well as the crystallinity the images showed spherical agglomerated and polydisperse nanoparticles for the SPIONs. The SPIONs were modified by directly coating them with gold using the direct gold coating method. These AuNPs were seen to have gold diffraction peaks that was confirmed by PXRD. Furthermore, this gold coated SPIONs were successfully reduced by using two different reducing agents ($NaBH_4$ and $Na_3C_6H_5O_7$), which reduced the gold directly onto the surface of the SPIONs. The ultraviolet visible spectroscopy clearly showed the difference in SPR peaks between the naked SPIONs and those catalysts that were reduced using the two different reducing agents. To prove that the reduction of these catalysts was successfully employed. The gold coated SPIONs were then stabilized with two difference phosphine ligands (1,3,5-Triaza-7-phosphaadamantane (PTA) and Triphenylphosphine (PPh_3). These ligands were successfully attached to the gold coated SPIONs as seen with the FTIR spectra that showed -CH, C=C and C-N stretching frequencies that were not present on the naked SPIONs. From the TEM micrographs obtained through the HRTEM technique it was shown that the agglomeration of the naked SPIONs and that of the gold coated SPIONs was resolved by the phosphine ligands stabilizer. The different metal loading ratios employed on these catalysts were proven to be successful as the ICP OES showed the different gold extracted from the metal loadings had an increasing trend from the catalysts that had the least gold coating to the catalysts that had the most gold coating mobilised on them.

2.4 Experimental

2.4.1 Materials

The chemicals used include methylene blue ($C_{16}H_{18}ClN_3S.2H_2O$, molecular weight 355.90 g/mol, not less than 96%, $C_{16}H_{18}ClN_3S$ on dried, May & Baker Ltd); sodium borohydride granular (99.99% trace metal bass, Sigma-Aldrich); iron trichloride hexahydrate ($FeCl_3.6H_2O$, ACS reagent, 97%, Sigma Aldrich); iron(II) sulfate heptahydrate ($FeSO_4.7H_2O$, ACS reagent, ≥99.0%, Sigma-Aldrich); triphenylphosphine (PPh_3, ReagentPlus®, 99%, Merck); ammonium hydroxide (NH_4OH, 28-30%, Sigma Aldrich); absolute ethanol (CH_3CH_2OH, 99.8%, Merck); gold(III) chloride trihydrate ($HAuCl_4.3H_2O$, ≥49.0, Sigma-Aldrich); sodium citrate tribasic dihydrate ($Na_3C_6H_5O_7$, ≥99.0%, Sigma-Aldrich) and Ultraspec solution gold (Au), 1000 ± 3 µg/ml, 20℃, Au metal 99.999% pure in 10 % HNO_3; De Bryn spectroscopic solution Iron (Fe), 1000 ± 3 µg/ml, 20℃, Fe metal 99.999% pure in 5 % HNO_3 and type II water (deionized); and 1,3,5-Triaza-7-phosphaadamandate (PTA) and triphenylphosphine (PPh_3).

2.4.2 Instruments

The Fourier-transform infrared (FT-IR) spectra were recorded using a PerkinElmer spectrum two IR spectrometer. A very small amount of the sample was mixed with dried KBr salt, then grounded into a fine powder using the mortar and pestel and there after pressed into a KBr-pellet. A pure KBr-pellet was used to obtain a background reference. The spectra were collected between 4000 and 400 cm^{-1}. All the FT-IR spectra were presented without background correction. Structural properties of the samples were analysed using powder X-ray diffraction (XRD) with a Siemens D8 Advance diffractometer using Cu Kα radiation (λ = 1.540 Å) operated at 40 kV and 30 mA. XRD patterns were recorded in the range 20º–80º (2θ) with a scan step of 0.02°. A Shimadzu UV-1800 UV-Vis spectrophotometer with a CPS that has a temperature control unit was used. Quartz cuvettes were used for spectrum and kinetic analysis, respectively. High resolution transmission electron microscopic (HRTEM) analysis was performed using a FEI Tecnai G2 Field Emission Gun (FEG) TEM, with a 2.5 Å point-to-point resolution, and operating at 200 kV. The samples were prepared by dropwise addition of the solution onto a copper grid. The average particle sizes of the NPs were determined by counting about 200 – 250 particles. By making use of the "ImageJ"

public software. Relative metal concentrations of the NPs were measured by Spectro Arcos inductively coupled plasma-optical emission spectrometer (ICP-OES) instrument.

2.4.3 Synthesis of uncapped superparamagnetic iron oxide nanoparticles

The synthesis of the naked SPIONs (**EJL1**) was carried out using the reported chemical co-precipitation method.[24] The solution of the metal ion precursors was prepared by dissolving iron trichloride hexahydrate $FeCl_3.6H_2O$ (3.4 g, 0.0127 M) and iron(II) sulfate heptahydrate $FeSO_4.7H_2O$ (4.2 g, 0.0275 M) in deionized water, in the molar ratio of 1:2 at room temperature of 23.5^oC An ammonium solution (NH_4OH, 28-30 %, 12 mL) was added dropwise to the solution of the metal precursors and the reaction mixture was vigorously stirred for 20 mins. A black precipitate was formed immediately, indicating the formation of the (**EJL1**) uncapped SPIONs. The reaction was stirred further for 60 min to ensure complete precipitation of the metal precursor ions. The black solid was washed with deionised water by using the magnetic decantation method until the pH of the supernatant was 7.0. The final black solid was washed with ethanol (50ml x 4). The SPIONs were dried in the oven at 60^oC.

2.4.4 Synthesis of gold coated SPIONs

The gold-coated SPIONs (**EJL2-EJL7**) were prepared using different gold loadings. In a typical reaction, uncapped SPION (**EJL1**) of a known amount (1mM) was weighed, and the amount of $HAuCl_4$ was varied (100-600 mM), to make gold-coated SPIONs with different metal loadings. These were added into a round bottom flask and dissolved in degassed deionised water (20 mL) and stirred vigorously for 3 hours. In addition, a known amount of a reducing agent, either being sodium borohydride ($NaBH_4$, $2.3x10^{-3}$ M) or sodium citrate ($Na_3C_6H_5O_7$, $2.0x10^{-4}$ M), was added to the round bottom flask and further stirred for 2 hours to ensure the complete reduction of the gold on the SPIONs surface. Direct gold coating onto the magnetic core can be achieved using magnetic particles that are in an aqueous or organic phase. For particles that are in an aqueous solution, the most common procedure to reduce Au^{3+} is using reducing agents such as sodium citrate and/or sodium borohydride. The ability of gold atoms to make a shell using the sodium citrate reduction of gold chloride is one of the simplest and most used methods.[25] The precipitate was separated by magnetic decantation and washed with deionized water (5 ml). The final gold-

coated SPIONs were placed in the oven to dry at 60 ^{o}C. The percentage yields achieved ranged from 70 – 98 %.

2.4.5 Stabilization of gold coated SPIONs

The method used for the preparation of the stabilized gold-coated SPIONs involves taking a known amount (3 mM) of the gold-coated SPIONs (2.4) and placing it into a round bottom flask. A phosphine ligand, either PTA (130 mM – 700 mM) or PPh_3 (80 mM – 400 mM), to match the metal loading ratio of a particular NP (**EJL8-EJL19**), was added to a round bottom flask and dissolved in a 50 mL of deionised water. These were stirred vigorously for 3 hours. The solid product was separated by magnetic decantation and washed with deionized water (5ml). The final phosphine-stabilized gold-coated SPIONs were placed in the oven to dry at 60 ^{o}C. All the gold-coated SPIONs were stored in a desiccator under an inert environment (nitrogen gas), sealed well with parafilm to ensure that they do not get exposed to air as they can easily oxidize.

2.5 References

[1] JT. Khutlane, K. R. Koch, R. Malgas-Enus, Competitive removal of PGMs from aqueous solutions via dendrimer modified magnetic nanoparticles, SN Applied Sciences, (2020), 1125.

[2] Y. Xia, T. D. Nguyen, M. Yang, B. Lee, A. Santos, P. Podsiadlo, Z. Tang, S. C. Glotzer, and N. A. Kotov, Self-assembly of self-limiting monodisperse supraparticles from polydisperse nanoparticles, Nature Nanotechnology, (2011) 6, 580-587.

[3] R. K. DeLong, C. M. Reynolds, Y. Malcolm, A. Schaeffer, T. Severs, and A. J. Wanekaya, Functionalized gold nanoparticles for the binding, stabilization, and delivery of therapeutic DNA, RNA, and other biological macromolecules, Nanotechnology Science and Applications, (2010) 3, 53-63.

[4] W. H. De Jong, W. I. Hagens, O. Krystek, M. C. Burger, A. J. A. M. Sips, and R. E. Geertsma, Particle size-dependent organ distribution of gold nanoparticles after intravenous administration, Biomaterials Elsevier, (2008) 29, no 12,1912-1919.

[5] R. B. Nasir Baig, and R. S. Varma, Magnetically retrievable catalysts for organic synthesis, Chemical Communications, (2013) 49, 752-770.

[6] P. Xu. G. Ming, D. Lian, C. Ling, S. Hu and M. Hua, Use of iron oxide nanomaterial in wastewater treatment: A Review, Science of the Total Environment, (2021) 424, 1-10

[7] A. Ito, Y. Kuga, H. Honda, H. Kikkawa, A. Horiuchi, Y. Watanabe and T. Kobayashi, Magnetite nanoparticle- loaded anti-HER_2 immunoliposomes for combination of anti-therapy with hyperthermia, Cancer Letters Journals, (2004) 212, 167.

[8] J. W. Moon, C. J. Rawn, A. J. Rondinone, W. Wang, H. Vali, L. W. Yeary, L. J. Love, M. J. Kirkham, B. Gu, and T. J. Phelps, Crystallite sizes and lattice parameters of nanobiomagnetite particles, Journal of Nanoscience and Nanotechnology, (2010) 10, 8298.

[9] P. Guardia, B. Batlle-Brugal, A.G. Roca, O. Iglesias, M.P. Morales, C.J. Serna, A. Labarta, and X. Batlle, Surfactant effects in monodisperse magnetite nanoparticles of controlled size, Journal of Magnetism and Magnetic Materials, (2007) 316, e756.

[10] I.O. Wulandari, D. J. D. H Santjojo, R. A. Shobirin and A. Sabarudin, Characteristics and magnetic properties of Chitosan-coated Fe3O4 nanoparticles prepared by ex-situ co-precipitation method, Rasayan Journal of Chemistry, (2017) Vol10, No 4, 1348-1358.

[11] Y. S. Kang, S. Risbud, J. F. Rabolt and S. Pieter, Magnetic nanoparticles, Chemistry of Materials, (2007) 34, 192-193.

[12] T. Ahn, J. H. Kim, H. M. Yang, J. W. Lee, and J. D. Kim, Formation pathways of magnetite nanoparticles by coprecipitation method, T. Phys. Chem. C, (2012) 116, 6069-6076.

[13] Lyon JL, Fleming DA, Stone MB, Schiffer P and Williams ME. Synthesis of Fe Oxide Core/Au Shell Nanoparticles by Iterative Hydroxylamine Seeding. Nano Letters ACS publications, 2004, 4:719-723

[14] K. Li, T. Jiao, R. Xing, G. Zou, J. Zhou, I. Zhang, and Q. Peng, Fabrication of tunable hierarchical magnetic coated gold nanoparticles nanocomposites constructed by self-reduction reactions with enhanced catalytic performances, Science China Materials, (2018) 61, 728-736.

[15] R.S. Hamida, M. A. Ali, A. Redhwan, M. M. Bin Meferij, Cyanobacteria – A promising platform in green nanotechnology: a review on nanoparticles fabrication and their prospective applications, International Journal of nanomedicine, (2020) 15, 6033-6066

[16] Y. Ofir, B. Samantha, and V. M. Rotello, Polymer and biopolymer mediated self-assembly of gold nanoparticles, Chemical Society Reviews, (2018) 37, 1814-1825.

[17] M. Kumari, A. Mishra, S. Pandey, S. P. Singh, V. Chaudhry, M. K. R. Mudiam, S. Shukla, P. Kakkar, and C. S. Nautiyal, Physico-chemical condition optimisation during biosynthesis lead to

development of improved and catalytically efficient gold Nanoparticles, Scientific Reports, (2016) 6, 27575-27583.

[18] J. Turkevich, P. C. Stevenson, and J. Hillier, A study of the nucleation and growth processes in the synthesis of colloidal gold, Discuss Faraday Soc, (1951) 11,55–75.

[19] K. Zabetakis, W. E. Ghann, S. Kumar, M. Daniel, Effect of high gold salt concentrations on the size and polydispersity of gold nanoparticles prepared by an extended Turkevich-Frens method, Gold Bull, Springer (2012) 45, 203-211.

[20] Z. Rahman, Y. Dong, C. Ren, Z. Zhang and X. Chen, Protein adsorption on citrate modified magnetic nanoparticles, Journal of Nanoscience (2012) 12, 2598-2606.

[21] H. Bonnemann and R. M. Richards, Nanoscopic metal particles – synthetic methods and potential applications, Eur. J. Inorg. Chem. (2001) 10, 2455.

[22] E. E. Foos, A. W. Snow, M. E. Twigg and M. G. Ancona, Prospects of colloidal nanocrystals for electronic and optoelectronic application, Chem. Mate (2003) 15, 1617.

[23] C. Ren, J. Li, X. Chen, Z. Hu, and D. Xue, Mater., Citrate conformation and chelation: enzymatic implications, Material Research Innovations, (2007) 11, 83.

[24] JT. Khutlane, K. R. Koch, R. Malgas-Enus, Competitive removal of PGMs from aqueous solutions via dendrimer modified magnetic nanoparticles. SN Applied Sciences, (2020) 12, 1125.

[25] S. M. Silva, R. Tavallaie, L. Sandiford, R. D. Tilley and J. Gooding, Gold coated magnetic nanoparticles: from preparation to surface modification for analytical and biomedical applications, Chemical Communications Journal, (2016) 52, 7528.

Chapter 3: Magnetic Au phosphine nanoparticles as catalysts in the reduction of methylene blue

3.1 Introduction

In the textile industry, synthetic dyes have been used to impart colour to fabrics; however, this poses a serious threat to the environment due to their toxicity. The complex structure of dyes makes them difficult to degrade. Therefore, a perpetual method is needed to eradicate the dyes. Conventional methods have been reported[1], some of these methods include coagulation-flocculation, sedimentation, membrane technologies (reverse osmosis, nanofiltration and dialysis), cloud point extraction, microbiological decomposition, aerobic and anaerobic degradation, chemical oxidation technologies (Fenton's reagent with hydrogen peroxide, photo-catalysis with UV radiation and ozonation), electrochemical treatment and adsorbents utilization (activated carbon, inorganic adsorbents such as silica or clays, synthetic ion-exchange resins and chitin-based adsorbents), but they are not efficient as the derivatives of the complex dyes remain in the water even after the treatment. The removal of these chemicals is expensive and complicated. In recent times, nanoparticles have been found to be an effective approach to water purification.[2] Dyes cause many problems in the industry and varying on the exposure time and dye concentration. The biggest environmental concern with dyes is their absorption and reflection of sunlight entering the water. Dyes can remain in the environment for an extended period of time, because of their high thermal and photostability. For instance, the half-life of hydrolysed Reactive Blue 19 is about 46 years at pH 7 and 25 °C. Many dyes and their breakdown products are carcinogenic, mutagenic and/or toxic to life.[3] Dyes are mostly introduced into the environment through industrial effluents.

Degradation, reduction, and removal of these compounds into non-toxic products is the biggest need that they must be treated before they are discharged into the water bodies. The first synthetic dye, Mauveine or aniline-purple, was discovered in 1856. Since then, dyes have come to be a crucial part of the textile and many other many industries.[4] There are a lot of dyes in the textile industry like methyl violet, bromophenol blue, ethyl violet, methyl green, brilliant green, cresol red, basic fuchsin, victoria blue and pararosaniline. There are some of the triarylmethane dyes that are commonly used in the textile industry for colouring.[5]

Furthermore, a study of dye wastewater treatment by removal was the next possible ways to deal with the issue. At present, the ways, such as adsorption, chemical oxidation, catalytic

oxidation, biological method, and membrane method, were often used[6]. Thereinto, adsorption could eliminate organic compounds which were resistant to degradation by biological method or general oxidation, for example, nitroaromatics and heterocyclic compounds, and it took on advantages such as simple operation, less land occupation, good effect and so on. So, adsorption was widely employed in printing and dyeing wastewater treatment.[7] Adsorption includes batch and column adsorption, but column adsorption plays a dominant role in the practical application. In order to reduce treatment cost and improve processing efficiency, the absorbent must be better adsorption and desorption performance. Therefore, batch adsorption, column adsorption and their regeneration for MB removal from aqueous solution were implemented previously and reported using home-made IOCPCF (interrupt-on-change Portc flag bit) as an absorbent. Adsorption and desorption mechanisms of MB were emphatically analysed, which hopes to provide theoretical basis for industrial wastewater treatment by porous ceramics filter. [8] There have also been many other technologies been developed for dye removal from aquatic environments, including flocculation, coagulation, precipitation, adsorption, membrane filtration, electrochemical techniques, ozonation and biosorption.[9] Among them, the wide application of adsorption is emerged from advantages including high efficiency, capacity and large-scale ability of generable adsorbents.[10] The design of novel procedures based on nontoxic, low cost and easily available adsorbents are the best choice for wastewater treatment. Nanoparticles possess distinguished properties such as a high number of reactive atoms and a large number of vacant reactive surface sites in addition to metallic or semi-metallic behaviour applicable for interaction of various functional and reactive groups (atoms) of target compound for their quantitative removal.[11]

Therefore, we propose the use of modified gold-coated magnetic nanoparticles, stabilized with phosphine ligands, as catalysts in the reduction and removal of dyes in textile industry wastewater. These catalysts can also be recyclable due to their magnetic abilities.

3.2 Results and discussion

The reductive discoloration of methylene blue (MB) was carried out as a reaction of cationic and anionic dyes since MB is a cationic dye. Initial optimisation studies were carried out using similar conditions to those reported by Saikaia *et al*. [1]

3.2.1 Methylene blue dye

MB ($C_{16}H_{18}ClN_3S$), which was used as an adsorbate in the present study, was prepared by dissolving the methylene blue (solid phase) in double-distilled water. The chemical structure and UV-Vs absorption spectrum of MB in the solution is shown in **Figure 3.1 a, b, and c**. Literature[12] showed four characteristic peaks (246, 292, 613 and 664 nm) and the one performed showed similar absorbance maxima (260, 293, 615 and 666 nm) which confirms that the MB was prepared correctly. The absorption spectra of the Methylene Blue are characterized by three main bands, one in the visible region (max = 666 nm), and two in the UV region (max = 293 nm and max = 260 nm). In our case, the most important band is at 666 nm (azo dye content). The MB absorption band (650 – 670 nm) can be assigned to monomeric (MB^+) species respectively. The UV-Vis spectra at 666 nm are monitored, at different time intervals for MB dye reduction (see **Figure 3.2)**. As the monitored absorbance maxima intensity decreases it depicts a slight noticeable shift. This is due to the addition of the stabilized AuNPs (**EJL8**) that helps in the electron relay from BH_4^- (donor) to MB (acceptor). Then the absorbance peak at about 260 nm is also monitored, as it shows an increase depicting that there is product being formed. Methylene blue is blue when it is in an oxidizing environment, but colourless Leuco methylene blue (LMB) if it is exposed to a reducing agent.[13] Refer to **Scheme 3.1**.

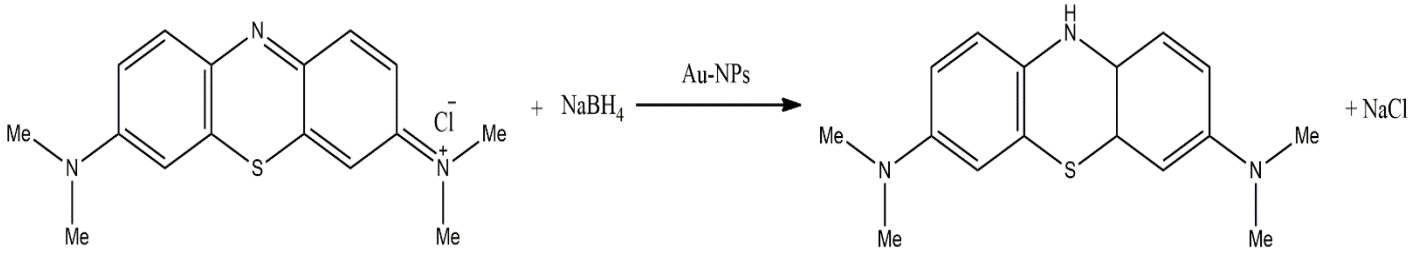

Scheme 3.1: Reduction reaction of MB to LMB.[13]

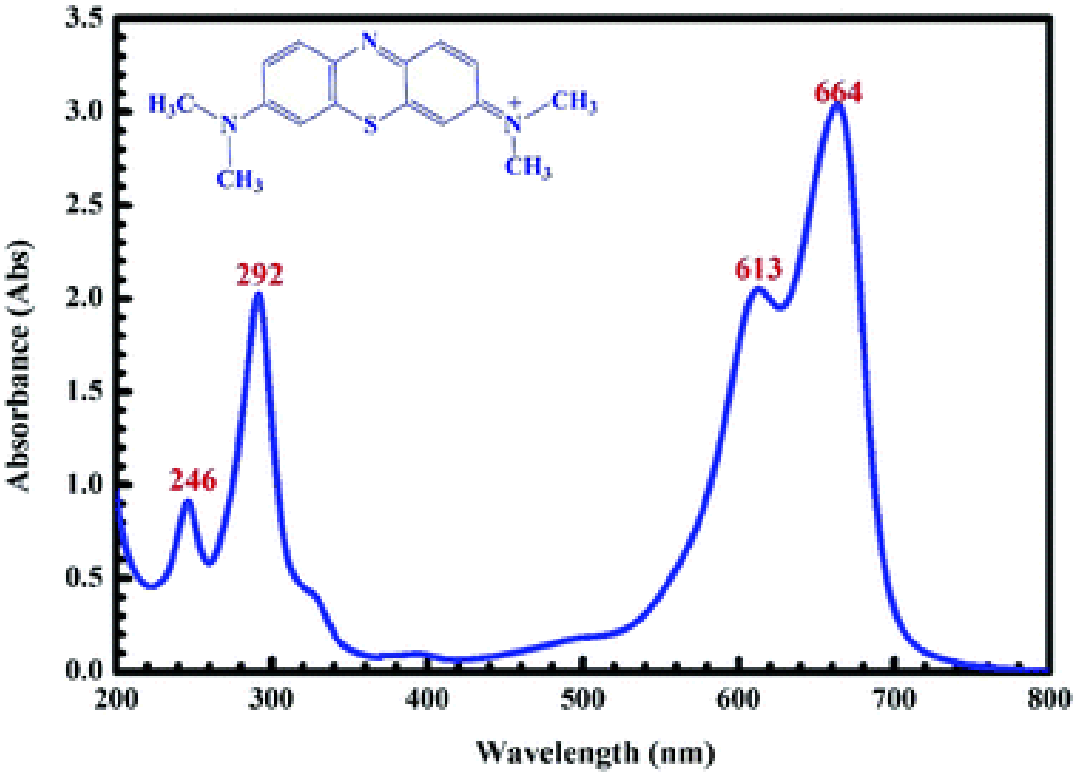

Figure 3.1a: Methylene Blue dye UV-vis spectra – $C_{16}H_{18}ClN_3S$, literature.[12]

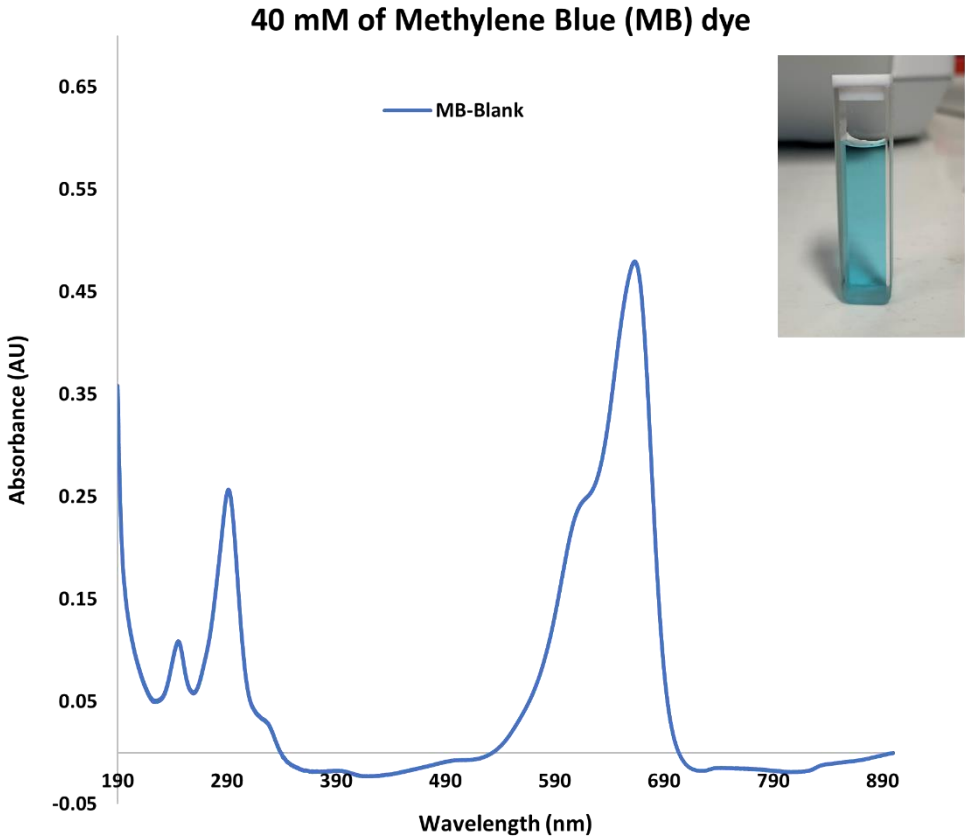

Figure 3.1b: Methylene Blue dye UV-vis spectra – $C_{16}H_{18}ClN_3S$

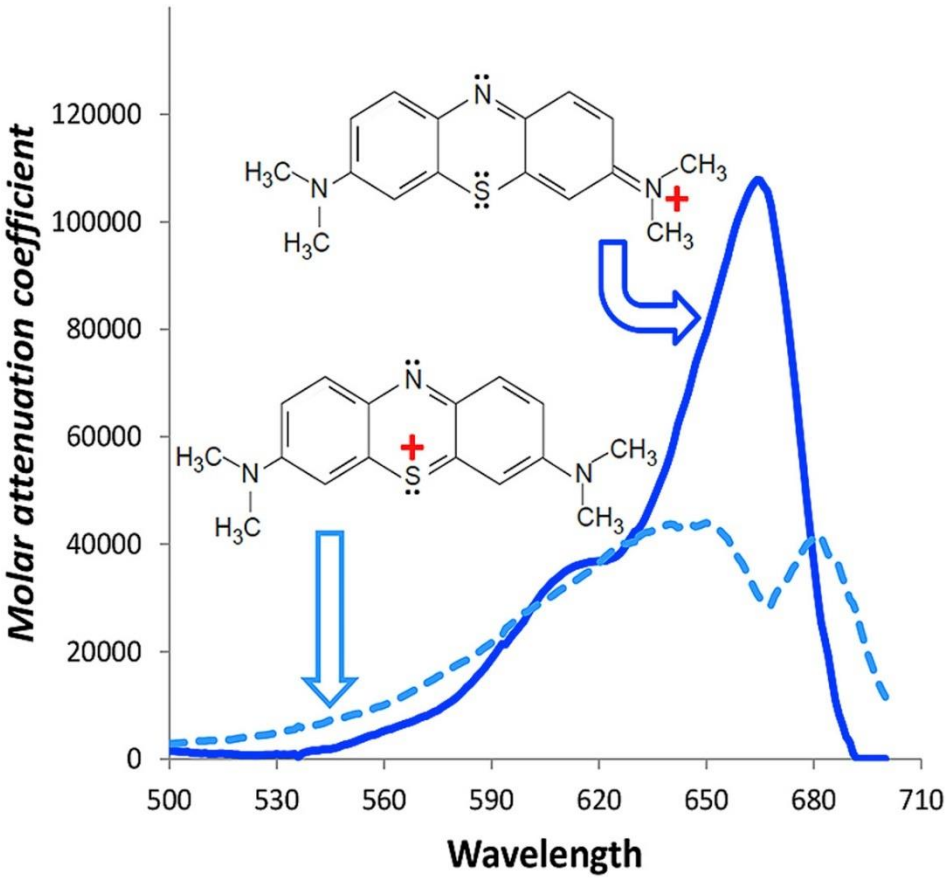

Figure 3.1c: Methylene Blue dye UV-vis spectra (peak assignment) – $C_{16}H_{18}ClN_3S$[14]

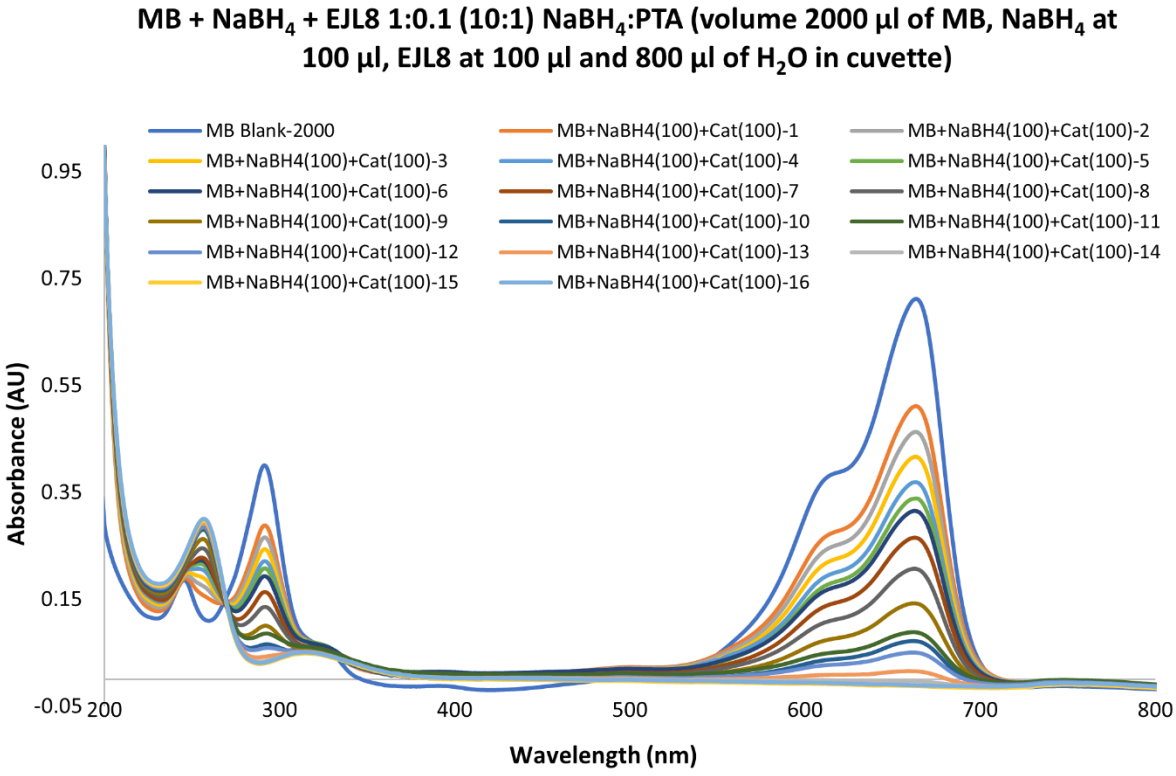

Figure 3.2: Study of MB reduction, with EJL8 and $NaBH_4$ against time interval (indicated on the graph labelled as 1 to 16 mins).

3.2.2 Optimisation studies on the UV-Vis spectroscopy for MB reduction

For the study of the method optimisation, a four-steps process was followed as per **Table 3.1**, where the concentrations of each parameter were varied and evaluated, using the same catalyst (**EJL8**) for the method optimisation using UV-Vis spectroscopy, see **Figure 3.3**:

1. The concentrations of methylene blue were varied from 6.4 µM to 1.6 µM. The best suitable concentration was found to be 6.4 µM of MB for this catalytic system.
2. Secondly, once the suitable concentration of MB was determined, this was then kept constant while the sodium borohydride ($NaBH_4$) concentrations were varied from 2 mM to 0.25 mM. The best suitable concentration was found to be 0.5 mM of $NaBH_4$ for this catalytic system.
3. Thirdly, once these optimized concentrations were established for MB and $NaBH_4$ at 6.4 µM and 0.5 mM, respectively. These were kept constant when the next variable concentration was varied thus being the catalyst loading (**EJL8**, was the catalyst used for the optimisation of the UV-Vis method), concentrations from 1ppm to 0.1 ppm. The best suitable concentration was found to be 1 ppm of catalysts loading for this catalytic system.
4. Lastly, the optimized concentrations for MB, $NaBH_4$ and catalysts loading was determined to be 6.4 µM, 0.5 mM and 1 ppm, respectively. Then the temperature at which the best suitable conditions for these reactions to take place was varied from 50 ℃ to 10 ℃. Subsequently the suitable temperature for our reaction was found to be 25 ℃.

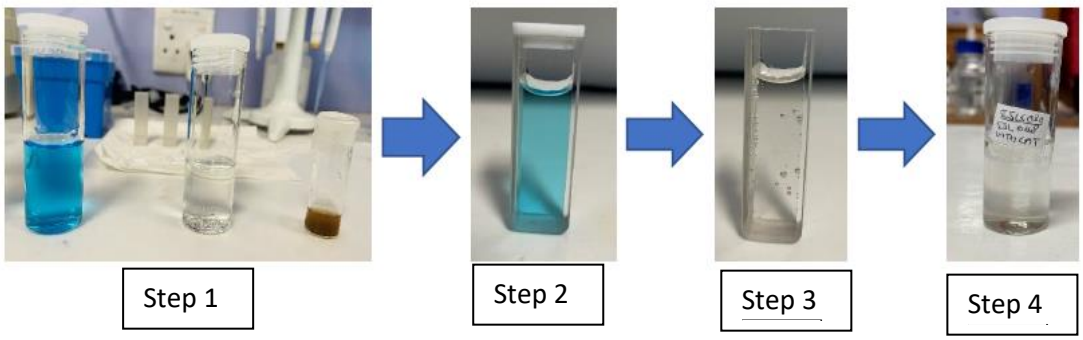

Table 3.1. UV-Vis conditions for the optimisation method used for reduction of MB.

Parameters	MB dye (µL)	H_2O (µL)	$NaBH_4$ (µL)	Catalyst (µL)	Temp (°C)
	2500	150	300	50	25
Varied MB conc					
	2000	650	300	50	25
	1500	1150	300	50	25
	1000	1650	300	50	25
	500	2150	300	50	25
Varied $NaBH_4$ conc					
	2000	550	400	50	25
	2000	750	200	50	25
	2000	850	100	50	25
	2000	900	50	50	25
Varied Catalyst loading conc					
	2000	800	100	100	25
	2000	825	100	75	25
	2000	875	100	25	25
	2000	890	100	10	25
Varied Temperature					
	2000	800	100	100	30
	2000	800	100	100	40
	2000	800	100	100	50
	2000	800	100	100	20
Reaction	2000	800	100	100	10

conditions for catalyst EJL8: **metal loading** ratio (Fe: Au) - 1:0.1; **reducing agent** – $NaBH_4$; **ligand** – PTA; time interval was 20 mins, each spectrum taken after 1 min interval for reaction interaction to take place, making total time per experiment to be 40 mins, and 5 mins between different parameters.

3.2.3 The kinetic studies for the optimisation method on UV-Vis spectroscopy

The optimisation method was obtained by following the steps as described in section 3.2.2. The reactions on the UV-Vis spectrophotometer were run in quadruplets for each change in parameter concentration as investigated using the conditions listed in **Table 3.1**. Once the UV-Vis spectra were obtained, the k_{abs} was then determined for the wavelength peaks at λ = 666 nm, λ = 293nm and λ = 260nm. The R^2 values were also taken into consideration. The k_{abs} and R^2 evaluated at λ = 666 nm were used to have a better understanding of each change in parameter

concentration. From the results, **Figure 3.4a, b and c**, it was seen that there is a correlation between the rate constant and the concentrations of the MB, $NaBH_4$ and catalysts loading were observed and will be discussed. For the concentration of MB, it was observed that as the MB concentration decreases with the increase in the rate constant. This proved that, when there is lowered MB concentration in the system, the reduction of MB occurs more rapidly. For the change in $NaBH_4$ concentration, it was shown that a higher concentration of $NaBH_4$ resulted in a higher rate constant. The catalysts loading concentration also showed a similar trend as for $NaBH_4$, in that a higher concentration results in an increased rate constant.

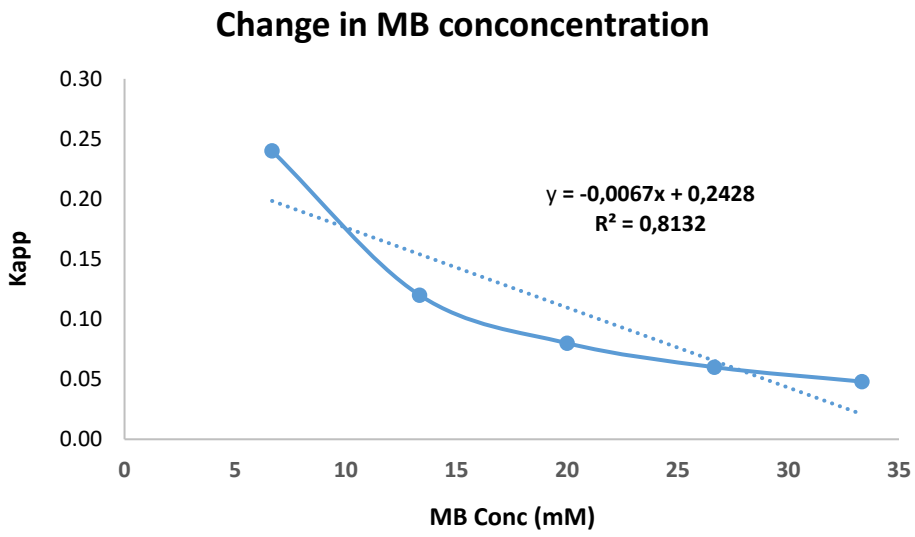

Figure 3.4a: The k_{abs} change in MB concentration for wavelength at 666.nm

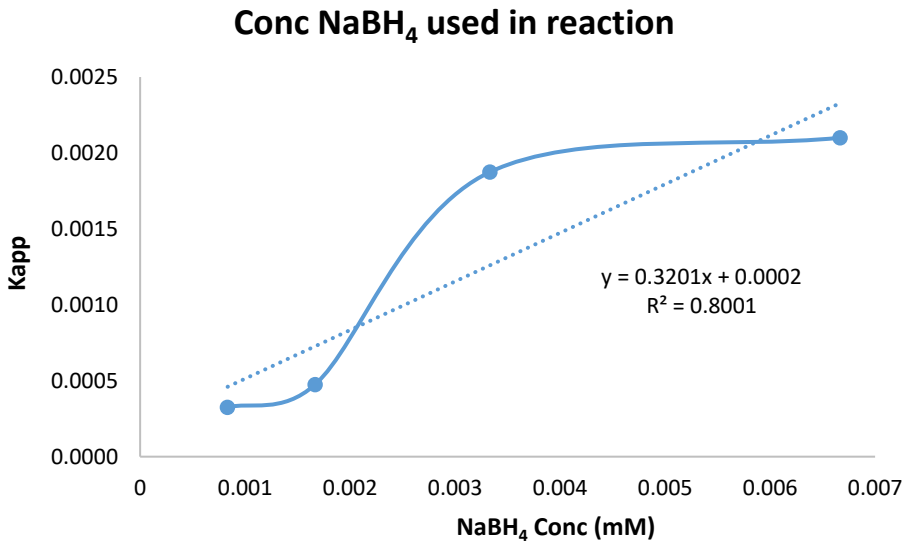

Figure 3.4b: The k_{app} change in $NaBH_4$ concentration for wavelength at 666.nm

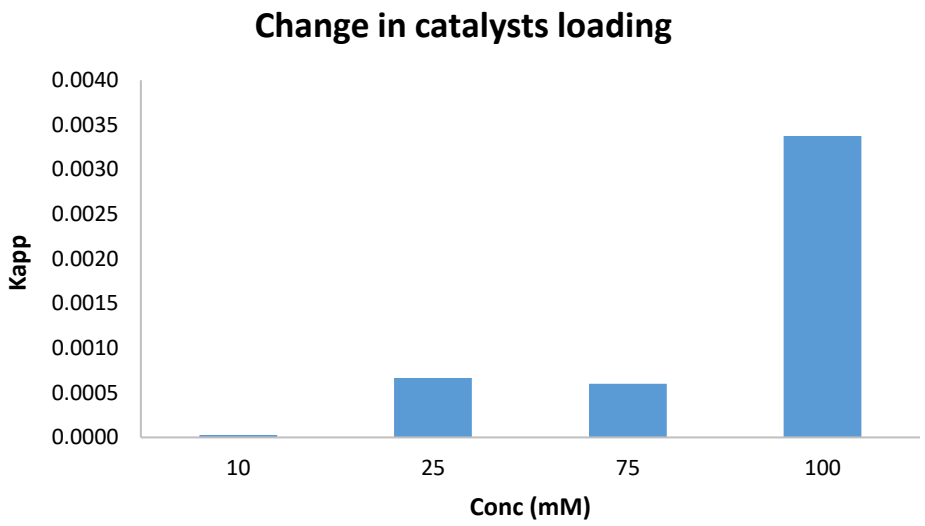

Figure 3.4c: The k_{app} change in catalyst loading concentration for wavelength at 666 nm.

3.2.3.1 The effect of temperature

The effect of temperature on the reduction of methylene blue in the presence of a catalyst for method optimisation using UV-Vis spectroscopy was investigated in the range of 283 – 323 K (10 – 50 °C). In order to calculate the activation energies for the MB reduction, kinetics runs were carried out at various temperatures (283 K, 293 K, 313 K and 323 K). The results in **Figure 3.5**, shows that the reduction efficiency has a direct proportionality to the reaction temperature. The increase in temperature may lead to an increasing reduction rate of methylene blue. This observation can be explained in terms of collision theory, i.e., particles not at 0 K tend to move around and therefore collide. During particle collisions, chemical reactions can occur. Higher temperatures result in an increased kinetic energy for the particles, increasing the frequency at which the particles collide. Resulting in faster reaction rates. [15]

The activation parameters associated with the reduction of methylene blue are calculated from the plot of Ink_{abs} versus $^1/_T$ **Figure 3.5**, which gives the value of activation energy (E_a), according to the Arrhenius equation:

$$In\ k_{abs} = \frac{-E_a}{RT} + In\ A \qquad (3.1)$$

If this Equation (**3.1**) is expressed in terms of Equation (**3.2**), the, the slope, $m = -\frac{E_a}{R}$

$$y = mx + c \qquad (3.2)$$

The activation energies for the reduction of methylene blue were calculated to be 20.237, 18.444, 18.160 and 17.080 kJ/mol at 283.15 K, 293.15 K, 313.15 K and 323.15 K, respectively.

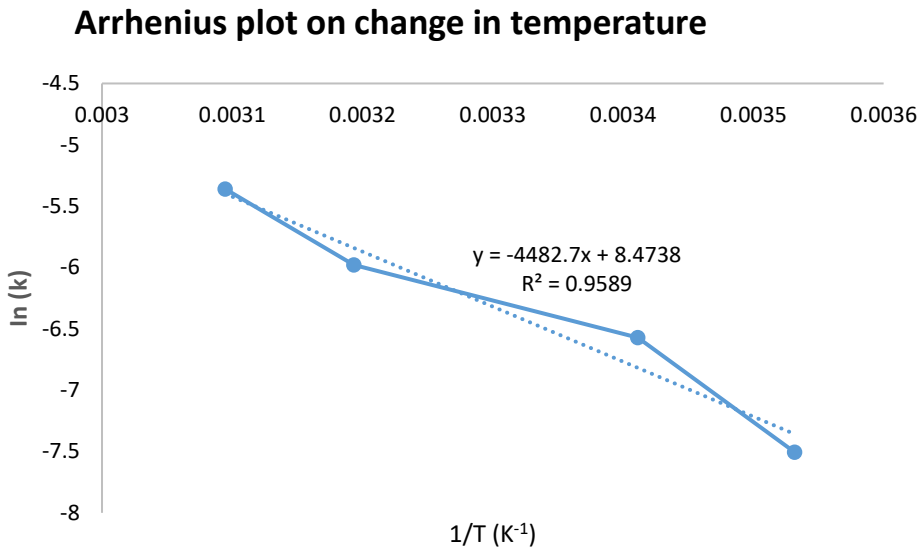

Figure 3.5. Arrhenius plot for the reaction of MB with Catalysts at constant concentrations but varying the temperature on the UV-Vis Spectroscopy.

Using an Equation 3.3, $k = Ae^{-Ea/RT}$ (3.3)

Where, A is Arrhenius constant at 2.71828, T is Temperature at unit Kelvin (K), and k is the rate constant. The Activation energy Ea, was obtained using equation 3.3. The natural logarithm of rate constant *ln(k)* vs. the inversed temperature $^1/_T$, tells of the corresponding orders as zero ($M*s^{-1}$), one (s^{-1}), two ($M^{-1}*s^{-1}$). For our purpose on this research, the corresponding order used was one (s^{-1}).

The value of $\Delta H^{\#}$ and $\Delta S^{\#}$ can be calculated from the plot of Erying equation (**3.4**) as follows:

$$In\left(\frac{k_{abs}}{T}\right) = \left(In\frac{k_B}{h} + \frac{\Delta S^{\#}}{R}\right) - \frac{\Delta H^{\#}}{RT} \qquad (3.4)$$

Where, k_B is the Boltzman's constant (1.381×10^{-23} J.K^{-1}); h is the Plank's constant (6.626×10^{-34} J.s), where $In\frac{k_B}{h} = 23.76$.

From the linear plot *of* $In(k_{abs}/T)$ versus $^1/_T$ **Figure 3.6**, values of $\Delta H^{\#}$ and $\Delta S^{\#}$ can be calculated. The Gibbs' free energy $\Delta G^{\#}$ can therefore be calculated from the relation 3.4:

$$\Delta G^{\#} = \Delta H^{\#} - T\Delta S^{\#} \qquad (3.5)$$

Table 3.2 shows the rate constants and activation energies in the range of temperature studied (283 – 323 K) with the thermodynamic parameters of $\Delta H^{\#}$, $\Delta S^{\#}$ and $\Delta G^{\#}$.

The positive values of $\Delta G^{\#}$ for the reaction (**Table 3.2**) indicate the non-spontaneous nature of decolorization of MB by AuNP catalyst at the temperatures studied. The negative value of $\Delta S^{\#}$ suggests the decrease randomness at the liquid/liquid solution interface during the decolorization of MB solution by AuNP ion, while the positive values of $\Delta H^{\#}$ show the endothermic nature of the reaction.

Table 3.2: Thermodynamic parameters for the reaction between MB and $NaBH_4$ in the presence of AuNP catalyst

Temperature (K)	K_{abs}	Activation energy (E_a) KJ/mol	$\Delta H^{\#}$ KJ/Mol	$\Delta S^{\#}$ KJ/Mol	$\Delta G^{\#}$ KJ/Mol
283.15	0.00055	20.237	30.963	-0.1094	61.940
293.15	0.00140	18.444	29.872	-0.1019	59.744
313.15	0.00253	18.160	30.566	-0.0975	61.098
323.15	0.00470	17.080	29.924	-0.0926	59.848

3.2.4 Catalysts used for the MB reduction on the optimised method on UV-Vis

After the method optimisation studies were performed, each of the 19 catalysts as synthesized in chapter 2 (from the naked SPIONs, to gold-coated set of catalysts and the stabilized gold coated SPIONs set of catalysts), were used on the optimized reaction conditions from UV-Vis spectroscopy. The composition of these reactions is shown in **Table 3.3.** These conditions were obtained after the optimisation of the method studies was performed on the UV-Vis as shown in **Table 3.1**. Based on the optimisation method, all the catalytic conditions for methylene blue reduction took place at 25 ℃. The methylene blue dye of 40 µM were added to the cuvette. The catalyst of 1ppm and the co-catalysts ($NaBH_4$ solution) of 50 mM was added to the MB solution in the cuvette in 100 µL aliquots. These were mixed together in a cuvette. The reactions were monitored by UV-Vis spectroscopy.

Table 3.3: UV-vis catalysts reaction conditions used on the optimized method.

Sample code	Ratio of Fe_3O_4: Au	Reducing agent	Stabilizer
EJL1	magnetite		
EJL2	10:1	$NaBH_4$	
EJL3	50:1	$NaBH_4$	
EJL4	100:1	$NaBH_4$	
EJL5	10:1	$Na_3C_6H_5O_7$	
EJL6	50:1	$Na_3C_6H_5O_7$	
EJL7	100:1	$Na_3C_6H_5O_7$	
EJL8	10:1	$NaBH_4$	PTA
EJL9	50:1	$NaBH_4$	PTA
EJL10	100:1	$NaBH_4$	PTA
EJL11	10:1	$Na_3C_6H_5O_7$	PTA
EJL12	50:1	$Na_3C_6H_5O_7$	PTA
EJL13	100:1	$Na_3C_6H_5O_7$	PTA
EJL14	10:1	$Na_3C_6H_5O_7$	PPh_3
EJL15	50:1	$Na_3C_6H_5O_7$	PPh_3
EJL16	100:1	$Na_3C_6H_5O_7$	PPh_3
EJL17	10:1	$NaBH_4$	PPh_3
EJL18	50:1	$NaBH_4$	PPh_3
EJL19	100:1	$NaBH_4$	PPh_3

Reaction conditions: **methylene blue** – 2000 µL; **$NaBH_4$** - 100 µL; **catalyst** – 100 µL: **temp**. - 25 ℃.

The change in the absorbance of MB with time was monitored by UV-Vis spectroscopy at λ = 666nm, λ = 293nm and λ = 260nm, as shown in **Figure 3.6**.

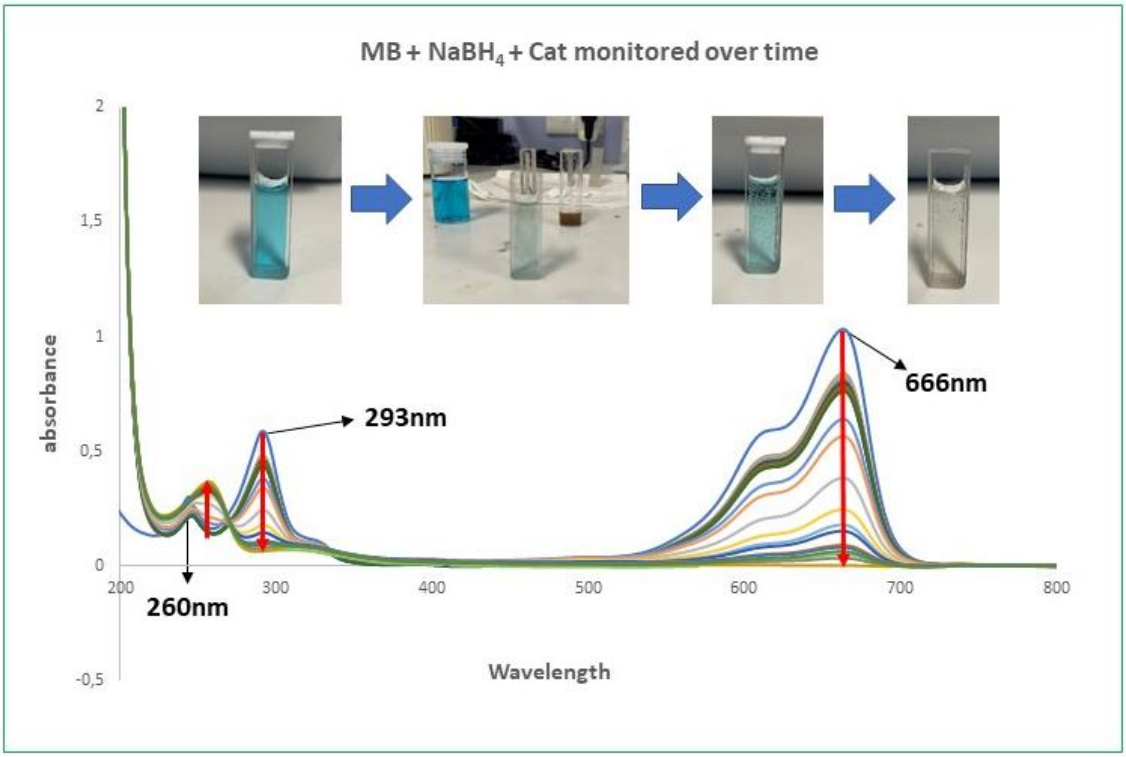

Figure 3.6: Time base UV-vis spectra monitoring MB reduction catalyzed by AuNPs with EJL8, stabilized with PTA ligand.

3.2.5 The kinetic studies on the different catalysts k_{abs} analysis on the MB reduction

The reactions on the UV-Vis spectroscopy were run in quadruplets for each catalyst using the reaction conditions listed in **Table 3.3**, after the UV-Vis spectra were obtained. The k_{abs} and R^2 were calculated at λ = 666nm, λ = 293nm and λ = 260nm. The k_{abs} and R^2 evaluated at λ = 666 nm were used to have a better understanding of the different catalysts used for the reduction of MB and their possible mechanisms. To evaluate the catalysts and their possible active mechanisms, a variety of reaction parameters were investigated and discussed: (**a**) The effect of SPIONs vs the two different reducing agents on MB reduction; (**b**) The phosphine ligands effect compared between the two reducing agents used; (**c**) The effect of two reducing agents on the catalysts which were stabilized with the same phosphine ligand stabilizers; (**d**) The metal loading effect on stabilized gold coated SPION; (**e**) The effect of $NaBH_4$ as a reducing agent used on the catalysts, one without a phosphine ligand, compared to the ones with phosphine ligands stabilizers; and (**f**)

The effect of $Na_3C_6H_5O_7$ as a reducing agent on the catalysts, one without a phosphine ligand compared to the ones with phosphine ligands stabilizers.

3.2.5.1 The effect of SPIONs vs. two different reducing agents used for MB reduction

From **Figure 3.7**, for the parameter (**a**) it can be concluded that the naked magnetite (**EJL1**) was observed to be a better catalyst compared to catalysts reduced with sodium borohydride (**EJL2**) /or by sodium citrate (**EJL5**) without any stabilizing phosphine ligands used. Even though the catalyst **EJL1** was better it was unable to retain the reduction of MB as there was a reverse reaction observed since MB retained a slight blue colour after 24 hrs of MB reduction, whilst this was not observed with **EJL2** and **EJL5**, where the reduction of MB was clear.

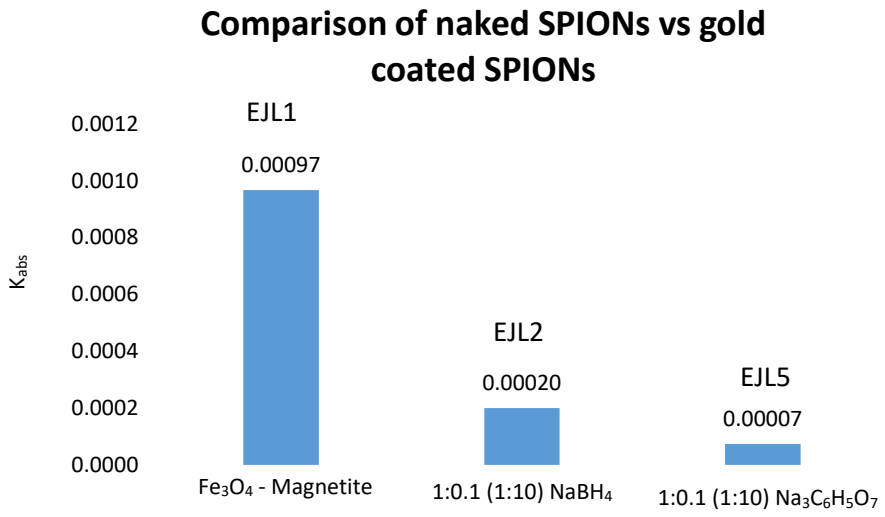

Figure 3.7: The k_{abs} histogram of naked SPION vs two reducing agents ($NaBH_4$ and $Na_3C_6H_5O_7$).

3.2.5.2 The phosphine ligands effect compared between the two reducing agents used

From **Figure 3.8a** and **b**, for the parameter (**b**), it can be concluded PTA and PPh_3, as stabilizers, showed that they react similarly when $NaBH_4$ is used as a reducing agent for MB reduction (**EJL8** vs. **EJL17**), as it has the highest k_{abs} value. It also can be concluded that the PPh_3 ligand, was the favorable catalysts compared to the PTA ligand when $Na_3C_6H_5O_7$ is used as a reducing agent for MB reduction. (**EJL11** vs. **EJL14**), as it has the highest k_{abs} value. PTA has a smaller chemical

structure compared to the bulkier PPh_3 structure. Making the PTA more easily accessible as a ligand for MB removal.

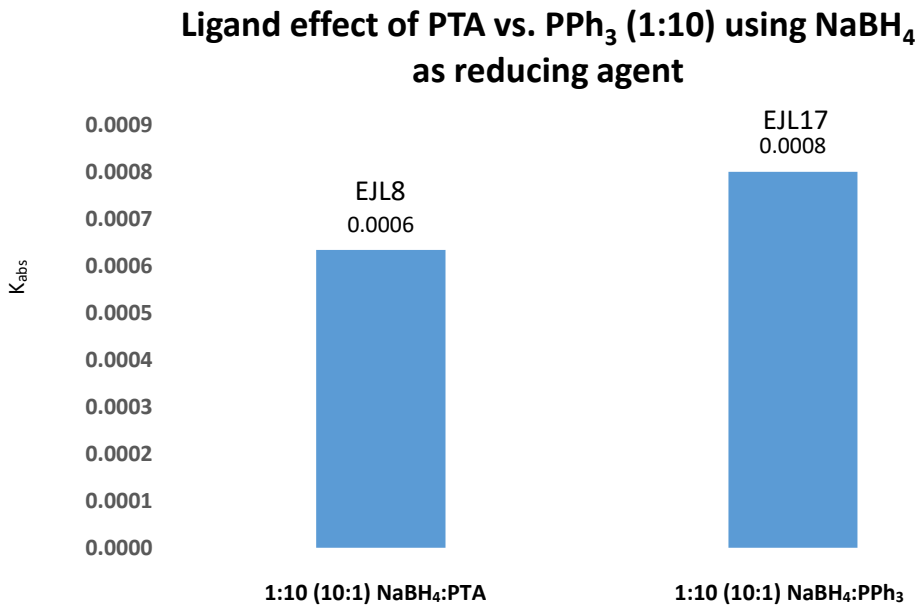

Figure 3.8a: The phosphine ligands effect at 1:10 (1:0.01) metal loading catalysts reduced with $NaBH_4$.

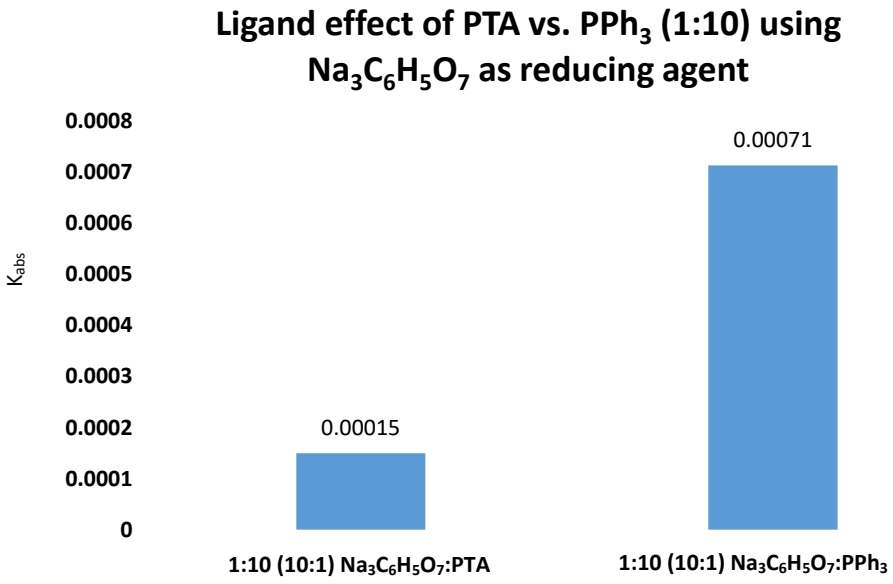

Figure 3.8b: The phosphine ligands effect at 1:10 (1:0.01) metal loading catalysts reduced with $Na_3C_6H_5O_7$.

3.2.5.3 The effect of two different reducing agents on the catalysts which were stabilized with the same phosphine ligand

From **Figure 3.9a and b**, for the parameter (**c**), it can be concluded from comparing the two different reducing agents used on the catalysts, with the PPh_3 as a stabilizer, that they react similarly for the MB reduction (**EJL17** vs **EJL14**). It also can be concluded that the use of NaBH4 as reducing agent with PTA as ligand resulted in the best catalysts for MB reduction. (**EJL8** vs **EJL11**), as it has the highest k_{abs} value.

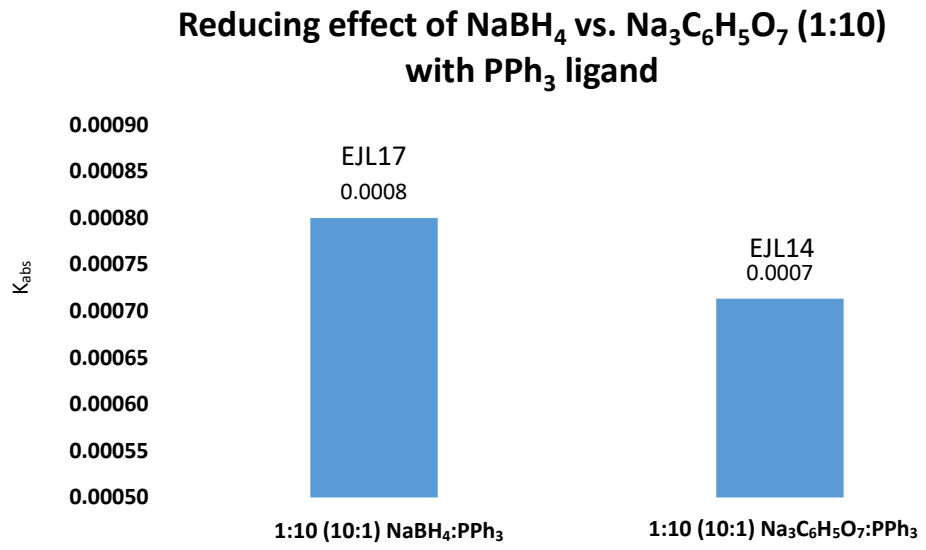

Figure 3.9a: The effect of two reducing agents on the catalysts which were stabilized with PPh_3.

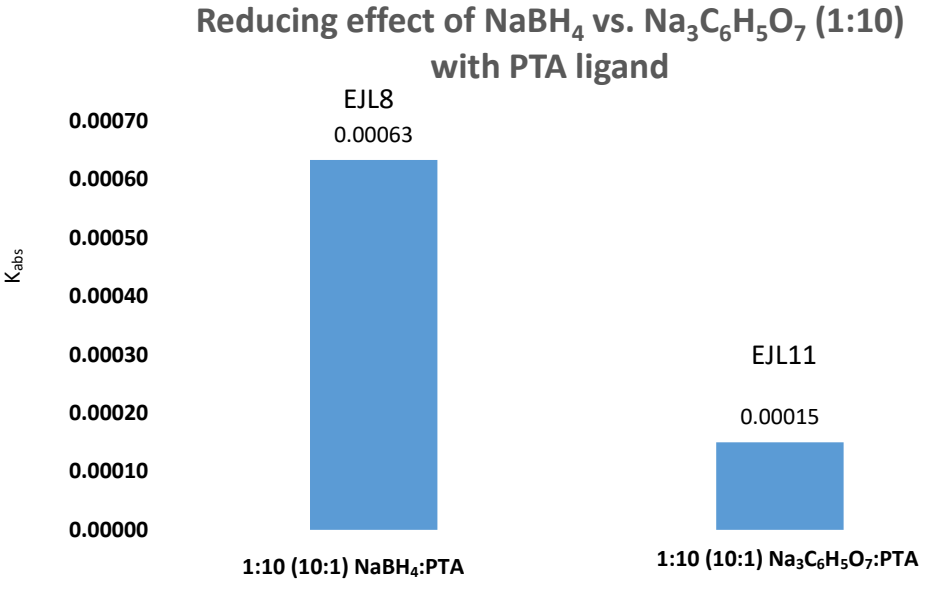

Figure 3.9b: The effect of two reducing agents on the catalysts which were stabilized with PTA.

3.2.5.4 The metal loading effect on stabilized gold coated SPIONs

From **Figure 3.10**, for parameter (**d**), the catalysts which were reduced with $Na_3C_6H_5O_7$ using PTA ligand stabilizer were used for this point. It can be concluded that the favorable Fe_3O_4:Au metal loading ratio for MB reduction is the 1:50 (1:0.05) compared to the 1:10 (1:0.01) and 1:100 (1:0.01), as it has the highest k_{abs} value. (**EJL11** vs **EJL12** vs **EJL13**).

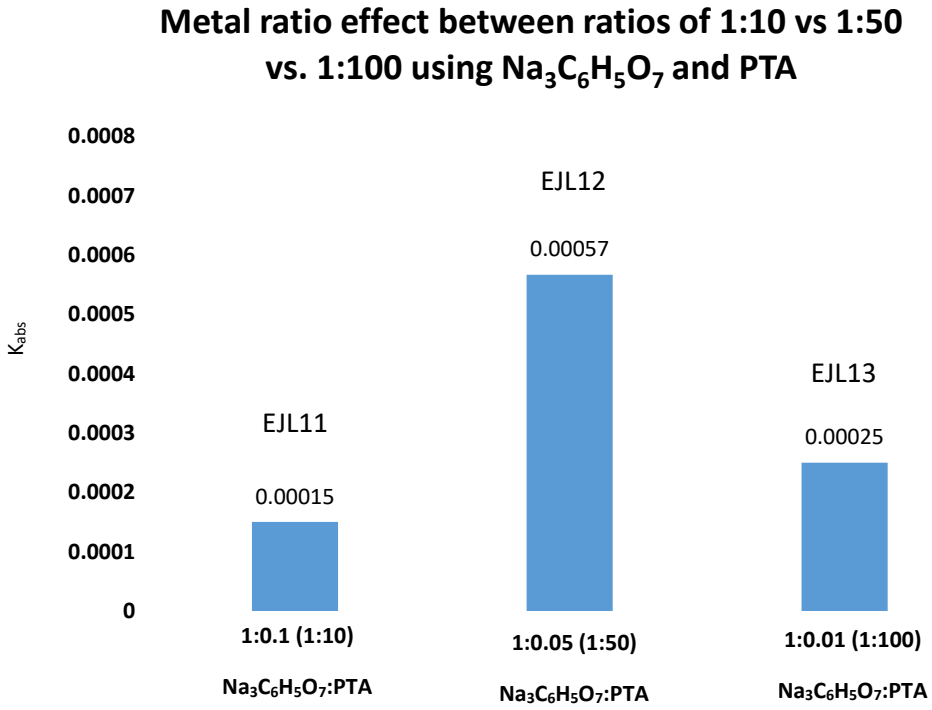

Figure 3.10. The effect of two reducing agents on the catalysts which were stabilized with the same phosphine ligand.

3.2.5.5 The effect of $NaBH_4$ as a reducing agent used on the catalysts, one without a phosphine ligand compared to the ones with phosphine ligands stabilizers

From **Figure 3.11a, b and c**, for parameter (**e**), the catalysts which were reduced with $NaBH_4$ with the different metal loading ratios, i.e., 1:10, 1:50 and 1:100, with one catalyst without being stabilized compared with two catalysts with one that was stabilized using PTA ligand stabilizer and the other was stabilized using PPh_3 ligand stabilizer, were used for this point. It can be concluded the effect of $NaBH_4$ at metal loading ratio 1:10, shows that the PTA ligand stabilized catalyst were preferential for the MB reduction (**EJL2** vs **EJL8** vs **EJL17**) as it has the highest k_{abs} value. For the metal loading ratio 1:50, it can be concluded that the PPh_3 stabilized catalysts were preferential for the MB reduction (**EJL3** vs **EJL9** vs **EJL18**), as it has the highest k_{abs} value. For the

metal loading ratio 1:100, showed no significant preference on any of the catalysts for the MB reduction (**EJL4** vs **EJL10** vs **EJL19**), as they all had similar k_{abs} values.

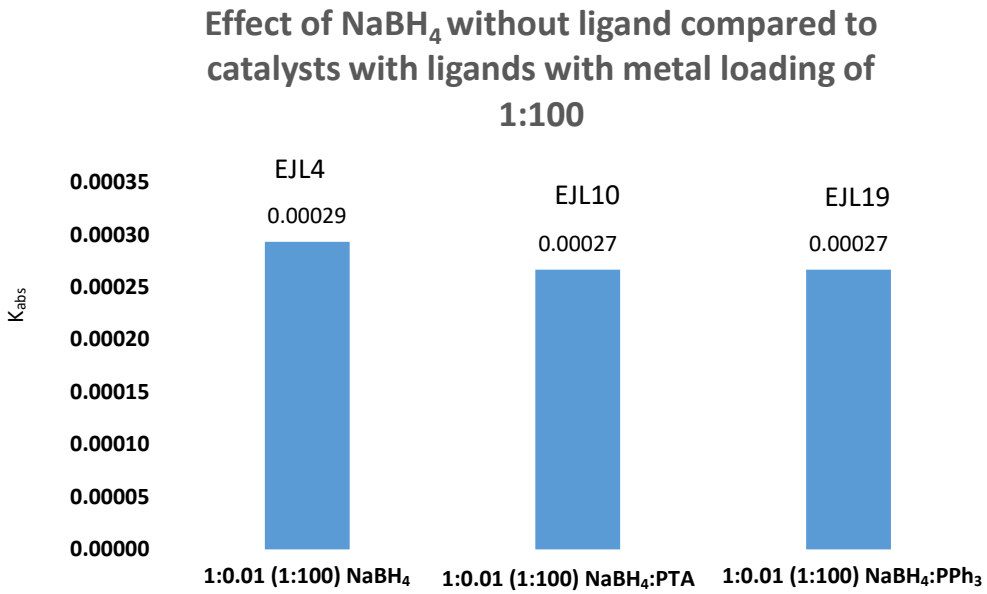

Figure 3.11a: The effect of $NaBH_4$ on catalysts with different metal loading ratios, one which was without a stabilizer and two with phosphine ligands stabilizers at 1:10

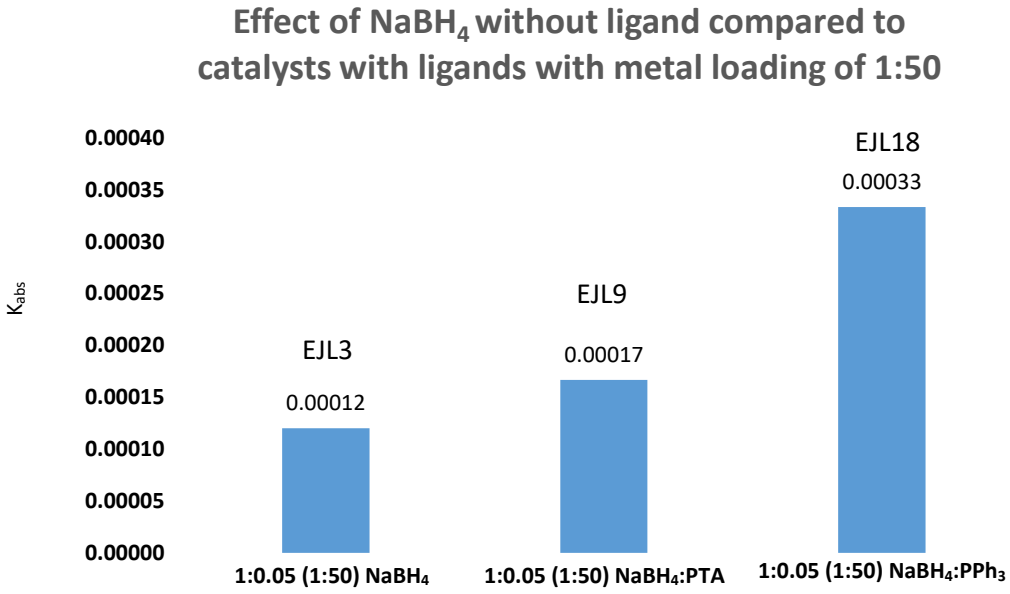

Figure 3.11b: The effect of $NaBH_4$ on catalysts with different metal loading ratios, one which was without a stabilizer and two with phosphine ligands stabilizers at 1:50

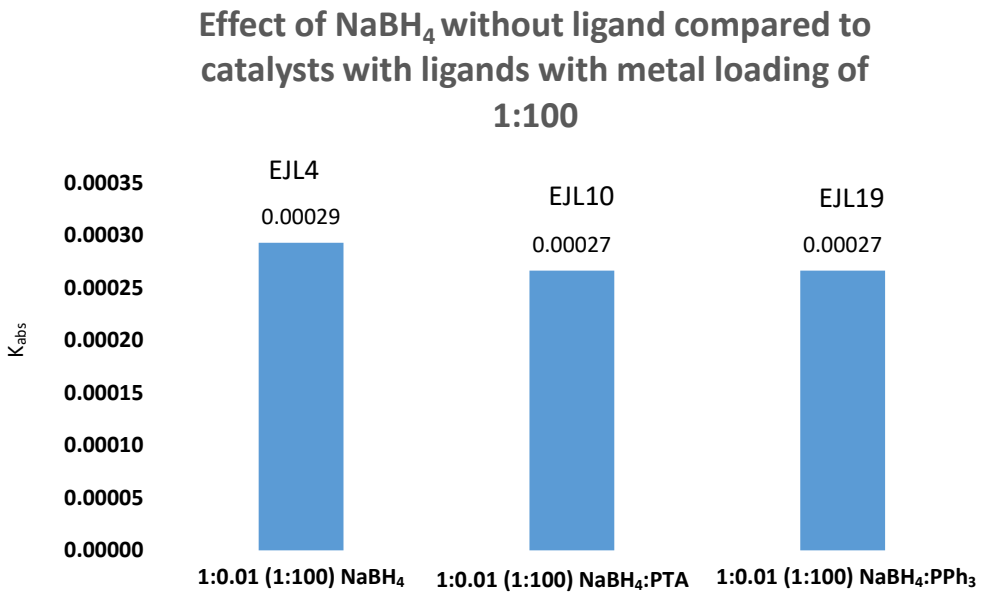

Figure 3.11c: The effect of $NaBH_4$ on catalysts with different metal loading ratios, one which was without a stabilizer and two with phosphine ligands stabilizers at 1:100

3.2.5.6 The effect of $Na_3C_6H_5O_7$ as a reducing agent used on the catalysts, one without a phosphine ligand compared to the ones with phosphine ligands stabilizers

From **Figure 3.12a, b, and c**, for parameter (**f**), the catalysts which were reduced with $NaBH_4$ with the different metal loading ratios at 1:10, 1:50, 1:100 with one catalyst without being stabilized compared with two catalysts with one that was stabilized using PTA ligand stabilizer and the other was stabilized using PPh_3 ligand stabilizer, were used for this point. It can be concluded that the effect of $Na_3C_6H_5O_7$ at a metal loading ratio of 1:10, shows that the uncapped catalyst was preferred for MB reduction (**EJL5** vs. **EJL11** vs. **EJL14**), as it has the highest k_{abs} value. But **EJL5** was unable to retain the reduction of MB as a slight blue colour was observed after 24 hrs of reduction. This is due to naked SPIONs being known to easily re-oxidised especially when they are not coated and stabilized, whilst it was not observed with **EJL11** and **EJL14**. The metal loading ratio 1:50, showed that the PTA stabilized catalysts were preferred for the MB reduction (**EJL6** vs **EJL12** vs **EJL15**), as it has the highest k_{abs} value. For the metal loading ratio 1:100, showed that the PPh_3 stabilized catalysts were preferred for the MB reduction (**EJL7** vs. **EJL13** vs. **EJL16**), as it has the highest k_{abs} value.

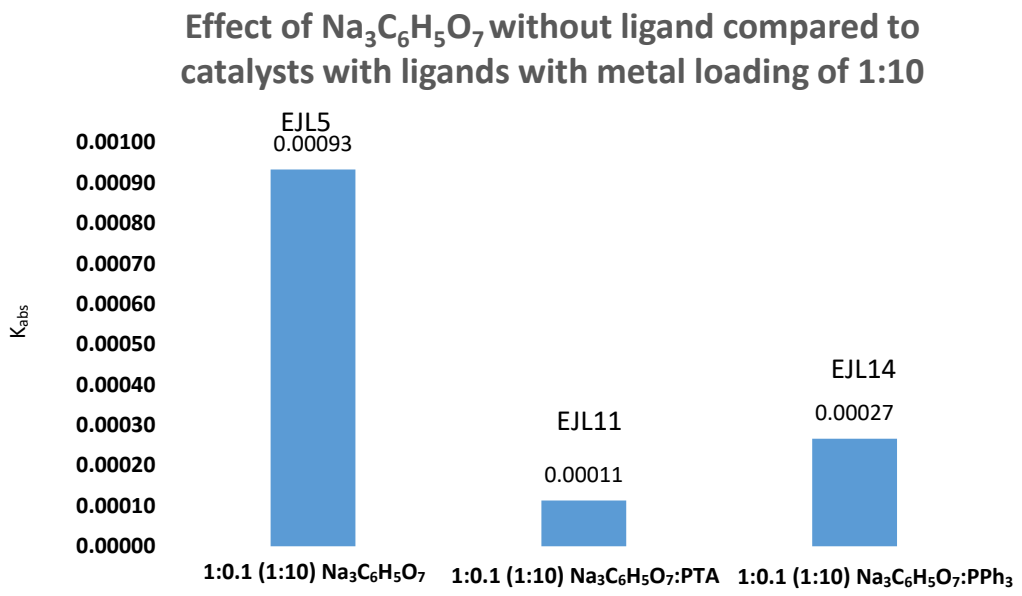

Figure 3.12a: The effect of $Na_3C_6H_5O_7$ on catalysts with different metal loading ratios, one which was without a stabilizer and two with phosphine ligands stabilizers at 1:10

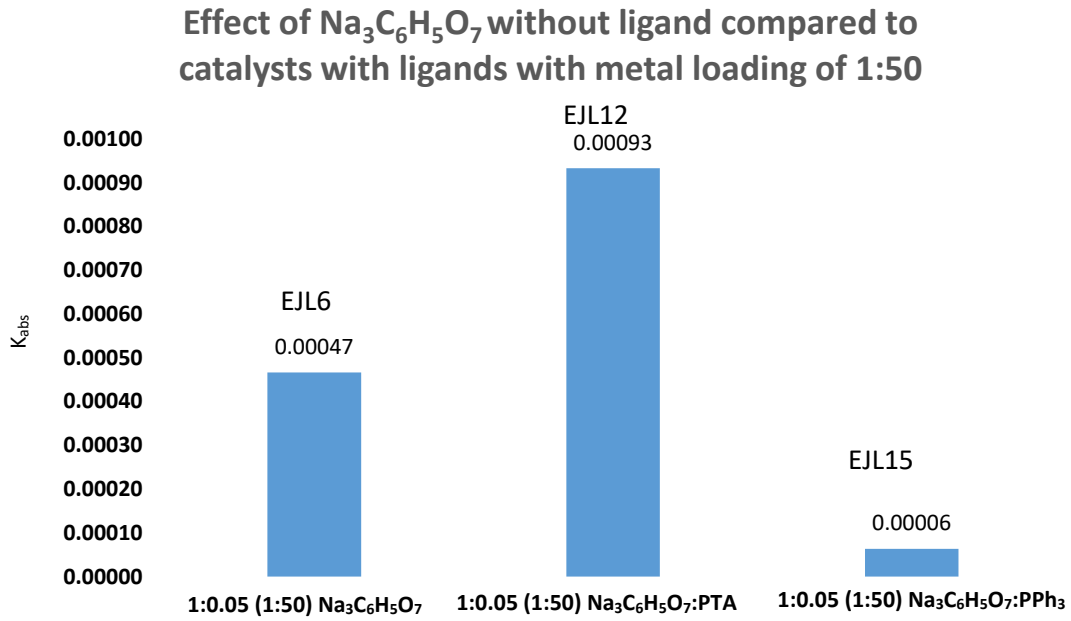

Figure 3.12b: The effect of $Na_3C_6H_5O_7$ on catalysts with different metal loading ratios, one which was without a stabilizer and two with phosphine ligands stabilizers at 1:50

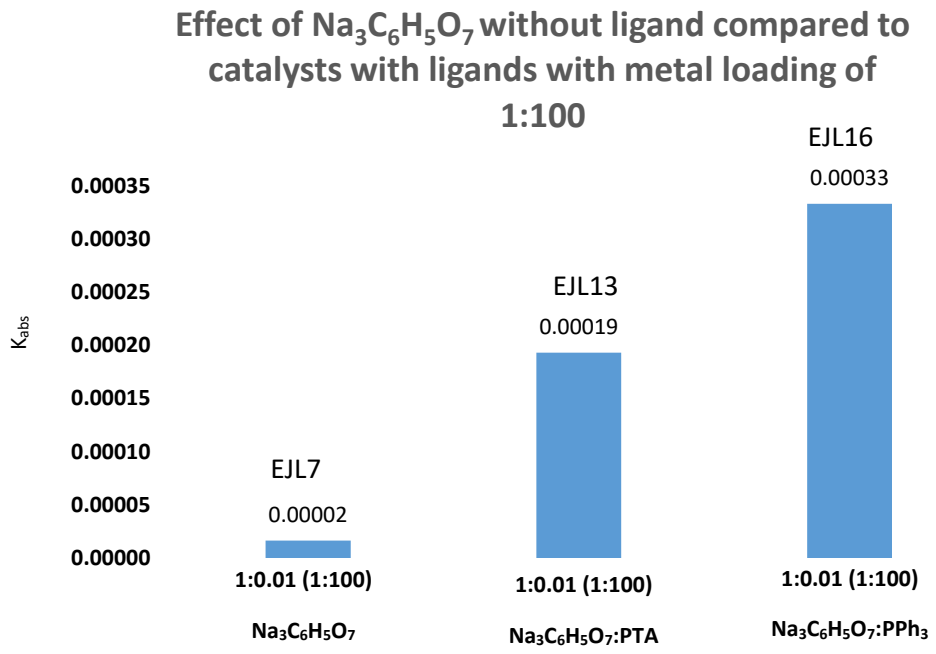

Figure 3.12c: The effect of $Na_3C_6H_5O_7$ on catalysts with different metal loading ratios, one which was without a stabilizer and two with phosphine ligands stabilizers at 1:100

3.2.6 The mechanism for MB reduction

From the literature[16], it is proposed that metal nanoparticles act as electron transfer systems, facilitating the transfer of an electron from $NaBH_4$ to the MB dye. The transfer can be unfavorable due to a large potential difference between the reagents. Hence, metal nanoparticles, with an intermediate potential assist in the transfer of the electron. [16] AuNPs help in the electron relay from BH_4^- (donor) to MB (acceptor). BH_4^- ions are nucleophilic, while MB is electrophilic in nature with respect to AuNPs, where electrons from BH_4^- ions and conveys them to the MB. [17] In order to confirm mechanism, the reaction conditions as above in **Table 3.5** were applied. The complete reduction was completed with all our catalysts different rate constant as per the discussion with the kinetic studies shown in point 3.4.6. The observation suggests that the electrons are transferred from $NaBH_4$ to the catalysts surface in the initial reaction and the excess electrons remaining on the catalysts surface then reduce the MB dye in the second step reaction, thus confirming that the catalysts used as AuNPs of different metal loading ratios, with different reducing agents used and different ligand stabilizers follow the proposed mechanisms, as shown in **Figure 13a and b**.

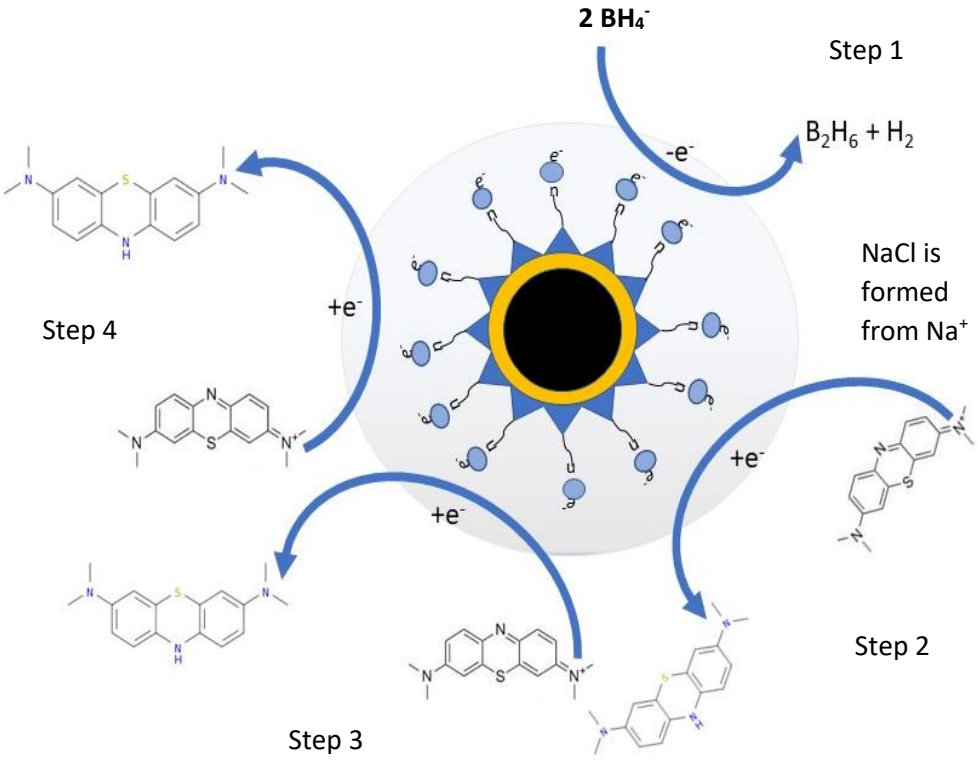

Figure 3.13a: Proposed electron transfer mechanism, where electrons from NaBH4 are transferred to methylene blue via catalyst surface.

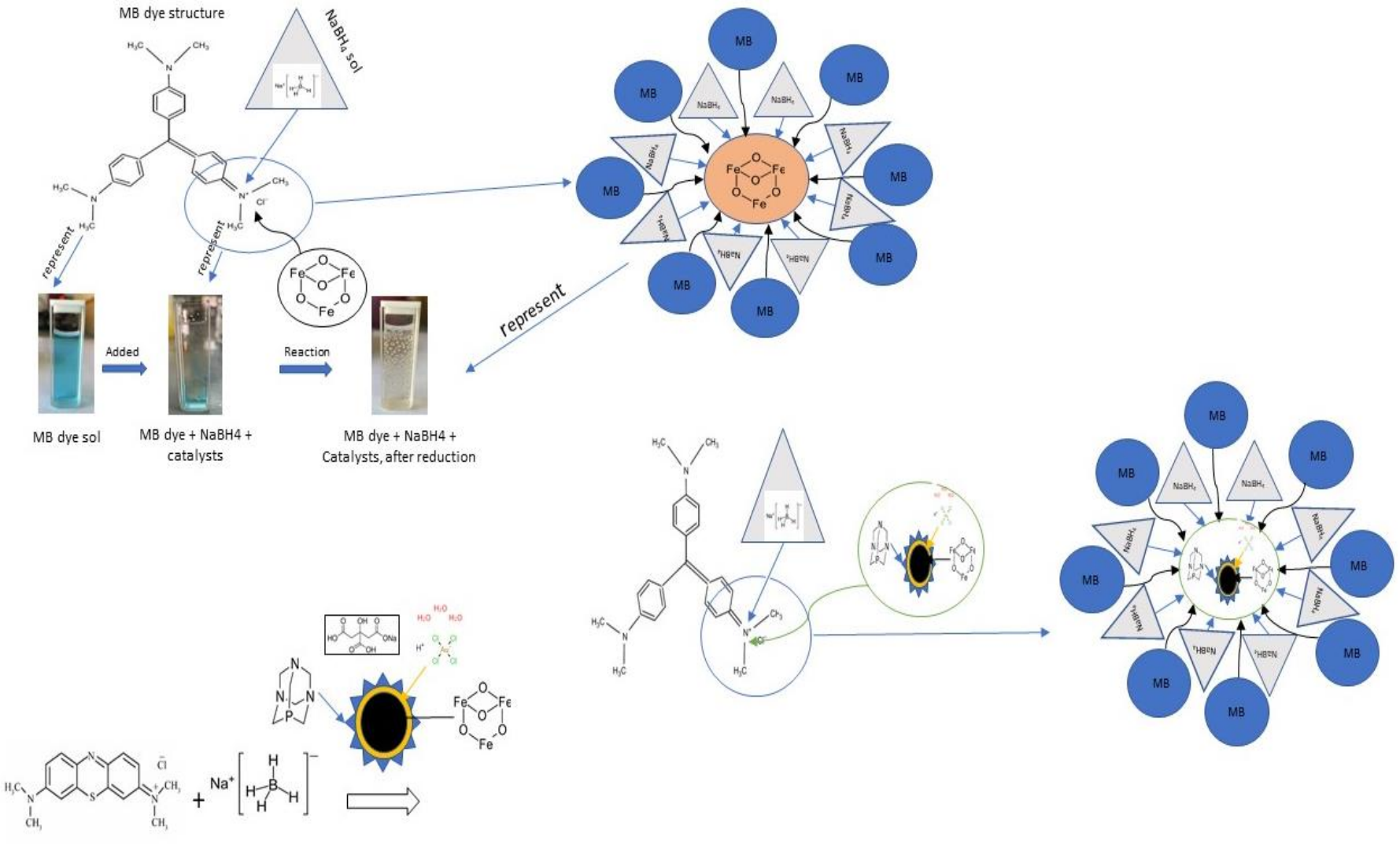

Figure 3.13b: Proposed mechanism showing what takes place within the MB reduction reaction.

3.3 Preliminary dye removal and recycling studies

From the MB dye reduction studies, we separated 50 % of the reduced MB solutions into two separate pill vials, one containing the catalyst and the other without catalyst. It was expected from previous research[17] that the absence of the catalysts will re-oxidise the MB in solution. The solution containing the catalysts was expected not to re-oxidize. However, it was observed that both solutions, with and without the catalysts remained clear over extended periods of time. This led to the investigation of possible MB dye removal from the solution by the magnetic catalyst. Therefore, we preliminarily investigated the possible removal of the MB dye and propose that the MB behaves as a stabilizer on our nanoparticle surface. Which allowed upon magnetic extraction the removal of the MB dye from the solution. The preliminary results using UV-Vis spectroscopy are presented below. **Scheme 3.2** shows how the recyclability studies was performed.

3.4 Monitor removal of MB via UV-Vis

The Shimadzu UV-1800 UV-Vis spectrophotometer with a CPS temperature control unit was used for all ultraviolet-visible (UV-Vis) spectroscopy experiments. The chemicals used include methylene blue ($C_{16}H_{18}ClN_3S.2H_2O$, molecular weight 355.90 g/mol, not less than 96%); sodium borohydride granular (99.99% trace metal bass, Sigma-Aldrich); some of the catalysts prepared as described in chapter 1 and type II water (deionized). There were three parameters used to monitor the removal of MB dye in an aqueous solution, and these will be discussed in this chapter. The first parameter will deal with using the nanomagnetic adsorbents (catalysts) with a co-catalyst ($NaBH_4$ solution) to investigate the removal of MB from an aqueous solution. The second parameter will deal with only using the nanomagnetic adsorbents (catalysts), this time without the co-catalyst to remove the MB dye in an aqueous solution. Lastly, the third parameter was to change the concentration of the MB dye solution and using the nanomagnetic adsorbents to remove the MB from aqueous solution.

3.4.1 Nanomagnetic adsorbents used with co-catalyst ($NaBH_4$) to remove the MB dye in aqueous solution

For this investigation, six nanomagnetic adsorbents (catalysts) were selected based on their characteristics (the phosphine ligands effect, the effect of two different reducing agents, the metal loading effect) already discussed previously with the kinetics studies of the nanomagnetic particles. From the kinetic studies, it was seen that the catalysts with the Fe_3O_4:Au metal loading ratios of 1:50 (1:0.05) were found to be the most preferable ones. From these set of nanomagnetic catalysts with the same Fe_3O_4:Au metal loading ratios of 1:50 (1:0.05), few were selected for this part of the research-based on modification (gold coated SPIONs), capping (stabilized gold coated SPIONs) and also with the unmodified (naked) SPIONs, refer to **Table 3.4**, to compare their adsorption capabilities in the removal of MB dye from aqueous solution.

Table 3.4: The nanomagnetic adsorbent (catalysts) used with co-catalyst (NaBH4) for the removal of MB dye in an aqueous solution.

Catalyst Code	Ratio Fe_3O_4:Au	Reducing agent	Stabilizer	Catalysts (mg)	Order of MB removal
EJL1	Magnetite			29.6	5
EJL3	1:0.05 (50:1)	$NaBH_4$		30.2	2
EJL6	1:0.05 (50:1)	$Na_3C_6H_5O_7$		29.9	4
EJL12	1:0.05 (50:1)	$Na_3C_6H_5O_7$	PTA	30.0	6
EJL15	1:0.05 (50:1)	$Na_3C_6H_5O_7$	PPh_3	29.7	3
EJL9	1:0.05 (50:1)	$NaBH_4$	PTA	100.0	1

Reaction conditions: **methylene blue** – 3000 µL; **$NaBH_4$** - 500 µL; **temp**. 25 ℃.

The method used for this experiment was as follows: An MB solution of 0.04 mM was prepared and placed into pill vials, see **Figure 3.14**. A co-catalyst ($NaBH_4$ solution) of 0.05 mM was prepared and added to the MB solutions. The nanomagnetic adsorbents (catalysts) were weighed at about 30 mg each, except for **EJL9** that was weighed at 100 mg, and added to the pill vials with MB and $NaBH_4$, see **Figure 3.15.** The mixture of solutions in pill vials was left to react further for 24 hrs on the benchtop. The catalysts were then extracted using a magnet from the solution, which left the solution colourless, see **Figure 3.16**.

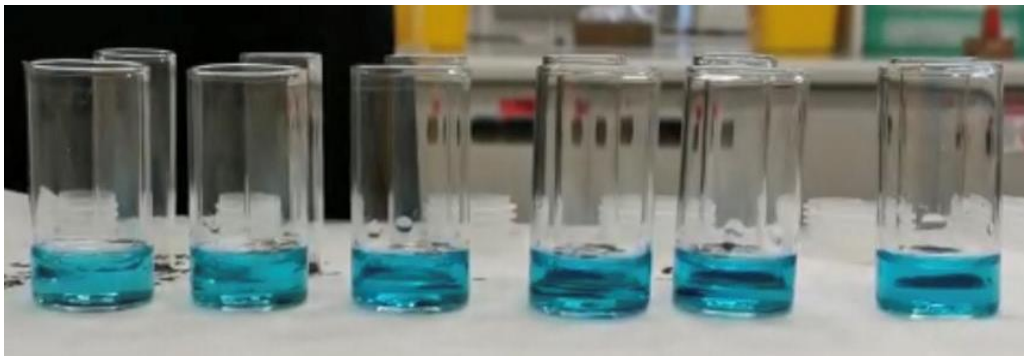

Figure 3.14: the samples of the 0.04 mM MB at 4000 µL in pill vials.

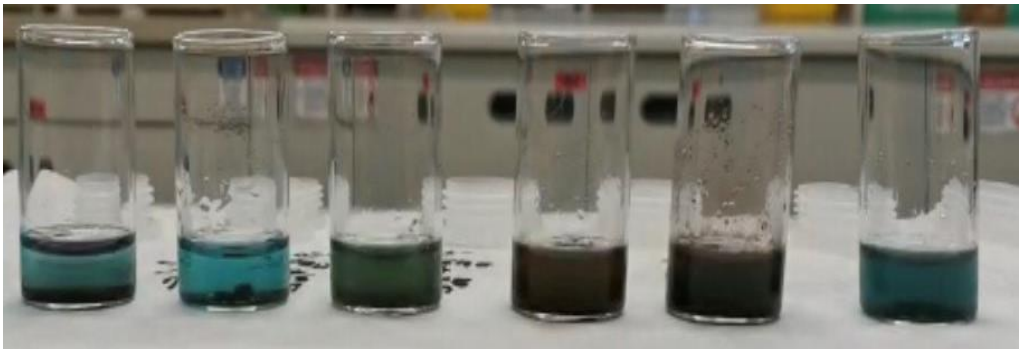

Figure 3.15: The samples mixture of MB with $NaBH_4$ and catalysts.

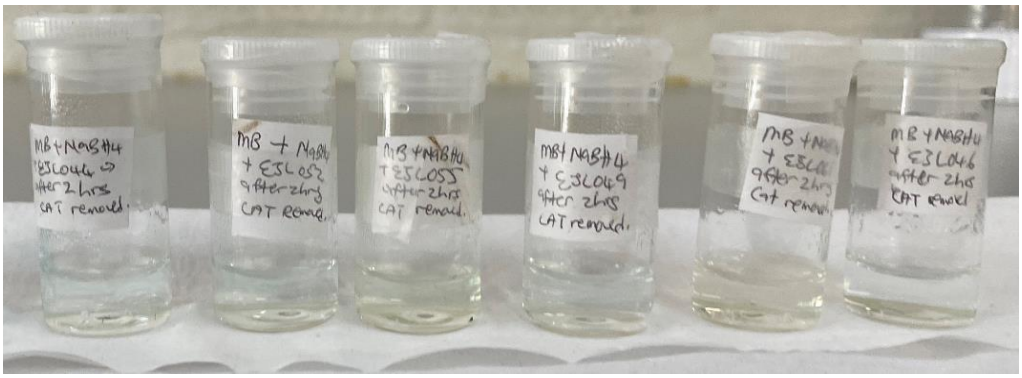

Figure 3.16: The solution after the catalysts were extracted – 24 hrs later.

These reactions were monitored using UV-Vis spectroscopy. The MB solutions before the $NaBH_4$ solution and catalysts was added, these were analyzed, to show where the MB Blank solution is on the UV-Vis spectra, see **Figure 3.17** blue spectrum.

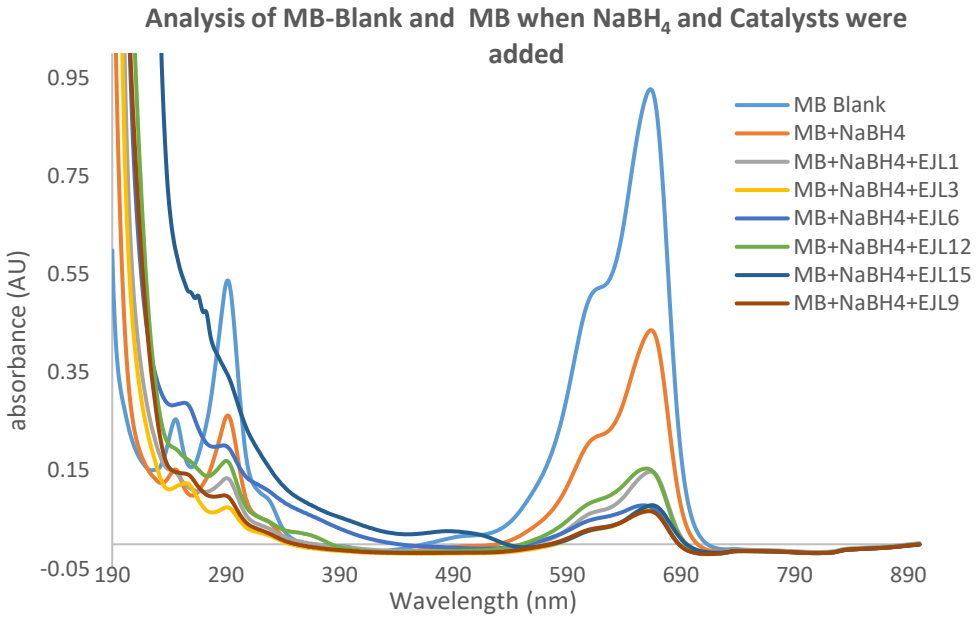

Figure 3.17: The UV-Vis spectra of MB solution with $NaBH_4$ and catalysts added.

After the addition of $NaBH_4$ and catalysts, the samples were mixed and analyzed to monitor the reaction taking place in the pill vials with different catalysts, refer **Figure 3.17**.

From Chapter 3, it was concluded that an increase in the catalyst loading led to an increase in the MB reduction. **EJL9** ($NaBH_4$ + PTA) was the fastest to reduce the MB, as it had a higher catalyst mass compared to the others. Furthermore, the other catalysts with similar masses showed that the second-best catalyst was found to be **EJL3** ($NaBH_4$), followed by **EJL15** ($Na_3C_6H_5O_7$ + PPh_3), then EJL6 ($Na_3C_6H_5O_7$), then by **EJL1** (uncapped -Fe_3O_4), then by **EJL4** ($Na_3C_6H_5O_7$ + PTA). MB blank with $NaBH_4$ without catalyst proved to be to be the slowest for MB reduction.

All the catalysts with $NaBH_4$, as a reducing agent, were the fastest to remove the MB dye, compared to the sodium citrate analogues. As expected, the naked magnetite catalyst was the least likely to remove the dye, although it was not as slow as the sample without any catalyst.

After the 24 hours, as seen in **Figure 3.17**, the catalysts were extracted from the MB solutions using a magnet and the solutions were analyzed on the UV-Vis spectrophotometer. The results were presented as seen in **Figure 3.18**. It can be clearly seen that the catalysts all removed the

MB dye from the aqueous solution, as the absorbance peak at λ = 666 nm showed no presence of MB dye on the aqueous solution.

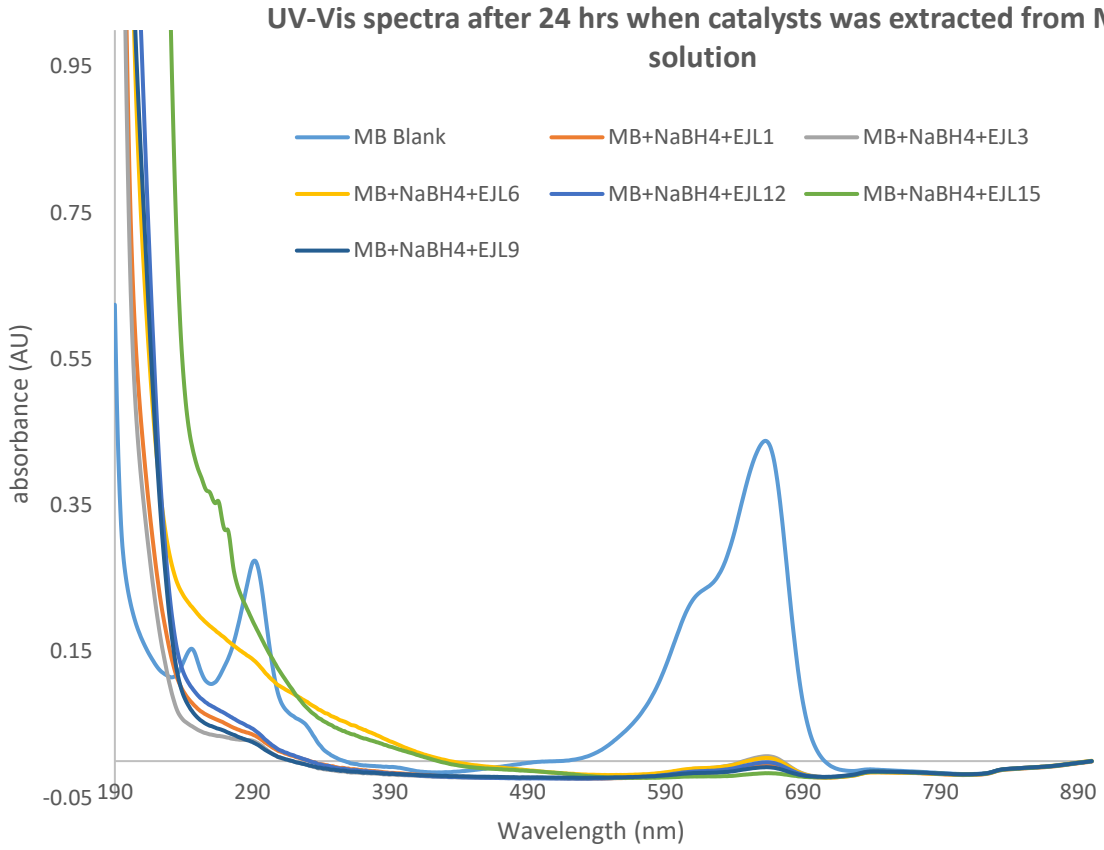

Figure 3.18: The UV-Vis spectra after 24 hrs once the catalysts were extracted from the MB aqueous solutions.

3.4.2 Nanomagnetic adsorbents used without co-catalyst ($NaBH_4$) to remove the MB dye in aqueous solution

A similar experiment was done, as section 3.1.1, but this time without the $NaBH_4$ solution to remove the MB dye from aqueous solution. The same approach was followed for the catalysts selection, but this time as mentioned without any co-catalyst ($NaBH_4$) being used. The Fe_3O_4:Au metal loading ratios of 1:10 (1:0.1), with the nanomagnetic catalysts at a mass of about 55 mg, were used. Seven nanomagnetic catalysts were selected for this part of the research based on modification (gold-coated SPIONs), capping (stabilized gold-coated SPIONs) and also with the unmodified (naked) SPIONs, refer to **Table 3.5**, to compare their adsorption capabilities in the removal of MB dye from aqueous solution.

Table 3.5: The nanomagnetic adsorbent (catalysts) used with co-catalyst (NaBH4) for the removal of MB dye in aqueous solution.

Catalyst Code	Ratio Fe_3O_4:Au	Reducing agent	Stabilizer	Catalysts (mg)	Order of MB removal
EJL1	Magnetite			55.1	7
EJL2	1:0.01 (10:1)	$NaBH_4$		54.2	3
EJL5	1:0.01 (10:1)	$Na_3C_6H_5O_7$		54.5	6
EJL11	1:0.01 (10:1)	$Na_3C_6H_5O_7$	PTA	54.8	4
EJL14	1:0.01 (10:1)	$Na_3C_6H_5O_7$	PPh_3	55.1	5
EJL8	1:0.01 (10:1)	$NaBH_4$	PTA	55.2	1
EJL17	1:0.01 (10:1)	$NaBH_4$	PPh_3	55.0	2

Reaction conditions: **methylene blue** – 3000 µL; **temp**. 25 ℃

This time the focus was only at the λ = 666 nm, and from **Figure 3.19**, it was seen that the nanomagnetic catalysts does reduce the MB dye from solution without using the co-catalysts ($NaBH_4$). This further supports the earlier conclusions that the nanomagnetic catalyst designed can reduce MB without a co-catalyst.

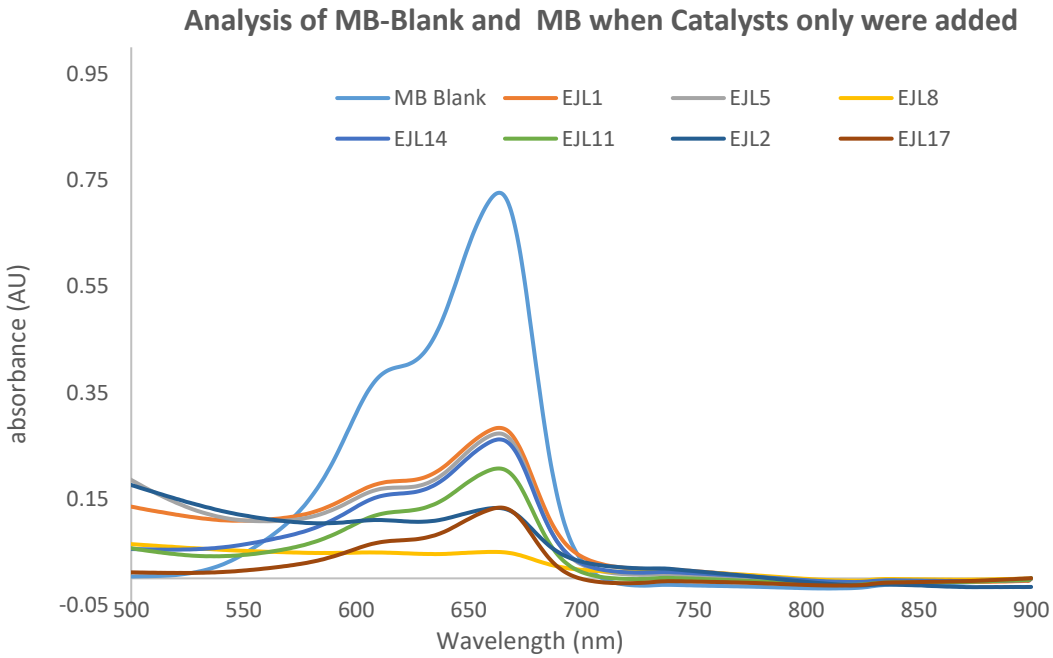

Figure 3.19: The UV-Vis spectra of MB solution with nanomagnetic catalysts added at λ = 666 nm.

3.5 Recyclability studies

For the recyclability studies, the Shimadzu UV-1800 UV-Vis spectrophotometer with a CPS temperature control unit was used for all ultraviolet-visible (UV-Vis) spectroscopy experiments. The chemicals used include methylene blue ($C_{16}H_{18}ClN_3S.2H_2O$); some of the nanomagnetic catalysts prepared as described in chapter 2, and type II water (deionized) was used. The nanomagnetic catalyst selected for the recyclability study was **EJL12** (1:50-1:0.05, $Na_3C_6H_5O_7$ + PTA). This catalyst was modified using sodium citrate and capped with PTA stabilizer. The recyclability of **EJL12** was performed 5 times, and each time on the fresh MB dye aqueous solution. The recyclability of nanomagnetic catalyst (**EJL12**) was evaluated in the removal of MB from an aqueous solution. The catalyst in the absence of a co-catalyst showed the successful removal of the MB dye from the solution. Subsequent recycles of the catalyst were also successful with negligible loss of activity between recycles. It is proposed that the MB act as a ligand on the nanoparticle surface, then it is magnetically extracted along with the catalyst from the solution. In order to recycle the catalyst, the MB is cleaved from the nanoparticle surface by the addition of acetonitrile, which substitutes the MB from the surface. Resulting in an acetonitrile stabilized nanoparticle and free MB in the acetonitrile solution. The nanoparticles were dried and subsequently reused up to 5 times, showing similar results throughout. Refer to Figure 3.21 -3.25.

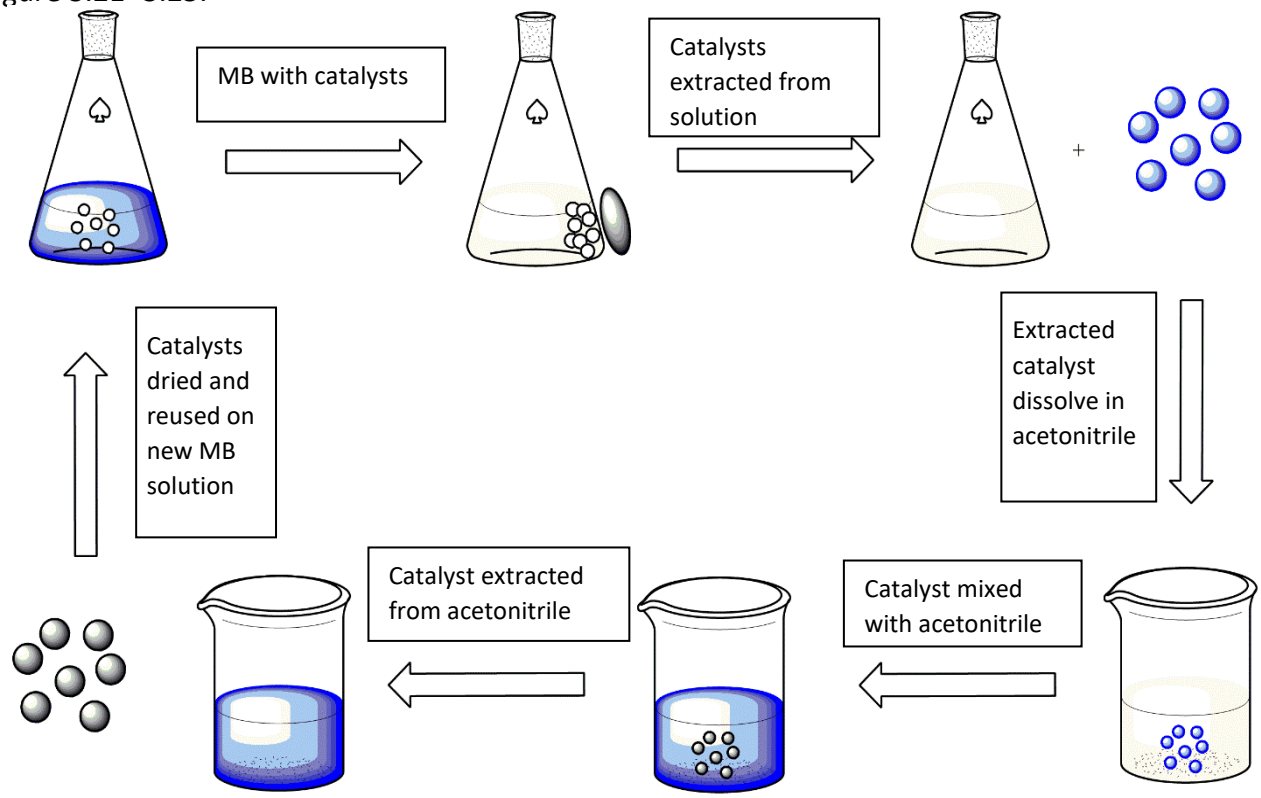

Figure 3.20: The recyclability study

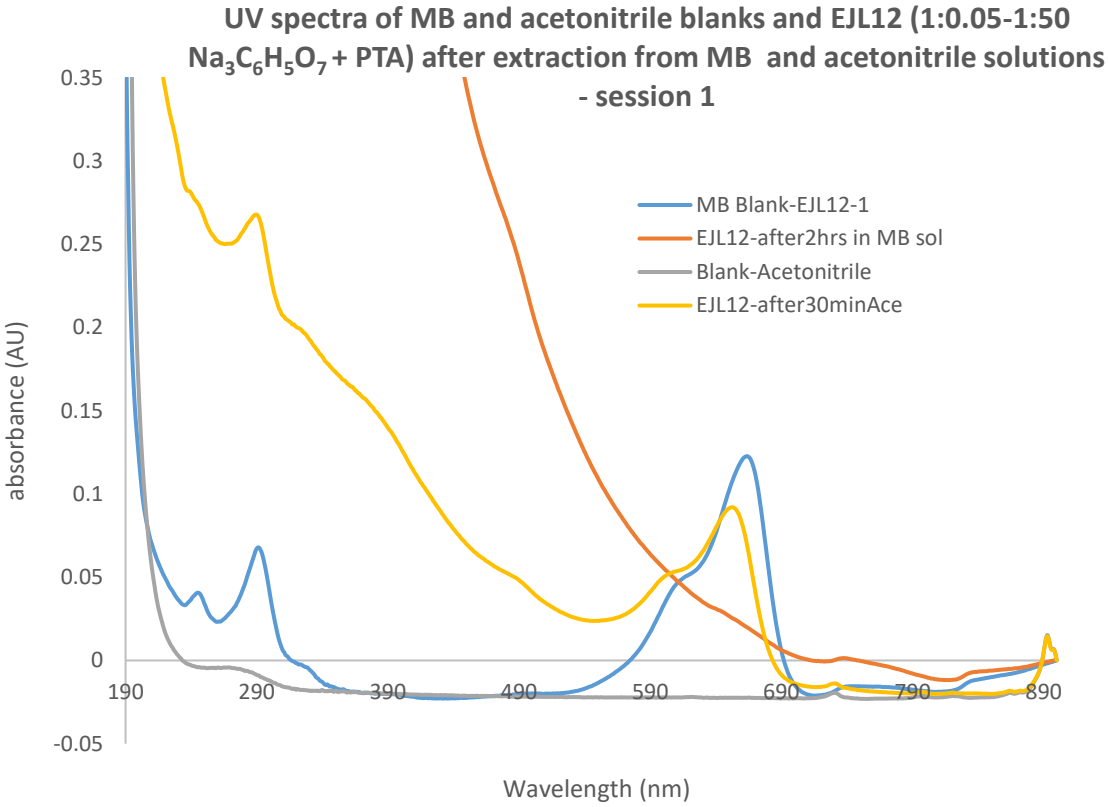

Figure 3.21: The UV-Vis spectra EJL12 used for recyclability studies on MB solution – session-1

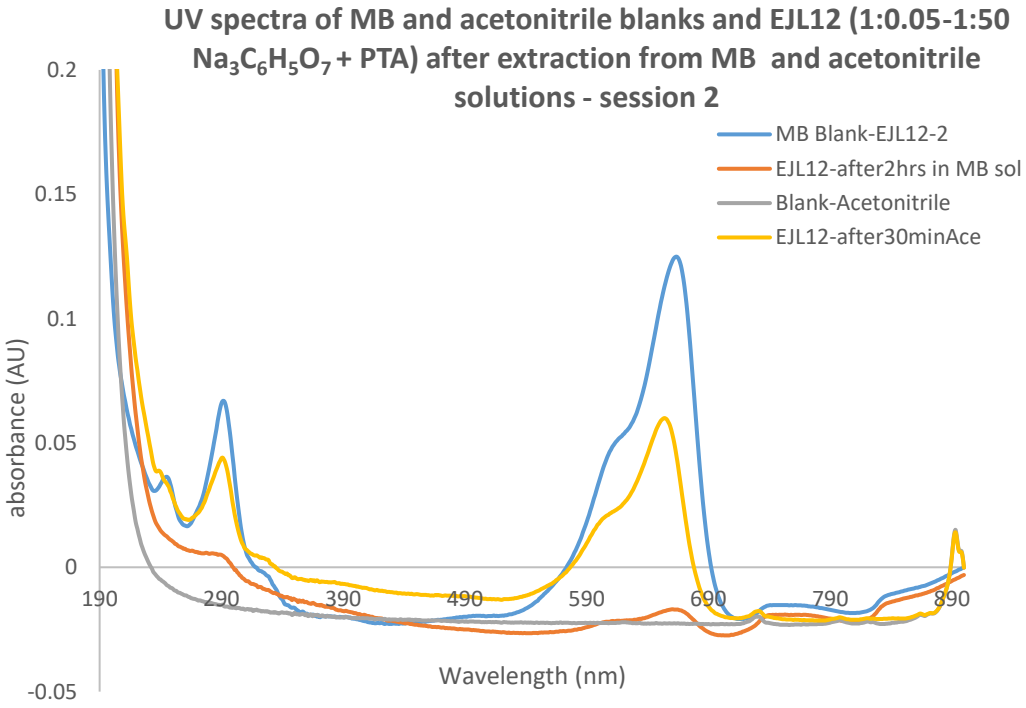

Figure 3.22: The UV-Vis spectra EJL12 used for recyclability studies on MB solution – session-2

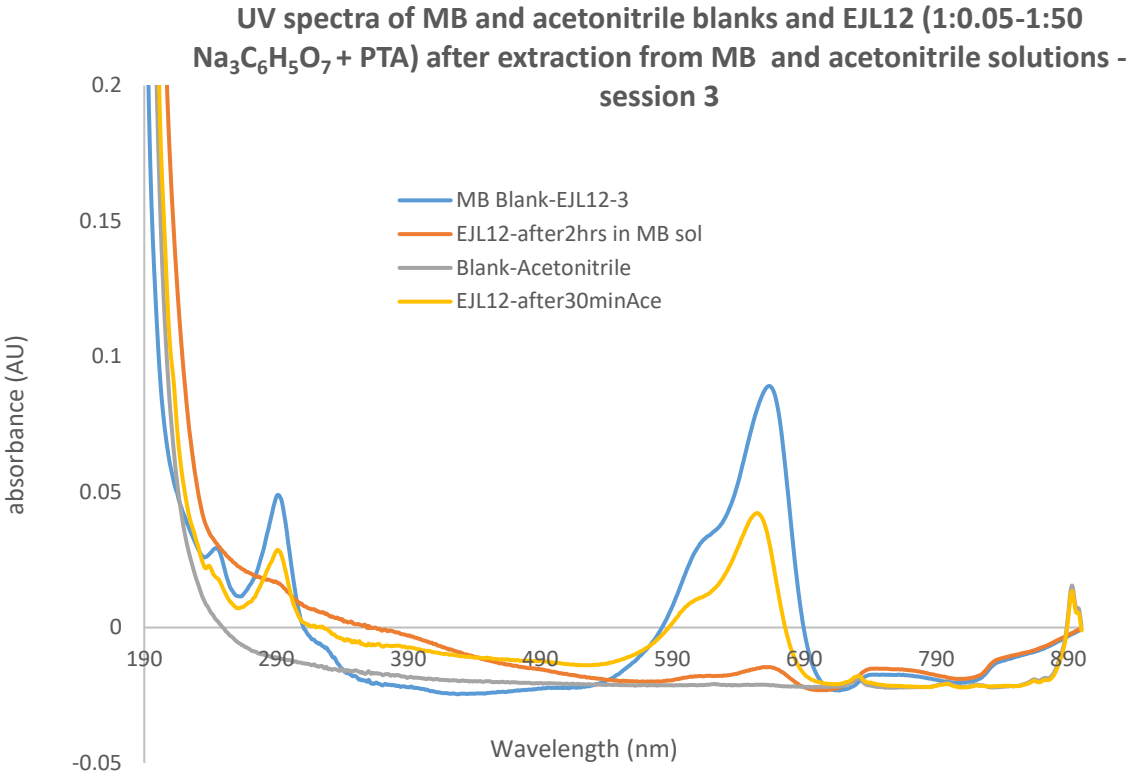

Figure 3.23: The UV-Vis spectra EJL12 used for recyclability studies on MB solution – session-3

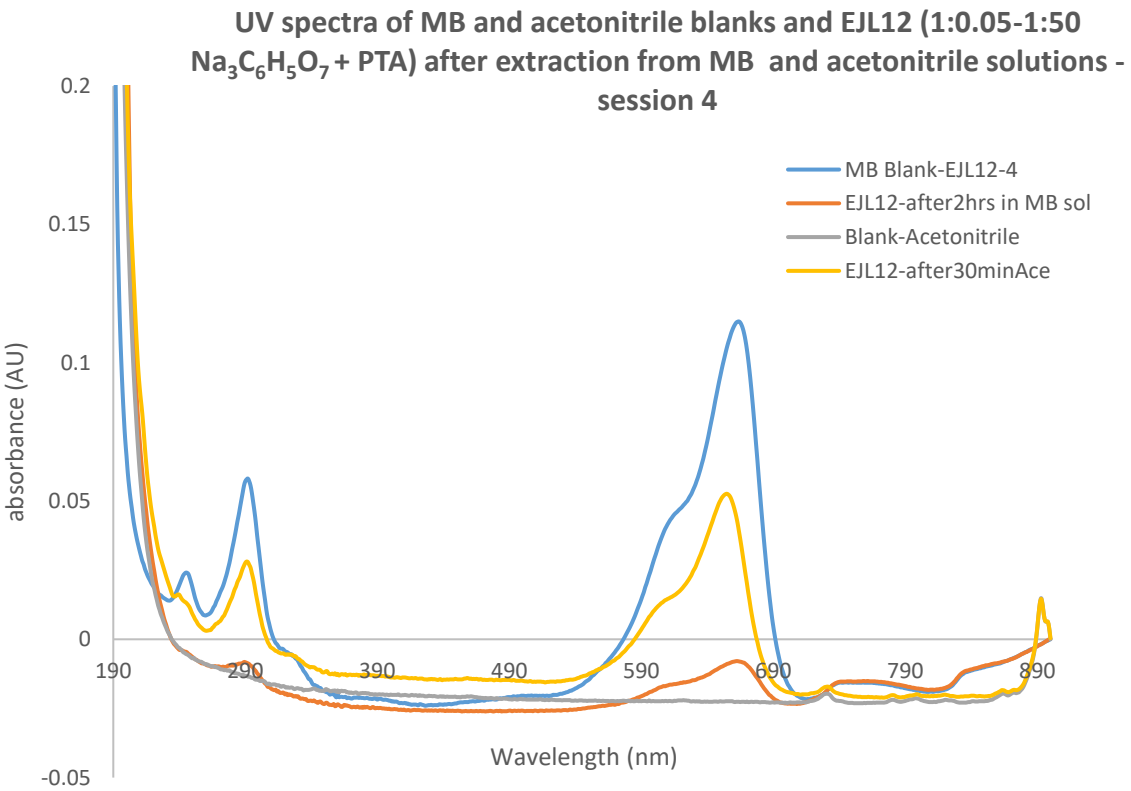

Figure 3.24: The UV-Vis spectra EJL12 used for recyclability studies on MB solution – session-4

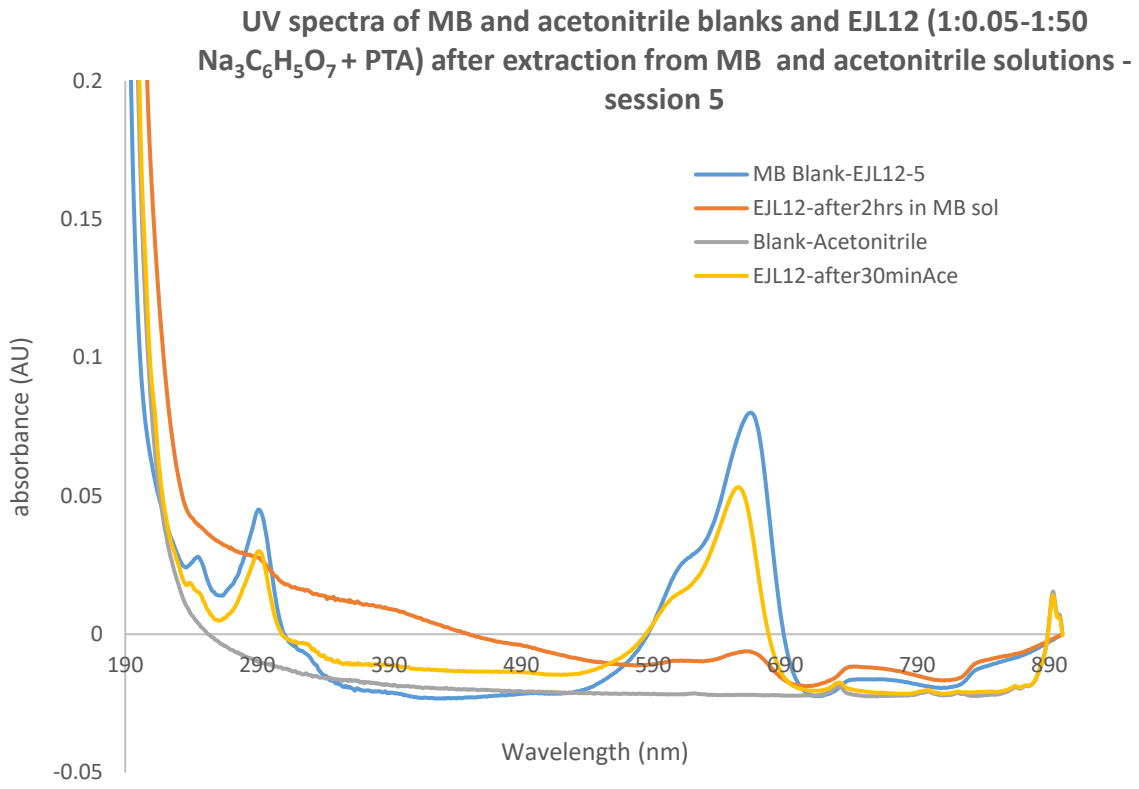

Figure 3.25: The UV-Vis spectra EJL12 used for recyclability studies on MB solution – session-5.

3.5 Conclusion

The gold-coated modified and stabilized SPIONs were tailored to be able to reduce the azo dyes in the textile industry. In this chapter, the azo dye used was methylene blue. Since these stabilized gold-coated SPIONs are easy to prepare, reusable, and can be recyclable as part of their characteristics due to being magnetic ability, it would be possible to improve the current expensive chemical usage on the treatment of wastewater azo dyes within the textile industry, as illustrated with the reduction of methylene blue. A total of 19 catalysts were successfully synthesized and used in the methylene blue reduction. These prepared stabilized AuNPs catalysts were catalytically active in the reduction of methylene blue dye in conjunction with $NaBH_4$. From the kinetic studies performed, it could be concluded that sodium citrate, as a reducing agent, works better than sodium borohydride on both ligands stabilizers and metal loading systems. As sodium citrate is a greener reducing agent compared to sodium borohydride, the catalytic system is more environmentally friendly. Furthermore, it was found that the 1,3,5-triaza-7-

phosphaadamantane (PTA) phosphine ligand was the best stabilizer compared to triphenylphosphine (PPh_3). The preferred magnetite (Fe_3O_4) to gold (Au) metal loading ratios for these catalysts was found 1:50 (1:0.05). This ratio was the most favourable catalytic parameter as it had the highest k_{abs} for the reduction of methylene blue dye. The complete reduction takes place in less than 20 mins using the catalysts that were most active. The rate of MB colour reduction depends on the concentration of reactants (the MB, $NaBH_4$ and catalysts), and as well as the temperature. It was concluded from the rate constant (k_{abs}) that, that an increase in temperature, catalysts and co-catalyst ($NaBH_4$) resulted in a more facile reduction of MB. Therefore, these reaction parameters can be tailored for the needs of wastewater treatment within the textile industry to be effective. The nanoparticles used are stable for a long period (years), and they can be easily isolated from the reaction system due to their magnetism. The catalytic and metal-mediated reactions showed a complete reduction of methylene blue from the UV-Vis spectroscopy on the optimised method. It was preliminarily shown that the phosphine stabilized nanoparticles were capable of removing the MB dye without the need for the co-catalysts ($NaBH_4$). It was proposed that the MB acts as a stabilizer for the nanoparticles which upon the extraction of the particles results in the removal of the MB. Subsequently, recyclability studies were also performed on **EJL12** up to 5 times. From the recyclability studies, it was shown that the removal of MB dye from an aqueous solution could be performed without the loss of activity over multiple reuses.

3.6 Experimental

3.6.1 Materials

The chemicals used include methylene blue ($C_{16}H_{18}ClN_3S.2H_2O$, molecular weight 355.90 g/mol, not less than 96%, $C_{16}H_{18}ClN_3S$ on dried, May & Baker Ltd); sodium borohydride granular (99.99% trace metal bass, Sigma-Aldrich); type II water (deionized); and acetonitrile anhydrous (CH_3CN, 99.8 %, Merck).

3.6.2 Instruments

The Shimadzu UV-1800 UV-Vis spectrophotometer with a CPS temperature control unit was used for all ultraviolet-visible (UV-Vis) spectroscopy experiments. Quartz cuvettes standard, 10 mm,

3.5 mL, spectrometer cell with a path length of 1.00 cm were used for spectrum and kinetic analysis, respectively. Branson Model B200 Ultrasonic Cleaner, 120 V, operates on 110-120 V AC, 50-60 Hz, includes a 5-minute timer, wide variety of other applications include: instrument and clock parts, small geological samples, metal and plastic machine parts, small electrical and electronic components, used for sonification of the nanoparticles used for the reduction of methylene blue studies.

3.6.3 Methylene blue studies

Methylene Blue dye concentration of 40 µM (taking a known amount of the crystal MB was weighed and dissolved in deionised water) was prepared as a stock solution of which an amount of 2000 µl was used for each reaction in the quartz cuvette for the UV-vis analysis especially on the optimised method. The $NaBH_4$ solution of 50 mM (taking a known amount of the crystal MB was weighed and dissolved in deionised water), was prepared as a stock solution of which an amount of 100 µl used for each reaction in the quartz cuvette for the UV-vis analysis especially on the optimised method. For the method optimisation studies using the catalyst **EJL8** (1 mg was weighed and sonicated well in 1 mL of H_2O) the different volumes were used as stipulated on **Table 3.1**. For the other catalysts on the optimized method a 1 ppm solution was prepared each time, and a volume of 100 µL was used in the cuvette for each reaction. Lastly, the cuvette was always topped up with deionized H_2O (on the optimized method, a volume of 800 µL was used) in the cuvette; this was always performed to ensure that the total volume of all reactants in the cuvette amounts to 3000 µL for all reactions for UV-vis analyses.

3.6.4 The kinetic study for the reduction of MB

The reduction of MB by using $NaBH_4$ and the catalysts was a complicated process probably due to various reduced forms of MB^+. The process could not easily be depicted by simple reaction kinetics. To estimate the kinetics rate of discoloration, an equation 3.5 form of power law is used:

$$-\frac{d[C]}{dt} = k[AuNPs]^n[C]^m \qquad (3.5)$$

Where k is the removal rate constant, [C] is MB concentration, m and n are the pseudo-order of reaction with respect to MB and catalyst respectively. The rate equation can be stated with observed rate constant (k_{abs}) as follows:

$$-\frac{d[C]}{dt} = k_{abs}[C]^m \quad (3.6)$$

Where,

$$k_{abs} = k[AuNPs]^n \quad (3.7)$$

For a zero-order reaction, the above equation after integration becomes:

$$C_t = k_o t \quad (3.8)$$

Also, for a first-order reaction, the above equation after integration becomes:

$$In(C_t) = In(C_o) - k_1 t \quad (3.9)$$

In which, C_0 is the initial MB concentration and C_t is the concentration at reaction time *t*.

From the pseudo first-order kinetic plots in **Figure 3.26**.

The reactions on the UV-Vis spectroscopy were run in quadruple for each catalysts using the reaction conditions listed in **Table 3.1 and 3.3**, after the UV-Vis spectrums were obtained. The k_{abs} where then calculated for wavelength peaks at λ 666nm, λ 293nm and λ 260nm. The R^2 values were also taken into consideration.

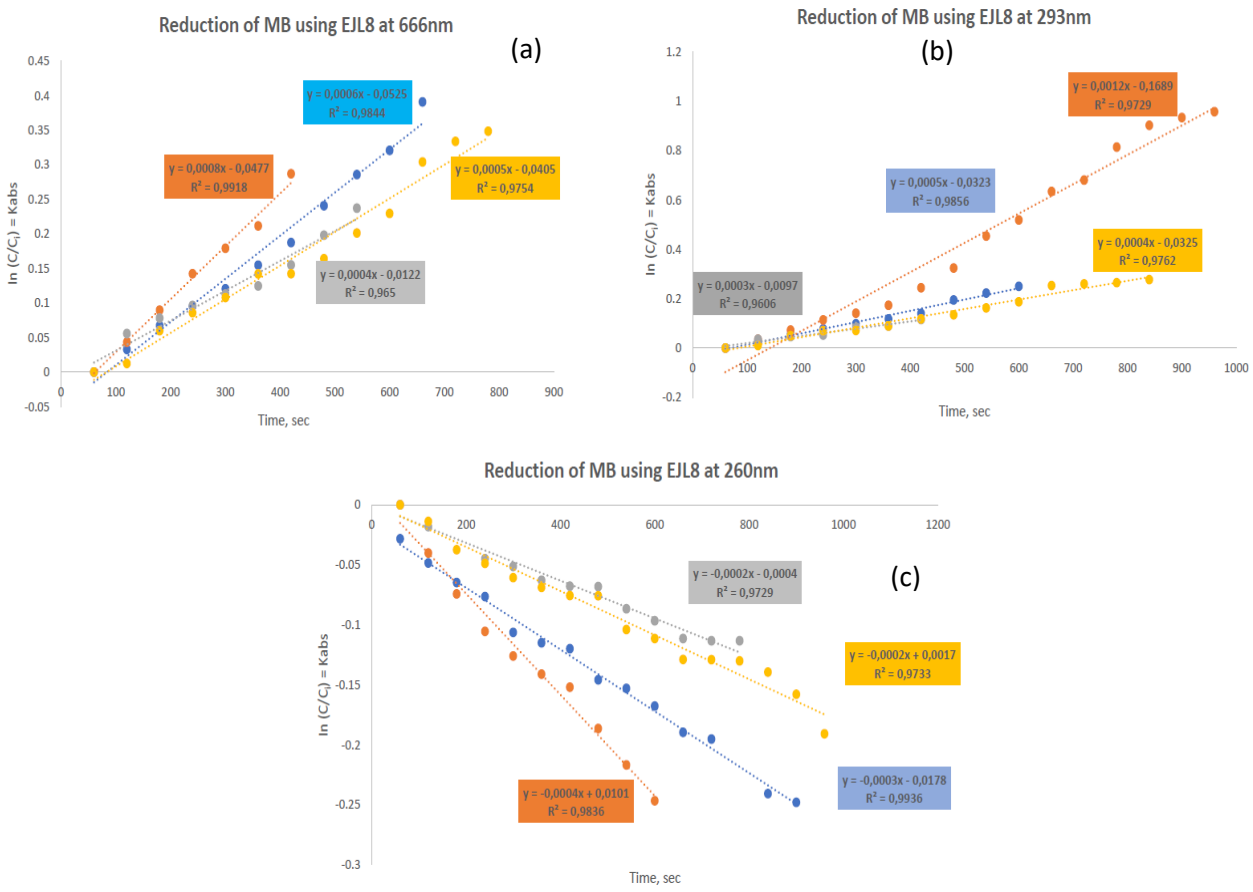

Figure 3.26: The k_{abs} calculations of catalysts EJL8 at wavelengths (a) 666, (b) 293 and (c) 260 nm.

3.7 References

[1] P. Saikia, A. T. Miah and P. P. Das, Highly efficient catalytic reductive degradation of various organic dyes by Au/CeO_2-TiO_2 nano-hybrid, Journal of Chemical Sciences (2017) 129, 81-93.

[2] N. T. Nandhini, S. Rajeshkumar, and S. Mythili, The possible mechanism of eco-friendly synthesized nanoparticles on hazardous dyes degradation, Biocatalysis and Agricultural Biotechnology, (2019) 19, 1-10.

[3] M. I. Kiron, Problems caused by textile dyes in the environment, Textile learner (one stop solution for textiles), (2011) 04, 4786-4787.

[4] W. H. Perkin, On Mauve or Aniline-Purple, Proceedings of the Royal Society of London, (1963) 12, 713-715.

[5] S. Singh, V. C. Srivastava, and I. D. Mall, Mechanism of dye degradation during electrochemical treatment, Journal of Physical Chemistry, (2013) C117 (29), 15229-15240.

[6] M. Joonghwan, H. Jeong-Eun, J, *et al*., Pre-treatment of a dyeing wastewater using chemical coagulants dyes and pigments, (2007) 72, 240-245.

[7] A. P. Pathelis, P. X. Nikolaos, and M. Dionissions, Treatment of textile dyehouse wastewater by TiO_2 photocatalysis, water research, (2006) 40, 1276-1286.

[8] L. I. Fangwen, W. U. Xiaoai, M. A. Songjiang, X. U. Zhongjian, L. I. U. Wenhua and L. I. U Fen, Adsorption and desorption mechanisms of methylene blue removal with iron oxide coated porous ceramic filter, J. water resources and production, (2009) 1, 1-57.

[9] A. Dabrowski, Absorption – from theory to practice, Adv. Colloid interface sci., (2001) 93, 135-224.

[10] M. Ghaedi, H. Khajehsharifi, A. H. Yadkuri, M. Roosta, A. Asghari, Oxidized multiwalled carbon nanotubes as efficient adsorbent for bromothymol blue, Toxicol. Environ. Chem., (2012) 94, 873-883.

[11] M. Ghaedi, S. Heidarpour, S. N. Kokhdan, R. Sahraie, A. Daneshfar, B. Brazesh, Studying the reparation of activated carbon from macadamia nut shells by chemical activation with NaOH in methylene blue treatment application, Powder Technol., (2021) 228, 18-25.

[12] Insight into the adsorption mechanisms of methylene blue and chromium (III) from aqueous solution onto pomelo fruit peel Van-Phuc Dinh, *a Thuy-Diem-Thuy Huynh, Royal Society of Chemistry, (2019) 9, 25847.

[13] Olajire AA and Olajide AJ, Kinetic study of decolorization of Methylene Blue with Sodium Sulphite in aqueous media: Influence of Transition Metal Ions, Journal of physical chemistry & Biophysics, (2014) 4,2.

[14] A. Fernandez-Perez, T. Valdes-Solis, and G. Marban, Visible light spectroscopic analysis of methylene blue in water; the resonance virtual equilibrium hypothesis, Dyes and Pigments (2019) 161, 448-456.

[15] Mulisa Nemanashi, Reinout Meijboom, Synthesis and characterization of Cu, Ag and Au dendrimer-encapsulated nanoparticles and their application in the reduction of 4-nitrophenol to 4-aminophenol, Journal of Colloid and Interface Science, (2013) 398, 260-267.

[16] Gupta N, Singh HP, Sharma RK, Metal nanoparticles with high catalytic activity in degradation of methyl orange: an electron relay effect. J Mol Catal A Chem (2011) 335, 248–252.

[17] Angelique Blanckenberg, Rehana Malgas-Enus, Raspberry-like gold-decorated silica (SSx-AMPS-Au) nanoparticles for the reductive discoloration of dyes, Spring Nature Switzerland AG, SN Applied Sciences, (2019) 1, 787.

Chapter 4: Summary, conclusion, and future work

4.1 Chapter summaries and concluding remarks

A literature review was performed to evaluate all relevant research in the literature pertaining to the use of different types of nanoparticles employed for wastewater treatment within the textile industry. A relevant background for this research was provided, discussing the various reasons why nanomaterials are used in wastewater treatment, including the advantages and disadvantages of different types of nanoparticles.

Chapter 2 dealt with the synthesis and characterization of magnetic nanoparticles, which involved the successful synthesis of uncapped superparamagnetic iron oxide (SPIONs), using the co-precipitation method. The synthesis of gold coated nanoparticles using two reducing agents respectively, sodium borohydride ($NaBH_4$) and sodium citrate ($Na_3C_6H_5O_7$), reduce the Au onto the surface of the SPIONs. These were successfully synthesized using the direct gold coating method. The through the FT-IR spectroscopy and UV-Vis spectroscopy, it could be concluded that the Au-NPs were immobilized on the surface of the naked SPIONs. These nanoparticles were then capped by employing two different phosphine ligands, 1,3,5-triaza-7-phosphaadamantane (PTA) and Triphenylphosphine (PPh_3), respectively. These were successfully capped, and the gold-coated nanoparticles showed increased stability due to the stabilizing effect of the ligands employed. From the HR-TEM analysis, it could be concluded that the stabilized gold-coated nanoparticles were much smaller and not as agglomerated compared to the naked SPIONs. Furthermore, these nanoparticles were also synthesized using various magnetite (Fe_3O_4): gold (Au) metal loading ratios of 1:10, 1:50 and 1:100.

Chapter 3 discussed the use of the 19 (**EJL1 – EJL19**) nanoparticle systems that were successfully synthesized from chapter 2, and their application in wastewater treatment, by reducing methylene blue dye in aqueous solution. From the UV-Vis studies it was concluded that these prepared stabilized AuNPs catalysts were catalytically active in the reduction of methylene blue dye in conjunction with $NaBH_4$. Using kinetic studies, it could be concluded that the sodium citrate as a reducing agent works better than sodium borohydride on both ligands stabilizers and metal loading systems. Furthermore, the 1,3,5-triaza-7-phosphaadamantane (PTA) phosphine ligand was found to be the best stabilizer compared to triphenylphosphine (PPh_3) ligand. The

preferred magnetite (Fe_3O_4) to gold (Au) metal loading ratios for these catalysts were found 1:50 (1:0.05) as this ratio was the most favourable. While the naked magnetite reduced the MB the fastest, it was also quick to oxidize back to methylene blue. The stabilized gold coated nanoparticles on the other hand, showed complete reduction of methylene blue, for a prolonged amount of time, even when the catalyst was removed for several months. It was also shown that the phosphine stabilized gold coated nanoparticles were capable of removing the MB dye from the aqueous solution, without the use of the reducing agent ($NaBH_4$). Subsequently, the recyclability studies were also performed on **EJL12**. These showed that the removal of MB dye from aqueous solution was possible up to 5 times, without the loss of activity over multiple reuses.

4.2 Suggestions for future work

The preliminary studies that we conducted using the stabilized gold coated nanoparticle **EJL12** (1:50-1:0.05, $Na_3C_6H_5O_7$ + PTA) showed very exciting MB dye removal conclusions. These need to be investigated further using the other set of stabilized gold coated nanoparticles with different Fe_3O_4 to Au metal loadings as well as the PPh_3 stabilized nanoparticles. The multiple reuses of these catalysts will also have to be studied further as **EJL12** was reused 5 without loss in its activity. The removal study was only used on the MB dye removal and these nanoparticles can be tested for other anionic and cationic dyes.

The use of bimetallic nanoparticles with a cheaper second metal, for the application of the wastewater treatment (in order to reduce the cost of the Au NPs) could make an interesting study for the reduction and removal of different azo dyes while the recyclability of the nanomaterials could be further probed.

The testing of typical concentration of MB that are found in the textile industry wastewater should be tested. The 6.4µM concentration used for this study was as close to the concentrations usually found in the textile industry. Testing of catalyst at the typical MB concentration in the textile industrial wastewater should also be considered.